Title

DECAY STUDIES OF NUCLEI NEAR THE PROTON DRIP LINE: [SUP]35 CO, [SUP]31 OR, [SUP]69 BR, AND [SUP]65 AS

Author

Reiff, J.E.

Publication Date

1989-06-01

LBL-27387

Lawrence Berkeley Laboratory
UNIVERSITY OF CALIFORNIA

Decay Studies of Nuclei Near the Proton Drip Line: ^{35}Ca, ^{31}Ar, ^{69}Br, and ^{65}As

J.E. Reiff
(Ph.D. Thesis)

June 1989

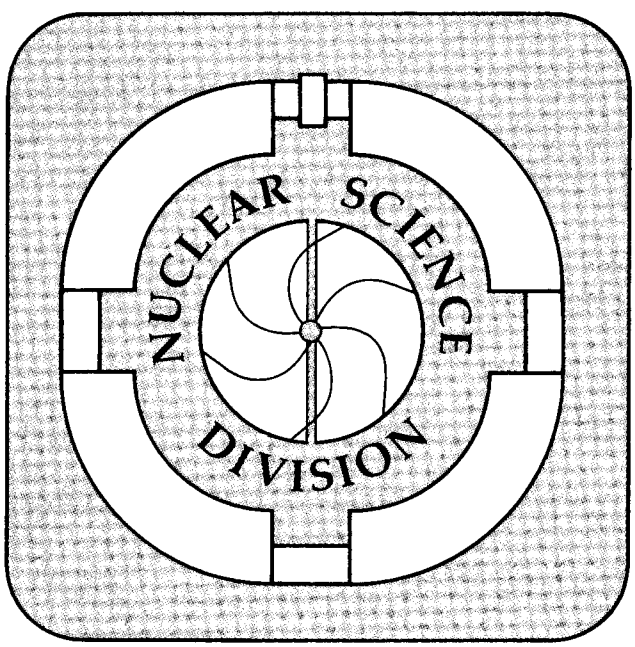

Prepared for the U.S. Department of Energy under Contract Number DE-AC03-76SF00098.

DISCLAIMER

Decay Studies of Nuclei Near the Proton Drip Line: ^{35}Ca, ^{31}Ar, ^{69}Br, and ^{65}As

by

Jay Edward Reiff

Nuclear Science Division
Lawrence Berkeley Laboratory
1 Cyclotron Road
Berkeley, California 94720
USA

*This work was supported by the Director, Office of Energy Research, Office of High Energy and Nuclear Physics, Nuclear Physics Division of the U.S. Department of Energy under Contract No. DE-AC03-76SF00098

Decay Studies of Nuclei Near the Proton Drip Line: ^{35}Ca, ^{31}Ar, ^{69}Br, and ^{65}As

by

Jay Edward Reiff

ABSTRACT

Studies of new beta-delayed two-proton emitters and a search for ground state proton radioactivity in medium mass nuclei were performed using various experimental techniques in conjunction with several detection systems. A helium-jet transport system and three-element (ΔE1, ΔE2, E) silicon telescopes were used to discover the existence and detect the decay of the first T_z = -5/2 nuclide, ^{35}Ca. Two-proton emission from the T = 5/2 isobaric analog state in ^{35}K at an excitation energy of 9.053 ± 0.045 MeV, fed by the superallowed beta decay of ^{35}Ca, resulted in transitions to both the ground state and first excited state of ^{33}Cl. The corresponding two-proton sum energies were 4.089 ± 0.030 MeV and 3.287 ± 0.030 MeV. Measurements of the individual proton energies indicated the prevalence of a sequential decay mechanism. Using the isobaric multiplet mass equation, the mass excess of ^{35}Ca was calculated to be 4.453 ± 0.060 MeV. By comparing the yield of ^{35}Ca with co-produced beta-delayed proton emitters, its half-life was determined to be 50 ± 30 ms.

In order to study nuclei whose half-lives were too short for the helium-jet system (~20 ms), an in-beam recoil catcher wheel was constructed. The wheel speed can be varied to study nuclides whose half-lives range from 100 μs to ~250 ms. The first new decay observed with the wheel system and traditional ΔE-E telescopes was the beta-delayed two-proton emission from ^{31}Ar. The two-proton sum energy of ~7.5 MeV corresponds to a transition from the isobaric analog state in ^{31}Cl to the ground state of ^{29}P.

The search for proton radioactivity required the development of low energy, particle identification detector telescopes. These telescopes, comprised of a gas ΔE and silicon E, were used in conjunction with the in-beam recoil catcher wheel to search for ground state proton emission from ^{69}Br and ^{65}As. No proton groups which could be assigned to either of these nuclides were observed. An upper limit of 100 μs has been placed on the half-life of ^{69}Br. ^{65}As, on the other hand, is believed to decay predominantly by beta emission but may possess a ground state proton decay branch which does not exceed 0.25%.

Acknowledgements

I would like to express my gratitude to the following people who have helped make my stay in Berkeley a rewarding and fruitful, albeit sometimes trying, experience:

Professor Joseph Cerny, my research advisor, for his support, enthusiasm and the seemingly endless amount of patience he has shown towards me and the projects on which I have worked.

The past and present members of the Cerny group: Dr. Mike Cable, Dr. Ed Schloemer, Dr. Masuma Ahmed, and Dr. Juha Äystö for getting me started on the road of experimental nuclear science; Dr. Mike Hotchkis and Dr. Fred Blönnigen for their help in designing the recoil catcher wheel; Dr. Dennis Moltz for his help with the gas detectors and associated electronics; Dr. J. David Robertson, a fellow graduate of the "new school", for his help and friendship during those long nights and early mornings of data analysis; Thomas Lang, the best office-mate I ever had, for being there when I needed someone with whom to talk, laugh, and commiserate; and Jon Batchelder, Ted Ognibene, and John Hoffman for their general help and companionship.

The entire staff and crew of the 88-Inch Cyclotron Facility, in particular: Ed Chubak, Don Fong, David Ruiz, Don Stiver, and John Wong for the fine pieces of precision machining I frantically asked them to produce, often on very short notice; Lon Chlosta, Dan Deutscher, Tim Foy, George Low, Pete McWalters, John Roberts, and Ed Wheeler for the excellent quality beams they tuned out; and Ruth-Mary Larimer for her warm smile and delicious cookies.

Sue Clifton for staying up late, often until 4 a.m.

Dr. Jim Corbett for having a beer with me when it was most urgent.

Dr. Stephen Fine and Stephanie Crane for getting me started in my matchmaking career.

Caty Furco for rooting for the Mets with me in Candlestick Park.

Mark Hurwitz for solving my problem whenever he saw one.

Dr. David Levine for being our doctor in the family.

Jon Marr for being the best apartment-mate in Berkeley.

Micah Nussbaum for listening to me tell him how much I love (expletive deleted) computers.

David Ruiz for helping me start many a weekend off on the right foot with a GB and an LIIT.

Carol Adams, co-founder of the Rose Club, for her endless supply of support, good cheer, and all-around friendliness.

Ruth, Maxwell, and Ira Reiff, and Sandy and Alex Kahn for their undying moral support and their constant rooting for me to find "the lost proton".

And most of all, my wife Michelle, who, in addition to doing everything that was mentioned above (with the possible exceptions of tuning beams and machining parts), put up with my bizarre hours, antics, and fits, and, despite working her own full schedule and being pregnant, was always there for me. Thank you for everything. I love you.

Table of Contents

I. Introduction

The study of light nuclei near the proton drip line is an important branch of nuclear physics as it investigates some very interesting problems far from the valley of beta stability. Among these are the effects of charge symmetry and charge independence in barely bound and slightly unbound proton-rich nuclei. The concept of charge symmetry considers the interaction between two protons equivalent to the interaction between two neutrons after the effects of non-nuclear forces are taken into account. Charge independence regards the interaction between a proton and a neutron in the same relative states to be equivalent to that between two protons or two neutrons. Models based on these concepts have been developed to predict various properties of nuclei including nuclear masses, the limits of nuclear stability (i.e., the proton and neutron drip lines), the onset of different modes of radioactive decay, and energy levels of a number of analog states. Studies of light proton-rich nuclei have revealed new modes of radioactivity while providing spectroscopic data on nuclides with unusually high proton to neutron ratios. A general review of the properties and decay modes exhibited by such nuclei is given by Äystö and Cerny [Äy 89].

For light nuclei, as the proton drip line is approached, the rapid decrease of the nuclear binding energy permits the existence of several "exotic" decay modes in addition to the more common processes of beta decay and gamma emission. These include beta-delayed proton decay, beta-delayed two-proton decay, ground state proton emission, and ground state two-proton emission. All but the ground state emission of two protons have been observed experimentally.

Beta-delayed proton emission is a two-step process where a nucleus beta decays to a state in its daughter which is unbound to the prompt emission of a proton. The observed proton reflects the half-life of the initial beta decay. In 1963, ^{25}Si became the first nucleus identified as having a beta-delayed proton branch [Ba 63]. Since then, many beta-delayed proton emitters have been discovered; perhaps the best known are the nuclei in the $A = 4n + 1$, $T_z = -3/2$ mass series extending from ^{9}C through ^{61}Ge [Ce 77].

As in beta-delayed proton emission, beta-delayed two-proton decay is a two-step process where the beta daughter is left in an excited state which is unbound to the emission of two protons. This process, predicted by Gol'danskii [Go 80] in 1980 as a potential decay mode for some proton-rich nuclei, has recently been reviewed by Moltz and Cerny [Mo 89]. In 1983, proton-proton coincidence experiments detected the first cases of beta-delayed two-proton radioactivity in the decays of ^{22}Al [Ca 83] and ^{26}P [Ho 83]. Subsequently, systematic searches for other beta-delayed two-proton emitters in this light mass region have been conducted. The beta-delayed two-proton decay of the first $T_z = -5/2$

nucleus to be discovered, ^{35}Ca, will be described, followed by the observation of this decay branch in another $T_z = -5/2$ nuclide, ^{31}Ar. To date, these are the only four nuclides known to possess such a decay branch.

Ground state proton emission is a single step process where a nucleus with a negative proton separation energy ($S_p < 0$) emits a proton. The decay time for this process will be determined by the energy available for the decay, the associated Coulomb and angular momentum barriers, and the degree of overlap between the initial and final state wave functions. Although discussed in the early days of nuclear physics, this decay mode was not highlighted again until the mid-1960's [Ka 64, Go 66]. In 1970, a high spin isomer in ^{53}Co was shown to emit a proton directly [Ja 70, Ce 70]; however the emission of a proton from a ground state was not observed until 1982, when it was discovered in the decays of ^{151}Lu [Ho 82] and ^{147}Tm [Kl 82]. Until now only two other nuclides have been observed to decay via ground state proton emission: ^{113}Cs [Fa 84] and ^{109}Cs [Gi 87]. In order to see if proton radioactivity could be seen in a lighter mass region, the search for proton emission from the $T_z = -1/2$ nuclides ^{69}Br and ^{65}As was performed and will be described. These nuclides were thought to be good candidates from which to either observe such decays, or to set half-life (and thus separation energy) limits. Their respective separation energies, predicted to be 810 ± 300 keV and 570 ± 270 keV, correspond to half-lives ranging from 1 ps to 1 μs and 100 ps to 1 ms, respectively.

Although direct two-proton radioactivity has yet to be observed, it was predicted and its main features were discussed by Gol'danskii in 1960 [Go 60]. Due to the additional stability imparted to a nucleus by the pairing of its nucleons, nuclei exhibiting two-proton radioactivity will be bound with respect to the emission of a single proton but unbound with respect to the emission of the pair, i.e., $S_p > 0$ but $S_{2p} < 0$.

The theoretical considerations involved in the decay of nuclei far from stability are discussed in Chapter II. A description of the various experimental apparati used in studying the decays of ^{35}Ca, ^{31}Ar, ^{69}Br, and ^{65}As is given in Chapter III. Chapter IV contains the results and ramifications of these studies. A brief summary and conclusions derived from these experiments are presented in Chapter V.

II. Theory

Charged particle emission, whether from the ground state or an excited state, is a process which is governed by several physical parameters. Among them are the centrifugal barrier, the Coulomb barrier, and the wave functions of the initial and final states. However, the most important quantity which determines whether charged particle emission can occur is the mass difference between the initial nucleus and the sum of the masses of the final products. It is this mass difference which is used to determine possible decay modes for a given nuclide as well as the location of the proton drip line (i.e., the onset of ground state proton and two-proton decays). It is therefore important to know or be able to predict the masses of the proton-rich nuclides approaching the drip line.

A. Nuclear Masses and the Proton Drip Line

A portion of the chart of the nuclides ($0 \leq Z \leq 36$) is presented in Fig. II - 1 (a, b, c). For each element shown, the lightest isotope known or predicted to "exist" (defined as having a half-life greater than or equal to 10^{-12} sec) and the lightest isotope whose mass has been experimentally determined is denoted. In addition, the first proton-rich isotope of each element which has been shown to be or is predicted to be unbound with respect to proton or two-proton emission is indicated. When experimental data are not available, the predictions are based on the Kelson-Garvey mass relation and/or Coulomb displacement energies (see Sections II. A. 1. and II. A. 3.). The definition of "existence" is taken from Gol'danskii [Go 66] and is based on the fact that this time (10^{-12} sec) is considerably greater than the lifetime of a compound nucleus (10^{-19} sec). This delay in the direct emission of protons is due to the Coulomb and angular momentum barriers.

The decays of all the proton-rich nuclei, i.e., nuclei where $Z > N$, through the aluminum isotopes ($Z \leq 13$) which are bound with respect to proton and two-proton emission have been observed. Moreover, the masses of these nuclei up to $Z = 12$ as well as that of at least one unbound proton-rich isotope of each element from helium through sodium have been experimentally determined. A total of 34 nuclides with $Z \leq 12$ and $Z > N$ have known masses. In the region from aluminum through titanium ($13 \leq Z \leq 22$), the masses of proton-rich nuclei have been measured up to the proton drip line for all the elements except aluminum, silicon and sulfur. This represents an additional 37 proton-rich nuclides whose masses are known. For elements heavier than titanium ($Z > 22$), mass measurements have been made on only 23 nuclides with $Z > N$. Thus, a total of 94 proton-rich nuclides have known masses.

Most mass formulae currently in use are intended for making predictions over fairly large mass regions. These formulae arise out of models which fall into four general

categories: 1) semi-empirical or phenomenological models, 2) fundamental approaches which include simple shell model corrections, 3) models which use detailed shell corrections, and 4) models based on mass relations. A survey of 10 different mass models is given by Haustein [Ha 88].

For light nuclei, the mass relations given by Garvey and Kelson in 1966 [Ga 66, Ke 66] are still considered some of the best predictive methods. The Garvey-Kelson mass relation is used to predict masses for those nuclei where N > Z, while the Kelson-Garvey relation is used for predicting masses for those nuclei where Z > N.

1. The Kelson-Garvey Mass Relation

Due to the charge symmetric nature of nuclear forces, binding energies between mirror nuclei differ mostly by their Coulomb energies. Thus, if the mass of a proton-rich nuclide is not known but that of its neutron-rich mirror is, then the mass of the proton-rich nuclide can be predicted. A generalized formula for this mass difference is

$$M(A, T_z) - M(A, -T_z) = \sum_{i=1}^{2T_z} \left[M(A-2T_z-1+2i,\ 1/2) - M(A-2T_z-1+2i,\ -1/2) \right]$$

where T_z is defined by

$$T_z = \frac{N - Z}{2}$$

This relation can be used to predict the mass of a proton-rich nuclide with $T_z = -T$ from the known masses of the appropriate T = 1/2 mirror pairs as well as the $T_z = +T$ mirror nucleus. The T = 1/2 masses are known through the zinc isotopes. Fig. II - 2 shows a schematic representation of this charge-symmetric relation for a T = 5/2 nuclide. The boxes represent nuclei from the chart of the nuclides. A plus or minus sign in a box indicates that the mass value of the corresponding nucleus is to be added or subtracted. As seen in Fig. II - 3 [Ha 88], comparing the Kelson-Garvey mass estimates with 90 known mass values, the Kelson-Garvey mass relation gives good agreement with a standard deviation of approximately 230 keV [Jä 88].

2. Isospin and the Isobaric Multiplet Mass Equation

The concept of isospin is attributed to Heisenberg [He 32] who postulated the theory of charge symmetry. He proposed that the neutron and proton be considered two states of one particle, the nucleon. Breit and Feenberg [Br 36] then compared the scattering of protons by both neutrons and protons and inferred that the forces acting between two protons and a proton-neutron pair are nearly identical (theory of charge independence). Charge independence is observed to be true to within 2% [Wi 57].

If all nucleons are considered equivalent and charge independence is accepted to be entirely true, it follows that all systems of A nucleons in the same states of relative motion will have the same spectra and energy levels, as it is irrelevant whether the nucleon is a proton or a neutron. This is illustrated schematically in Fig. II - 4a [Wi 57] where the A = 6 nuclei all have the same spectra, that of ^{6}Li. This, however, cannot be true due to the Pauli exclusion principle; while all proton-neutron combinations are compatible with the exclusion principle, all the corresponding proton-proton or neutron-neutron combinations are not. This eliminates some of the low lying levels in nuclei where $Z \neq N$. As the difference between Z and N increases, so does the number of levels which are eliminated. This is shown in Fig. II - 4b [Wi 57] where ^{6}Li (Z = N) has the same spectrum as in the preceding figure, but some of the levels for ^{6}Be and ^{6}He ($|Z - N| = 2$) have been eliminated. All the levels within the energy range shown for ^{6}B and ^{6}H ($|Z - N| = 4$) have also been eliminated.

Although the nuclear interactions between the nucleons may be considered equivalent, the non-nuclear forces are not. The major non-nuclear interaction is the electrostatic or Coulomb force. This force only pertains to the proton-proton interaction, and has the effect of raising the energy of the states with the higher number of protons as compared with states with fewer protons and more neutrons. When this is taken into account, the degeneracy of the corresponding levels in the A = 6 isobars is broken, as depicted in Fig. II - 5.

The degenerate levels in Fig. II - 4b form isobaric multiplets and are assigned a quantum number T such that the number of degenerate levels in each multiplet is $2T + 1$. Each nucleus has an isospin projection, T_z, which was defined in section II. A. 1. It should be noted that the members of an isobaric multiplet (known as analog states), while not energetically degenerate, have identical spins, isospins, and parities, thereby aiding in identifying which levels belong to the multiplet. The masses of the analog states in an isobaric multiplet can be given by the quadratic expression [Wi 57]

$$M(A, T, T_z) = a(A,T) + b(A,T)\, T_z + c(A, T)\, T_z^2$$

This quadratic equation is known as the isobaric multiplet mass equation, or IMME. Deviations from the IMME are expressed by the additional terms dT_z^3 and eT_z^4. These can arise from higher order charge related effects as well as isospin mixing effects. The coefficients d and e can be derived from second order perturbation theory.

The mass of a proton-rich nuclide can be predicted from the mass of its neutron-rich mirror and the corresponding b coefficient by taking the difference between the respective IMME equations:

$$M_{-Tz} = M_{+Tz} - 2bT_z$$

The b coefficient can be determined in two different ways. The more reliable method is solving the simultaneous equations when the masses of three or more members of the multiplet are known. This permits a direct calculation of the three IMME coefficients with quite reliable results. However, due to limited experimental data on high isospin multiplets, this method of mass prediction is limited to $A \leq 40$ and $T_z \geq -2$. Above $A = 40$, the masses of only a few $T_z = -3/2$ nuclei can be predicted in this manner.

The second predictive method for obtaining proton-rich ground state masses using the b coefficient is given by Antony *et al.* [An 86]. Here, the b coefficient is calculated by the expression

$$b_{calc}\,(\text{keV}) = \Delta_{nH} - E_c^{(1)} = \Delta_{nH} - \frac{1440.8}{2} A^{2/3} + 1026.3 = -720.4\, A^{2/3} + 1808.6$$

where Δ_{nH} is the neutron-hydrogen mass difference (782.3 keV), and $E_c^{(1)}$ is the vector part of the nuclear Coulomb energy. (The term "vector" refers to the transformation properties of the operator that causes the Fermi part of beta decay; the Gamow-Teller part arises from an "axial-vector" type of interaction. See section II. B.) This expression for b_{calc}, which agrees well with the experimental b values for $A = 9 - 60$ [An 85, An 84], assumes that the value of b is constant for all multiplets of a given mass, thereby providing a simple way of predicting the masses of proton-rich nuclides up to mass 60.

3. Coulomb Displacement Energy Formulae

Antony *et al.* [An 86] also provide a formula for calculating the mass of an analog state in a nucleus of mass A, given that the ground state of the $T_z = T$ nucleus has a known mass and is a member of the isobaric multiplet. For nuclei in the range $9 \leq A \leq 60$, the expression for ΔE_c, the Coulomb displacement energy, is

$$\Delta E_C \text{ (keV)} = 1440.8 \left(\frac{Z_{av}}{A^{1/3}} \right) - 1026.3$$

where Z_{av} is the average atomic number between the pair, and the constants are determined from a fit to experimental data [An 85]. The mass of each successive member of the isobaric multiplet can be obtained from the equation [Co 75]

$$\Delta E_C = M_{Z>} - M_{Z<} + \Delta_{nH}$$

where $M_{Z>}$ is the mass of the isobaric analog state in the higher Z nucleus and $M_{Z<}$ is that of the lower Z nucleus. Thus,

$$M_{Z>} \text{ (keV)} = 1440.8 \left(\frac{Z_{av}}{A^{1/3}} \right) - 1808.6 + M_{Z<}$$

For $44 \leq A \leq 239$, the Coulomb displacement energy data suggest

$$\Delta E_C \text{ (keV)} = 1412 \left(\frac{Z_{av}}{A^{1/3}} \right) - 861$$

so that

$$M_{Z>} \text{ (keV)} = 1412 \left(\frac{Z_{av}}{A^{1/3}} \right) - 1643 + M_{Z<}$$

The difference between the ground state mass and an isobaric analog state mass gives the excitation energy of the analog state. By using either the Kelson-Garvey mass relation or the IMME in conjunction with the appropriate Coulomb displacement energy formula, it is possible to predict the center-of-mass decay energy of the protons resulting from beta-delayed proton or beta-delayed two-proton emission, assuming a superallowed beta decay to the isobaric analog state (see below).

B. Beta Decay

By a standard application of time dependent perturbation theory [Ma 69], the probability of emitting a beta particle with energy E and momentum p is given by

$$P(E)\,dE = \frac{g^2}{2\pi^3\,\hbar^7\,c^3}\;|M_\beta|^2\;F(Z,E)\,(E_0 - E)^2\,p^2\,dp$$

where

g = beta decay strength constant

M_β = matrix element connecting the initial and final nuclear states

F(Z,E) = Fermi function which takes into account the distortion of the beta particles' wave function from that of a free particle (a plane wave) due to the Coulomb interaction with the nucleus

Z = atomic number of the beta daughter

E_o = maximum beta energy

The derivation of this formula may be found in Appendix 1. The beta decay transition rate, λ, is obtained by integrating this probability over all possible momenta:

$$\lambda = \frac{g^2}{2\pi^3\,\hbar^7\,c^3}\;|M_\beta|^2 \int_0^{p_{max}} F(Z,E)\,(E_o - E)^2\,p^2\,dp$$

The integral in the above equation is known as the statistical rate function, f, and contains all factors not dependent upon the details of nuclear structure. This function has great control over the absolute magnitude of the decay constant λ. By rewriting this relationship in terms of the partial half-life for a specific transition ($t = \ln 2/\lambda$), one obtains the expression for the comparative half-life of the transition:

$$ft = \frac{2\pi^3\,\hbar^7\,c^3\,\ln 2}{g^2\;|M_\beta|^2} = \frac{1.230618 \times 10^{-94}}{g^2\;|M_\beta|^2}\ \text{erg}^2\,\text{cm}^6\,\text{s}$$

Comparative half-lives (often quoted as $\log_{10}$ft) tend to fall into groups which enable beta decay transitions to be classified in terms of allowed, superallowed, or forbidden.

An allowed transition is defined as one in which the beta particle and the neutrino (or anti-neutrino) carry away no orbital angular momentum; the only change in the angular momentum of the nucleus must result from the spins of the emitted leptons, each of which has a value of s = 1/2. If the leptons are emitted with their spins anti-parallel (total S = 0), then there can be no change in the nuclear spin: $\Delta J = |J_i - J_f| = 0$. This type of transition is known as Fermi decay. If, on the other hand, the leptons are emitted with their spins

parallel (S = 1), they carry a total angular momentum of 1$\hbar$, and J_i and J_f must be coupled through a vector length of 1: $\Delta J = |J_i - J_f| = 0, 1$. This is known as Gamow-Teller decay. In both cases of allowed beta decay, the parity of the initial and final states is the same since parity is associated with the orbital angular momentum: $\pi = (-1)^l$. Allowed transitions have very similar log ft values, generally ranging from 2.5 to 6.0, the bulk of which fall between 4 and 6.

A subset of allowed transitions is superallowed transitions. Superallowed transitions are decays between initial and final states that have maximal overlap between their wave functions. This type of transition is mostly found among beta emitters of low Z, particularly between mirror nuclei, as well as between isobaric analog states. Given that the theory of charge symmetry holds, the wave functions characterizing two mirror nuclei as well as those characterizing isobaric analog states are expected to be very nearly the same. Nuclei undergoing a superallowed beta transition have the lowest log ft values, generally falling between 2.7 and 3.2.

When the emitted leptons carry away units of orbital angular momentum the decays are more hindered than allowed decays and are called forbidden transitions. The most frequent type of forbidden transition occurs between states of opposite parities. In order to accomplish this, the leptons must carry away an odd number of units of orbital angular momentum relative to the parent. For each unit of angular momentum carried away, the order of forbiddenness increases by one and the beta transition probability decreases by several orders of magnitude. The log ft ranges for first, second, and third forbidden transitions are 6 - 12, 11 - 18, and 17 - 20. Again, there is a mixture of Fermi and Gamow-Teller type transitions for each case, depending on whether the leptons are emitted with their spins parallel or anti-parallel. These selection rules are summarized in Table II - 1 [Fr 81].

Selection Rules for Beta Decay Transitions

Transition Type	ΔJ	Change in Parity	log ft
Superallowed (Fermi)	0	No	2.7 - 3.2
Allowed (Gamow-Teller)	0, ±1 (not 0 →0)	No	4 - 7
First Forbidden	0, ±1, ±2	Yes	6 - 15
Second Forbidden	±2, ±3 (0 →0)	No	11 - 18
Third Forbidden	±3, ±4	Yes	17 - 19

Table II - 1

For light proton-rich nuclei far from stability, beta decay generally consists of a superallowed Fermi component plus a Gamow-Teller component when allowed by the selection rules. Such a decay leaves the daughter either in the isobaric analog state, in one of several states clustered around the analog state, or in a low-lying level. The role of forbidden transitions is generally not important for these nuclei.

The expression for the comparative half-life can now be rewritten with the beta decay matrix element and the accompanying interaction strength constant in terms of a Fermi decay matrix element and a Gamow-Teller decay matrix element:

$$ft = \frac{K}{G_V^2 \langle 1 \rangle^2 + G_A^2 \langle \sigma\tau \rangle^2}$$

where

$K = 1.230618 \times 10^{-94}$ erg^2 cm^6 s
G_V = weak interaction vector coupling constant
$\langle 1 \rangle$ = Fermi decay matrix element
G_A = axial vector coupling constant
$\langle \sigma\tau \rangle$ = Gamow-Teller decay matrix element

The above expression for the comparative half-life is simplified and several corrections are needed [Ra 75]. Electromagnetic radiative corrections which arise from the exchange of virtual photons between the charged particles involved in the beta decay are not included in the statistical rate function. These corrections are divided into two parts: the model dependent, or inner part, and the model independent, or outer part.

The inner correction is applied to the vector, or Fermi, coupling constant such that

$$G_V'^2 = G_V^2 (1 + \Delta_R)$$

This yields an "effective" coupling constant G_V'. Δ_R is independent of the momentum transfer but does depend on the details of the weak and strong theory. For this reason, no unambiguous value for this correction has been obtained.

The outer correction, which has no dependence on the models of the strong or weak interactions but does depend on the momentum transfer, is applied to the statistical rate function such that

$$f \rightarrow f(1 + \delta_R)$$

where $\delta_R = \delta_1 + \delta_2 + \delta_3$. The δ_i are corrections in the i^{th} order of the fine structure constant α. δ_1 is tabulated in [Wi 70] and is less than 2% for most light nuclei. Expressions for δ_2 [Ja 70a] and δ_3 [Ja 72] are

$$\delta_2 \sim 4.0 \times 10^{-4} Z$$
$$\delta_3 \sim 3.6 \times 10^{-6} Z^2$$

Radiative corrections also enter into the calculation of the statistical rate function as do other modifications to account for such effects as screening and the finite nuclear mass and size. These effects, which differ slightly for Fermi transitions and Gamow-Teller transitions [Wi 74], are denoted by f_V and f_A, respectively.

The Fermi matrix element, <1>, also requires some modification. Pure Fermi decay requires that $\Delta J = 0$, $\Delta\pi$ = no, and $\Delta T = 0$; the initial and final state wave functions are considered to be identical. However, the number of protons in the parent differs from that in the daughter by one, so that these states will have slightly different wave functions. Because the nuclear Hamiltonian is charge dependent, the assumption that the states are isospin pure is no longer valid. The result is the introduction of isospin impurities and a decrease in the Fermi matrix element by a factor of $1 - \delta_C$ [Ra 75]. While all calculated values of δ_C are model dependent, they agree that δ_C is positive and less than 1.5%.

Inclusion of these correction factors produces the new expression

$$(1 + \delta_R)t = \frac{K}{f_V G_V'^2 \langle 1 \rangle^2 (1 - \delta_C) + f_A G_A^2 \langle \sigma\tau \rangle^2}$$

The values for the coupling constants G_V' and G_A have been determined experimentally.

The value of G_V', obtained from the superallowed $0^+ \rightarrow 0^+$ (pure Fermi) transitions, is

$(1.41561 \pm .00044) \times 10^{-49}$ erg cm^3 [Si 87]. The ratio of the coupling constants G_A/G_V', is $1.262 \pm .005$ [Bo 86]. Substituting these values into the above equation yields

$$(1 + \delta_R)\, t = \frac{6170 \pm 4}{f_V \langle 1 \rangle^2 (1 - \delta_C) + 1.4546\, f_A \langle \sigma\tau \rangle^2} \text{ sec}$$

The Fermi transition probability $\langle 1 \rangle^2$ can be written as

$$\langle 1 \rangle^2 = T(T + 1) - T_{zi} T_{zf}$$

where T is the isospin of the initial and final states and T_{zi} and T_{zf} are their corresponding z-projections. For transitions between T = 1/2 mirror nuclei, $\langle 1 \rangle^2 = 1$; however, for transitions in nuclei with the highest isospin transition yet observed, T = 5/2, $\langle 1 \rangle^2 = 5$.

The Gamow-Teller matrix element $\langle \sigma\tau \rangle$, which can be written as

$$\langle \sigma\tau \rangle = \left\langle f \left| \sum_k^A \sigma(k)\, \tau(k) \right| i \right\rangle$$

is composed of a sum over all the nucleons in the nucleus. Its magnitude is much more difficult to determine as it depends on the details of the nuclear wave functions involved. Probabilities for specific Gamow-Teller transitions have been calculated using large basis shell model calculations [Wi 84, Br 85].

C. Proton Emission

Proton emission, whether from an excited state as in beta-delayed proton decay, or the ground state, depends on the proton penetrability through the Coulomb and angular momentum barriers as well as the degree of overlap between the initial and final state wave functions. The relationship between these factors can be written as

$$\Gamma = 2P_l \gamma^2$$

where

Γ = proton decay width
P = proton penetrability
l = angular momentum of the emitted proton
γ^2 = proton reduced width

The penetrability factor can be calculated using the regular and irregular Coulomb wave functions, F_l and G_l, which are obtained from the solution of the radial Schrödinger equation using a Coulomb potential. The penetrability is then given by

$$P_l = \frac{kR_o}{F_l^2 + G_l^2}$$

where k is the wave number of the proton calculated by

$$k = \frac{(2\mu E)^{1/2}}{\hbar} = .2187(\mu E)^{1/2} \ \text{fm}^{-1}$$

in which μ is the reduced mass of the system in amu and E is the center-of-mass energy of the proton in MeV and R_o is the nuclear radius at which the Coulomb wave functions are evaluated, given by

$$R_o = r_o(A_1^{1/3} + A_2^{1/3})$$

where A_1 is the mass number of the proton decay daughter and A_2 is that of the proton, i.e. 1. Penetrability values have been calculated by the program COCAGD [Se 73].

The reduced width is more difficult to calculate as it depends on wave function information. It is given by

$$\gamma^2 = \frac{\hbar^2}{2\mu} S_{lj} \ |R_{nlj}(R_0)|^2 \ R_0$$

where S_{lj} is a spectroscopic factor equal to

$$S_{lj} = \frac{2j + 2 - n}{2j + 1}$$

and $R_{nlj}(R_o)$ is the radial wave function evaluated at the nuclear surface. The radial wave function at the nuclear surface can be approximated [Bo 69] by

$$R_{nlj}(R_o) \approx \sqrt{\frac{1.4}{R_o^3}}$$

because at the nuclear surface, the radial wave function is approximately independent of n, l, and j. The Wigner Sum Rule puts an upper limit given on the reduced width:

$$\gamma^2 \leq \frac{3\hbar^2}{2\mu R_o^2} = \frac{62.7}{\mu R_o^2} \text{ MeV}$$

Using this result, an upper limit for the proton decay width and the lower limit for the proton partial half-life may be deduced:

$$\Gamma \leq 125.4 \frac{P_l}{\mu R_o^2} \text{ MeV}$$

and

$$t_{1/2} = \tau \ln 2 = \frac{\hbar}{\Gamma} \ln 2 \geq \frac{\hbar \ln 2 \, \mu R_o^2}{125.4 \, P_l} \text{ sec}$$

Based on these relations and their proton separation energies, the proton partial half-life has been calculated for the first proton unbound isotope from lithium through krypton that does not have a heavier isotope predicted to be unbound with respect to two-proton emission. The results are presented in Table II -2. It should be noted that although ^{26}P has a negative proton separation energy, its proton partial half-life is expected to be 4 x 10^9 sec. Discovered in 1983 via its beta-delayed proton decay branch [Ca 83a], it was determined to have a half-life of 20^{+25}_{-15} ms. Based on the proton partial half-life, ^{26}P should have a direct proton decay branch of 4 x 10^{-10}%.

Ground state proton decay was first observed in 1982 from the decays of ^{151}Lu ($t_{1/2}$ = 85 ± 10 ms) [Ho 82] and ^{147}Tm ($t_{1/2}$ = 560 ± 40 ms) [Kl 82]. Despite intensive searches in various mass regions [Fa 88], the only other nuclides positively identified as ground state proton emitters are ^{109}I ($t_{1/2}$ = 33 ± 7 μs) and ^{113}Cs ($t_{1/2}$ = 109 ± 17 μs) [Fa 84, Gi 87].

For the ground state proton emitters near A = 150, the ratio of the experimentally observed proton partial half-lives to the values predicted by the WKB approximation (see, for example, [Li 80]) is quite good: 1.3 for ^{151}Lu and 0.9 for ^{147}Tm [Gi 87]. In sharp contrast, however, the corresponding ratios for the two nuclei near A = 110 are 47 for ^{113}Cs and 8.4 for ^{109}I [Gi 87]. Because the penetrability of a proton through the Coulomb

Predicted Ground State Proton Emitters and Their Half-Lives

Nucleus	l	S_p (MeV) [a]	Half-Life (sec)
^{5}Li	1	-1.970 ± 0.050 [b]	2×10^{-22}
^{7}B [c]	1	-2.210 ± 0.070 [b]	4×10^{-22}
^{11}N	0	-1.920 ± 0.150 [b]	2×10^{-22}
^{16}F	0	-0.540 ± 0.010 [b]	2×10^{-18}
^{19}Na	2	-0.320 ± 0.010 [b]	6×10^{-16}
^{21}Al	2	-1.090 ± 0.030	6×10^{-19}
^{21}Si [c]	2	-1.470 ± 0.670	3×10^{-19}
^{26}P [d]	2	-0.070 ± 0.020	4×10^{9}
^{26}S [c]	0	-0.610 ± 0.080	4×10^{-18}
^{30}Cl	2	-0.720 ± 0.060	1×10^{-9}
^{34}K	2	-0.630 ± 0.030	1×10^{-15}
^{39}Sc	3	-0.630 ± 0.040 [e]	4×10^{-13}
^{42}V	1	-0.400 ± 0.020	7×10^{-10}
^{45}Mn	3	-1.010 ± 0.050	9×10^{-15}
^{49}Co	3	-0.910 ± 0.120	2×10^{-13}
^{55}Cu	1	-0.170 ± 0.070	3×10^{1}
^{54}Zn [c]	1	-0.160 ± 0.100	2×10^{3}
^{60}Ga	1	-0.020 ± 0.070	1×10^{31}
^{65}As	3	-0.530 ± 0.270	7×10^{-8}
^{69}Br	3	-0.810 ± 0.300	2×10^{-10}

[a] Predictions made by using the Kelson-Garvey mass relation and/or the formulae from Antony *et al.* Error bars arise solely from the errors on the input masses. See text.

[b] These values have been determined experimentally [Wa 83].

[c] These nuclei are also predicted to be unbound with respect to ground state two-proton emission.

[d] This nuclide has been observed to possess beta-delayed proton and beta-delayed two-proton decay branches [Ca 83a, Ca 83].

[e] This value has been determined experimentally [Mo 88].

Table II - 2

and angular momentum barriers is well understood, these discrepancies must arise from a reduction in the proton reduced width with respect to the theoretical calculations. The differences are most likely due to a change in the nuclear configuration between the parent and the daughter which is not taken into account in the calculations.

As can be seen in Table II - 2, ^{69}Br and ^{65}As are predicted to be the lightest T_z = -1/2 nuclides that are proton unbound; the proton separation energy (S_p) of ^{69}Br is predicted to be -810 ± 300 keV and that of ^{65}As is predicted to be -530 ± 270 keV. Plots of the emitted proton energy versus the predicted proton partial half-life for both l = 1 and l = 3 protons from ^{69}Br and ^{65}As are shown in Fig. II - 6. Based on their separation energies, the half-life of ^{69}Br should fall between 1 ps and 1 μs and the half-life of ^{65}As should be in the range of 100 ps to 1 ms. However, it has been found that the mass predictions often underestimate the binding energy of a nucleus, sometimes by up to 200 keV. Thus, if the proton separation energy of ^{69}Br is as small as -610 ± 300 keV, or if its reduced width for proton emission is smaller than what is predicted, the proton partial half-life can, in principle, range from 10 ps to 1 sec, and if the proton separation energy of ^{65}As is as small as -370 ± 200 keV, or it has a smaller than predicted reduced width for proton decay, its proton partial half-life can range from 100 ns to 2.8 h. Beta decay could then be a competitive decay mode in these decays at the upper end of this range. These values assume that the emitted protons have an angular momentum of l = 3; this expectation is based on the proposed spin and parity of 5/2$^-$ for the parents.

By searching for ground state proton emission in the A = 70 region, it is hoped to determine whether or not the discrepancy between the observed reduced width and the theoretical calculations continues in this lighter mass region on the proton drip line.

D. Two-Proton Emission

Two-proton radioactivity, the emission of a pair of protons from the ground state, is a decay mode which, while predicted in the early sixties [Go 60, Go 61], has yet to be observed. A ground state two-proton emitter is defined as one for which the direct single-proton decay channel is energetically closed but, because of the added stability from nucleon pairing, the direct two-proton decay channel remains open. As with ground state proton emission, direct two-proton radioactivity is expected to occur at the proton drip line. Several light nuclei, including ^{6}Be, ^{8}C, ^{12}O, and ^{16}Ne, are known not to exist due to their instability with respect to two-proton decay (their respective two-proton separation energies, S_{2p}, are -1.371 MeV, -2.143 MeV, -1.780 MeV, and -1.404 MeV). The half-lives of such nuclei are on the order of 10^{-22} seconds.

In ^{2}He emission, the protons will leave the nucleus coupled to a $^1S_0$ configuration. The virtual state, ^{2}He, has been studied in reaction work [Co 80, St 79] and can be thought of as a proton pair penetrating the Coulomb and angular momentum barriers of the nucleus with a virtual energy, ε, shared between the protons. This center-of-mass energy of the proton pair then "returns" at some distance from the nucleus as the kinetic energy of the protons which are now correlated at small angles. For simplicity, it is assumed that this break-up occurs well outside the Coulomb and angular momentum barriers.

This decay mode requires that the protons are emitted at 180° to each other in their center-of-mass reference frame. Momentum and energy conservation give the following expression for the summed laboratory energy of the two protons:

$$E_{LAB} = \frac{mE_{cm} + 2m_p\varepsilon + \varepsilon^2}{m + 2m_p + \varepsilon}$$

where

m = mass of the two-proton daughter
E_{cm} = center-of-mass decay energy for the two protons
m_p = mass of the proton
ε = relative energy of the two protons (the break-up energy)

The quantity ε is determined by the nucleon-nucleon interaction of the proton pair (the final state interaction) and is expected from the aforementioned reaction studies to appear as a distribution with a maximum value of ~500 keV and a full width at half the maximum of ~600 keV.

Given a value for ε, the kinematic expression for the laboratory energies and angles of the protons can be derived [Sy 71, Oh 65]. The resulting expression is

$$\cos\eta = \frac{E_1^L + E_2^L - 2\varepsilon}{2\sqrt{E_1^L E_2^L}}$$

In this equation

η = laboratory angle between the emitted protons

E_1^L = laboratory energy of one proton

E_2^L = laboratory energy of the other proton

η is maximized when the laboratory energies of the two protons are equal. As this is also expected to be its most probable value, the individual proton energy spectrum resulting from ^{2}He emission should be a distribution symmetric about this energy with its shape determined by the distribution in ε and by the variation of the detector efficiency as a function of η.

Gol'danskii [Go 60, Go 61] showed two ways to calculate the probability for the simultaneous emission of two protons. Either the penetrability for a doubly charged particle (^{2}He) with an energy E_0 through the corresponding Coulomb barrier may be calculated, or alternatively, the penetration factors for two single protons of energy E and E_0 - E may be multiplied. Again, the latter product is maximized when $E = E_0/2$. Furthermore, Gol'danskii showed that both methods led to the same result with the caveat that the protons come from an s shell, i.e., $l = 0$; otherwise, the centrifugal barrier for the protons comes into effect and suppresses the uncorrelated emission of the two protons. Table II - 3 gives the two-proton separation energies (S_{2p}) for the heaviest proton-rich nuclei of $3 \leq Z \leq 36$ which are expected to be unstable with respect to two-proton emission and do not have a heavier isotope predicted to be unbound with respect to single proton emission. In addition, the table lists the shell from which the two protons are emitted, the predicted half-life for the emission of a diproton (^{2}He) with a final state interaction of $\varepsilon = 0$, the predicted half-life for diproton emission with a final state interaction of $\varepsilon = .500$ MeV, and the half-life for the emission of an uncorrelated pair of protons which share the decay energy equally ($Ep_1 = Ep_2$) and have angular momenta of $l = 0$ and $l = l_{sm}$ where l_{sm} is the angular momentum of the shell from which the protons are emitted.

Beta-delayed two-proton radioactivity is quite similar to ground state two-proton decay, but does have some notable differences. First, beta-delayed two-proton emitters are not energetically restricted from emitting a single proton after the beta decay. As a result, the sequential emission of two protons must be considered as well as the simultaneous emission. Second, beta-delayed two-proton radioactivity normally involves the emission of higher energy protons than ground state two-proton decay and is therefore easier to observe.

Predicted Ground State Two-Proton Emitters and Their Two-Proton Half-Lives

Nucleus	S_{2p} (MeV) [a]	2p Shell	$\varepsilon = 0$ ^{2}He $T_{1/2}$ (sec)	$\varepsilon = .5$ ^{2}He $T_{1/2}$ (sec)	2p $T_{1/2}$ (sec)
^{6}Be	-1.370 ± 0.010 [b]	$1p_{3/2}$	2×10^{-22}	3×10^{-22}	8×10^{-21}
^{7}B [c]	-1.610 ± 0.090 [b]	$1p_{3/2}$	2×10^{-22}	3×10^{-22}	1×10^{-20}
^{8}C	-2.140 ± 0.030 [b]	$1p_{3/2}$	2×10^{-22}	3×10^{-22}	7×10^{-21}
^{12}O	-1.780 ± 0.040 [b]	$1p_{1/2}$	1×10^{-21}	5×10^{-21}	7×10^{-20}
^{16}Ne	-1.400 ± 0.020 [b]	$1d_{5/2}$	3×10^{-20}	1×10^{-18}	7×10^{-17}
^{19}Mg	-1.170 ± 0.060	$1d_{5/2}$	3×10^{-18}	4×10^{-15}	9×10^{-15}
^{21}Si [c]	-4.690 ± 0.600	$1d_{5/2}$	5×10^{-22}	9×10^{-22}	3×10^{-20}
^{26}S [c]	-2.140 ± 0.070	$2s_{1/2}$	7×10^{-19}	2×10^{-17}	9×10^{-18}
^{31}Ar [d]	-0.230 ± 0.180	$1d_{3/2}$	1×10^{8}	∞	3×10^{13}
^{34}Ca	-2.210 ± 0.050	$1d_{3/2}$	4×10^{-17}	2×10^{-15}	1×10^{-14}
^{39}Ti	-0.790 ± 0.020	$1f_{7/2}$	6×10^{-6}	3×10^{13}	4×10^{-1}
^{42}Cr	-0.690 ± 0.050	$1f_{7/2}$	7×10^{-2}	1×10^{26}	5×10^{3}
^{45}Fe	-1.140 ± 0.050	$1f_{7/2}$	7×10^{-7}	3×10^{2}	1×10^{-2}
^{49}Ni	-0.190 ± 0.060	$1f_{7/2}$	3×10^{36}	∞	3×10^{43}
^{54}Zn [c]	-1.690 ± 0.100	$2p_{3/2}$	7×10^{-9}	4×10^{-4}	3×10^{-7}
^{59}Ge	-1.250 ± 0.200	$2p_{3/2}$	3×10^{-3}	4×10^{6}	2×10^{-1}
^{64}Se	-0.360 ± 0.290	$1f_{5/2}$	2×10^{28}	∞	7×10^{33}
^{68}Kr	-0.760 ± 0.560	$1f_{5/2}$	7×10^{10}	$>10^{22}$	2×10^{15}

[a] Predictions made by using the Kelson-Garvey mass relation and/or the formulae from Antony *et al.* Error bars arise solely from the errors on the input masses. See text. [b] These values have been determined experimentally [Wa 83]. [c] These nuclei are also predicted to be unbound with respect to ground state proton emission. [d] This nuclide has been observed to possess beta-delayed proton and beta-delayed two-proton decay branches [Bo 87, Re 89].

Table II - 3

In principle, the emission of two protons following beta decay can result from several mechanisms. These include ^{2}He (diproton) emission, sequential emission, and uncoupled simultaneous emission. ^{2}He emission has already been discussed. Uncoupled emission may be thought of as two protons leaving the nucleus with a time, Δt, between the first and second proton. If Δt is long enough for the formation of an intermediate state, this will be referred to as sequential emission. The alternative case ($\Delta t \leq 10^{-21}$ s) will be referred to as pre-equilibrium emission.

Sequential emission is a two-step process; two protons are emitted, each with a discrete energy dependent upon the intermediate state formed. The expressions for the laboratory energies of two protons emitted sequentially are [Ca 84]

$$E_1^L = \left(\frac{m_1}{m_2}\right) E_1$$

and

$$E_2^L = \frac{m}{m_1}\left(E_{cm} - E_1\right) + \frac{E_1 \left(m_p\right)^2}{m_1\ m_2} - \frac{2m_p \cos\theta}{m_1} \sqrt{\frac{mE_1\left(E_{cm} - E_1\right)}{m_2}}$$

where

E_1^L = laboratory energy of the first proton

m_1 = mass of the intermediate state between proton emissions

m_2 = mass of the state of the beta daughter emitting the protons (usually the isobaric analog state)

E_1 = center-of-mass energy of the first proton

E_2^L = laboratory energy of the second proton

m = mass of the two-proton daughter

E_{cm} = center-of-mass sum energy of the two protons

m_p = mass of the proton

θ = center-of-mass angle between the protons

Although the first proton in the sequential emission has the usual center-of-mass to laboratory energy conversion as calculated for single proton emission, the laboratory energy of the second proton is dependent upon the relative angle of emission between the protons. This angle needs to be considered because the second proton is being emitted from an already recoiling nucleus. The center-of-mass angle may be calculated from the laboratory angle via the equation

$$\cos\theta = \cos\eta\,(1 - k^2 \sin^2\eta)^{1/2} - k \sin^2\eta$$

where k is defined as

$$k = \frac{m_p}{\sqrt{m\ m_2}}$$

To fully describe the third possible mechanism, pre-equilibrium emission, a knowledge of the evolution of the nucleus following the emission of the first proton is required. Such a treatment is quite difficult and only the qualitative features of the relatively simple, limiting case of $\Delta t = 0$ will be discussed. If spin dependent angular correlations are negligibly small as in sequential emission, and if barriers are ignored, then phase space limitations will determine the proton energy spectrum. Individual proton spectra for this limiting case are similar to that for ^{2}He emission and will consist of a continuum of proton energies with equal proton energies being the most probable. However, unlike ^{2}He emission, these protons are not restricted to small angles and there is an angular dependence on their laboratory energies similar to that for sequential emission.

Figure Captions

Figure II - 1a: A portion of the chart of the nuclides from $0 \leq Z \leq 14$ showing nuclei from the proton drip line to the valley of stability. For each element, this chart shows stable isotopes, the lightest isotope which "exists" (see text), the lightest isotope whose mass has been determined, and which nuclei at the proton drip line are predicted to be unbound with respect to proton and two-proton emission.

Figure II - 1b: Continuation of Figure II - 1a from $15 \leq Z \leq 23$.

Figure II - 1c: Continuation of Figure II - 1b from $24 \leq Z \leq 36$.

Figure II - 2: A schematic representation of the charge symmetric Kelson-Garvey mass relation for a $T_z = -5/2$ nucleus.

Figure II - 3: Delta values (calculated mass values - experimental mass values) for known nuclides using the Kelson-Garvey mass relation [Ha 88].

Figure II - 4a: A level scheme of ^{6}B, ^{6}Be, ^{6}Li, ^{6}He, and ^{6}H as they might be if the Pauli exclusion principle and electrostatic forces were not taken into account.

Figure II - 4b: The effect of the Pauli exclusion principle: some of the lowest levels of ^{6}He and ^{6}Be, and all the low-lying levels of ^{6}H and ^{6}B are eliminated.

Figure II - 5: The resulting level scheme of the $A = 6$ isobars when electrostatic forces are taken into account. Isotopic spin multiplets are indicated.

Figure II - 6: Plots of the proton partial half-life versus the proton energy for ^{69}Br and ^{65}As.

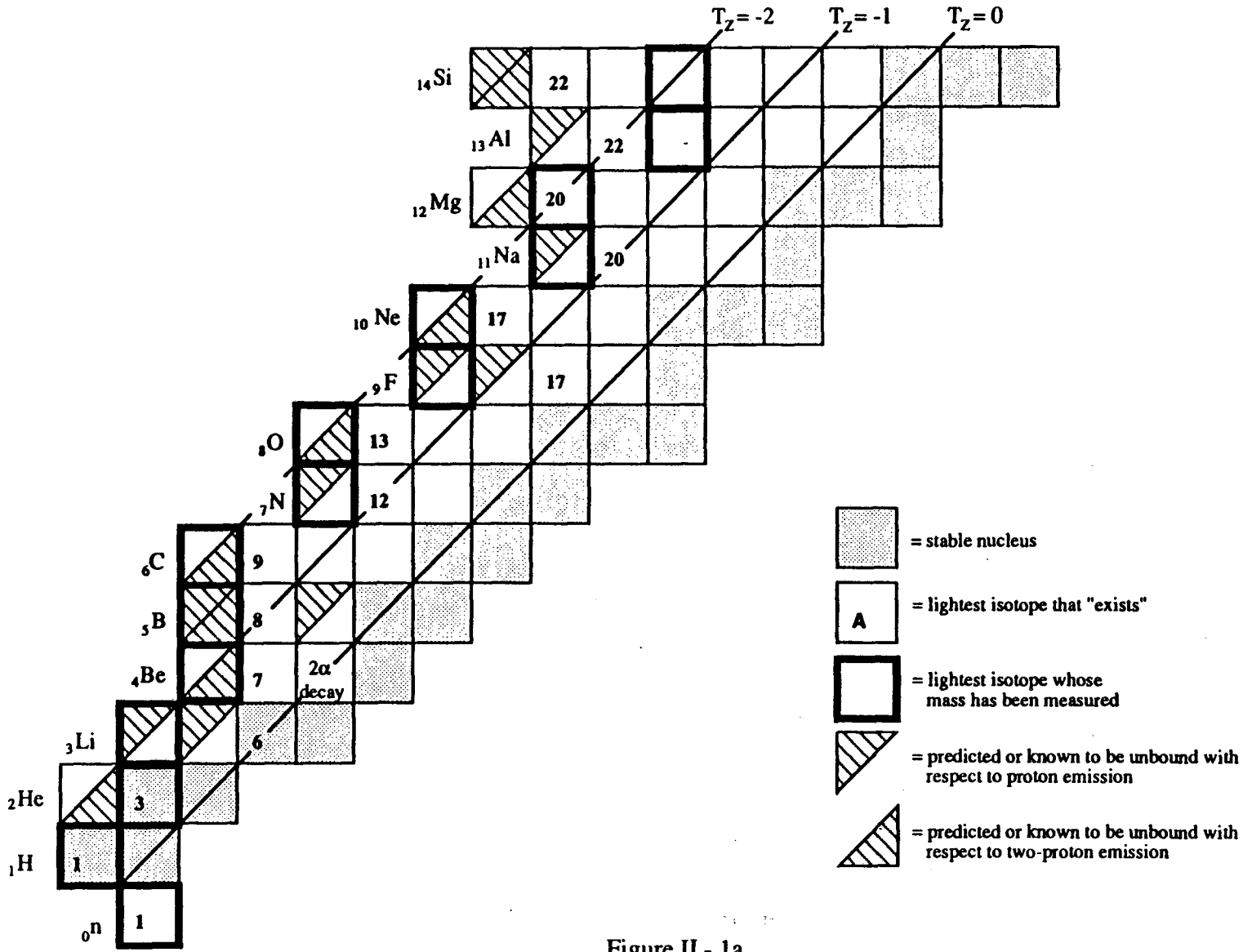
$T_z = -2$
$T_z = -1$
$T_z = 0$
$_{14}Si$
$_{13}Al$
$_{12}Mg$
$_{11}Na$
$_{10}Ne$
$_{9}F$
$_{8}O$
$_{7}N$
$_{6}C$
$_{5}B$
$_{4}Be$
$_{3}Li$
$_{2}He$
$_{1}H$
$_{0}n$
22
22
20
20
17
17
13
12
9
8
7
6
3
1
1
2α decay
= stable nucleus
A
= lightest isotope that "exists"
= lightest isotope whose mass has been measured
= predicted or known to be unbound with respect to proton emission
= predicted or known to be unbound with respect to two-proton emission

Figure II - 1a

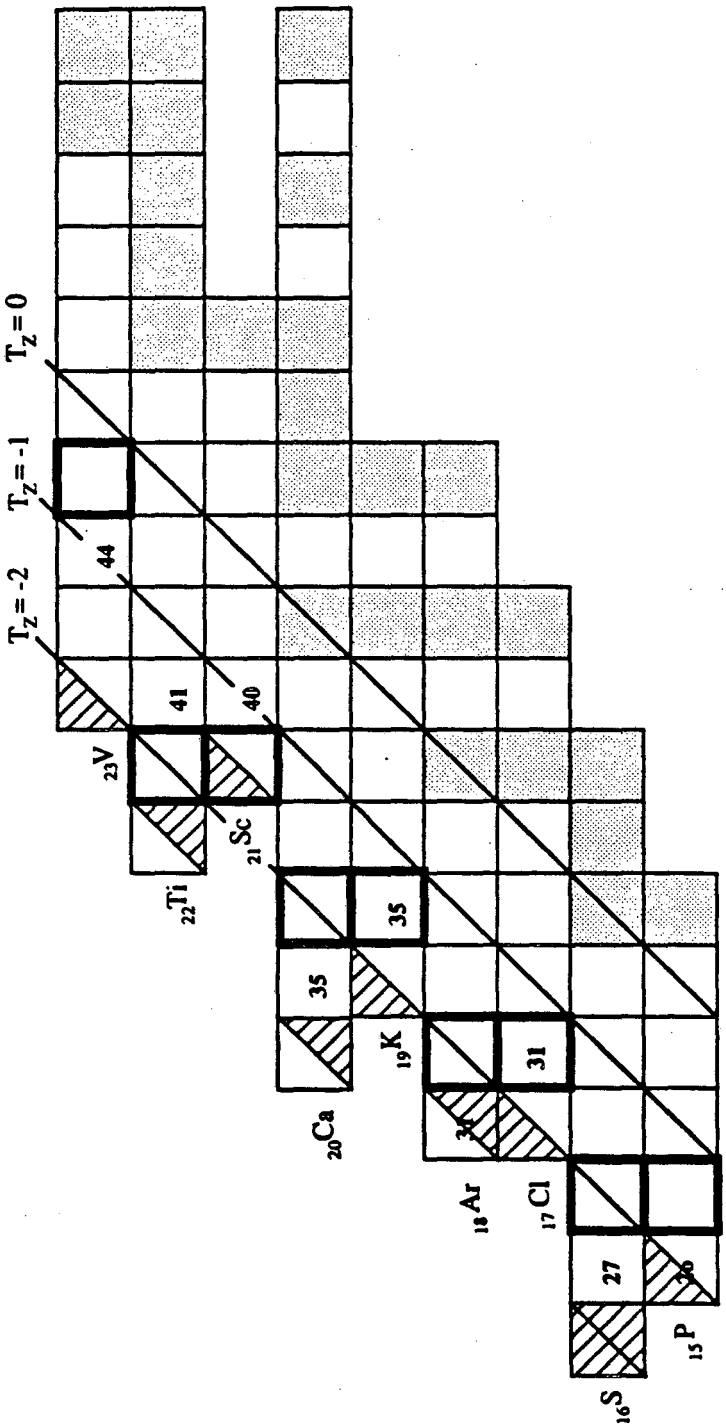
$T_z = 0$
$T_z = -1$
$T_z = -2$
44
41
40
35
35
31
27
$_{23}V$
$_{22}Ti$
$_{21}Sc$
$_{20}Ca$
$_{19}K$
$_{18}Ar$
$_{17}Cl$
$_{16}S$
$_{15}P$

Figure II - 1b

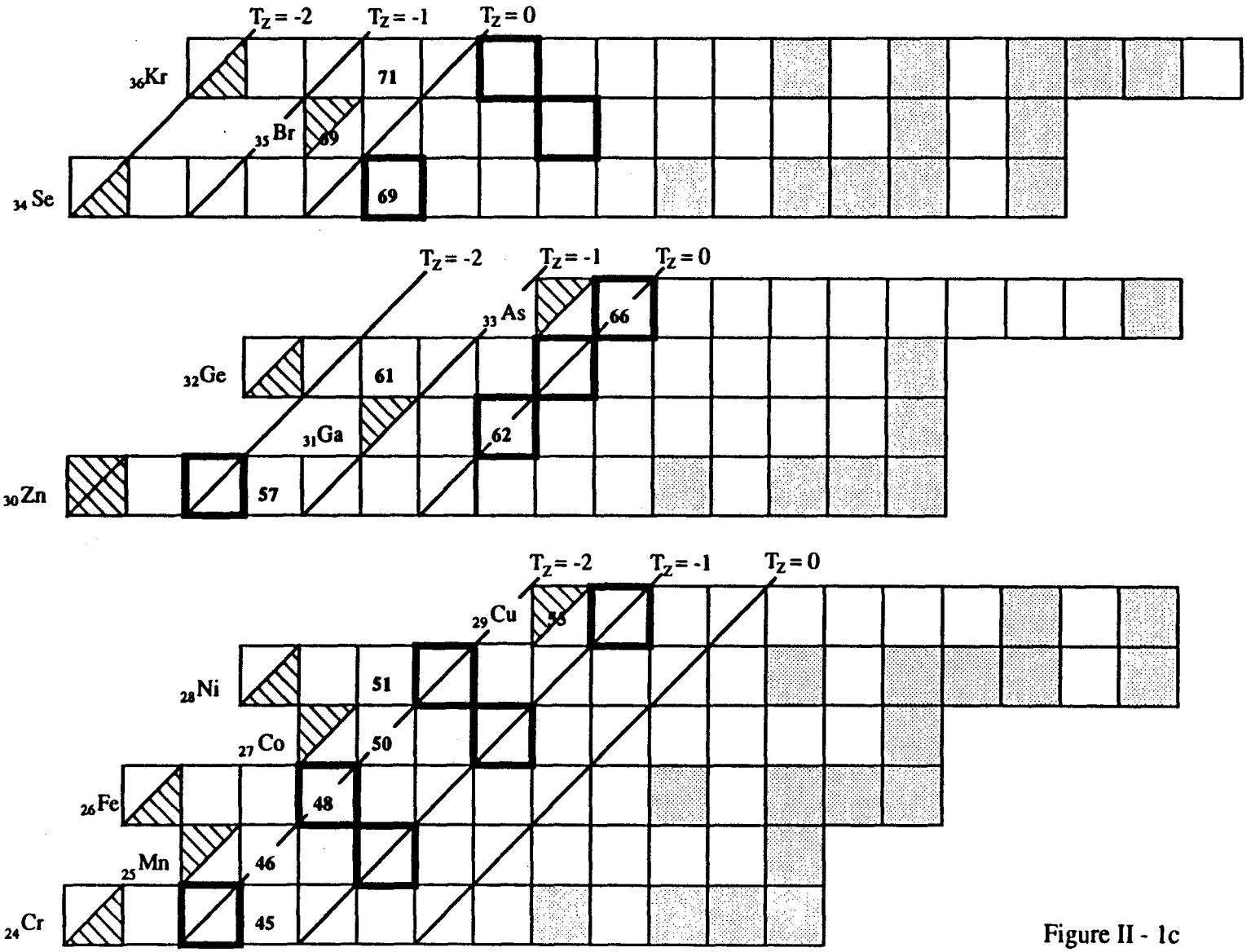
$T_z = -2$
$T_z = -1$
$T_z = 0$
$_{36}Kr$
71
$_{35}Br$
69
$_{34}Se$
69
$T_z = -2$
$T_z = -1$
$T_z = 0$
$_{33}As$
66
$_{32}Ge$
61
$_{31}Ga$
62
$_{30}Zn$
57
$T_z = -2$
$T_z = -1$
$T_z = 0$
$_{29}Cu$
$_{28}Ni$
51
$_{27}Co$
50
$_{26}Fe$
48
$_{25}Mn$
46
$_{24}Cr$
45

Figure II - 1c

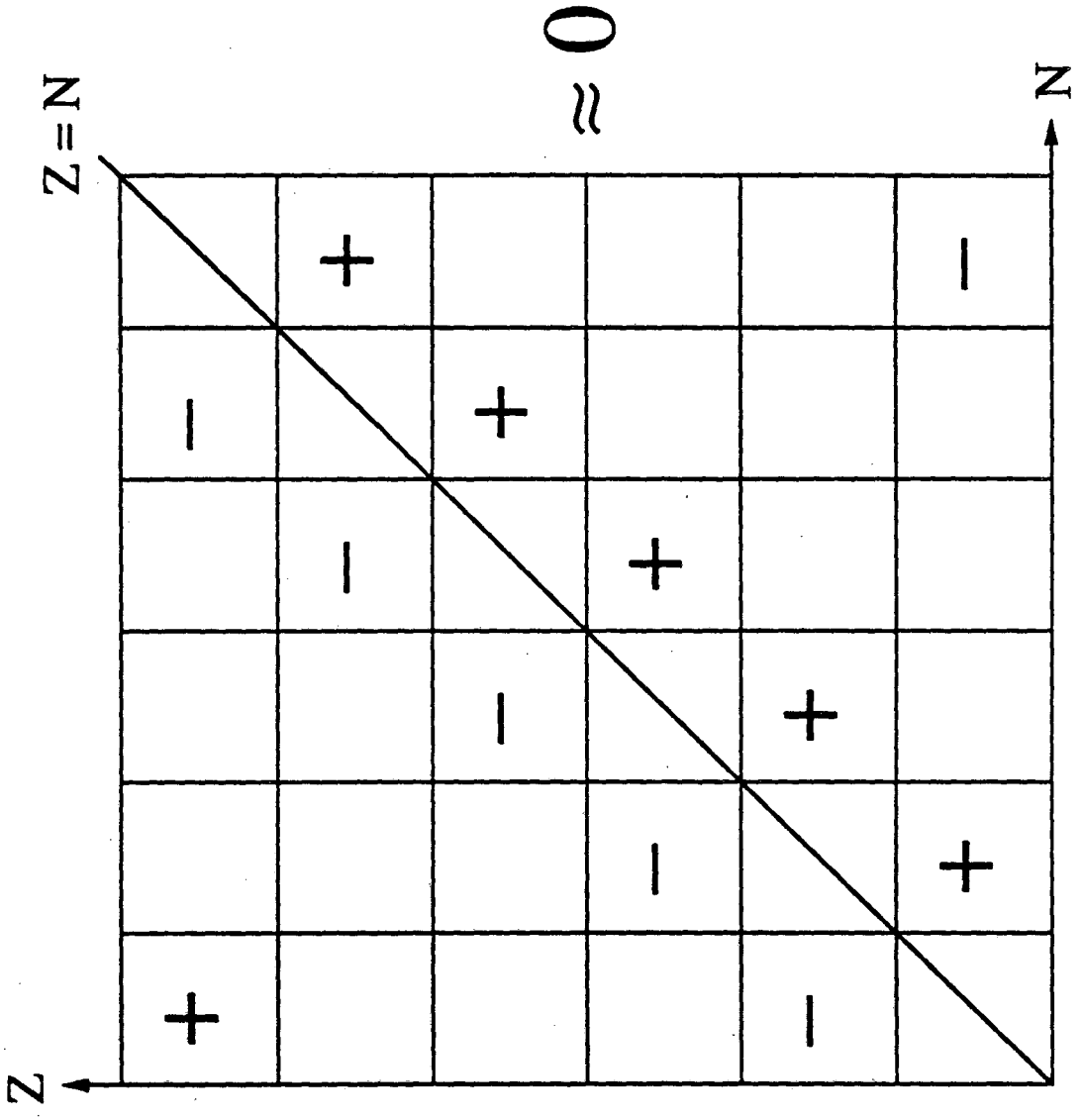

Figure II - 2

Comparison of Kelson-Garvey Relation With Known Masses

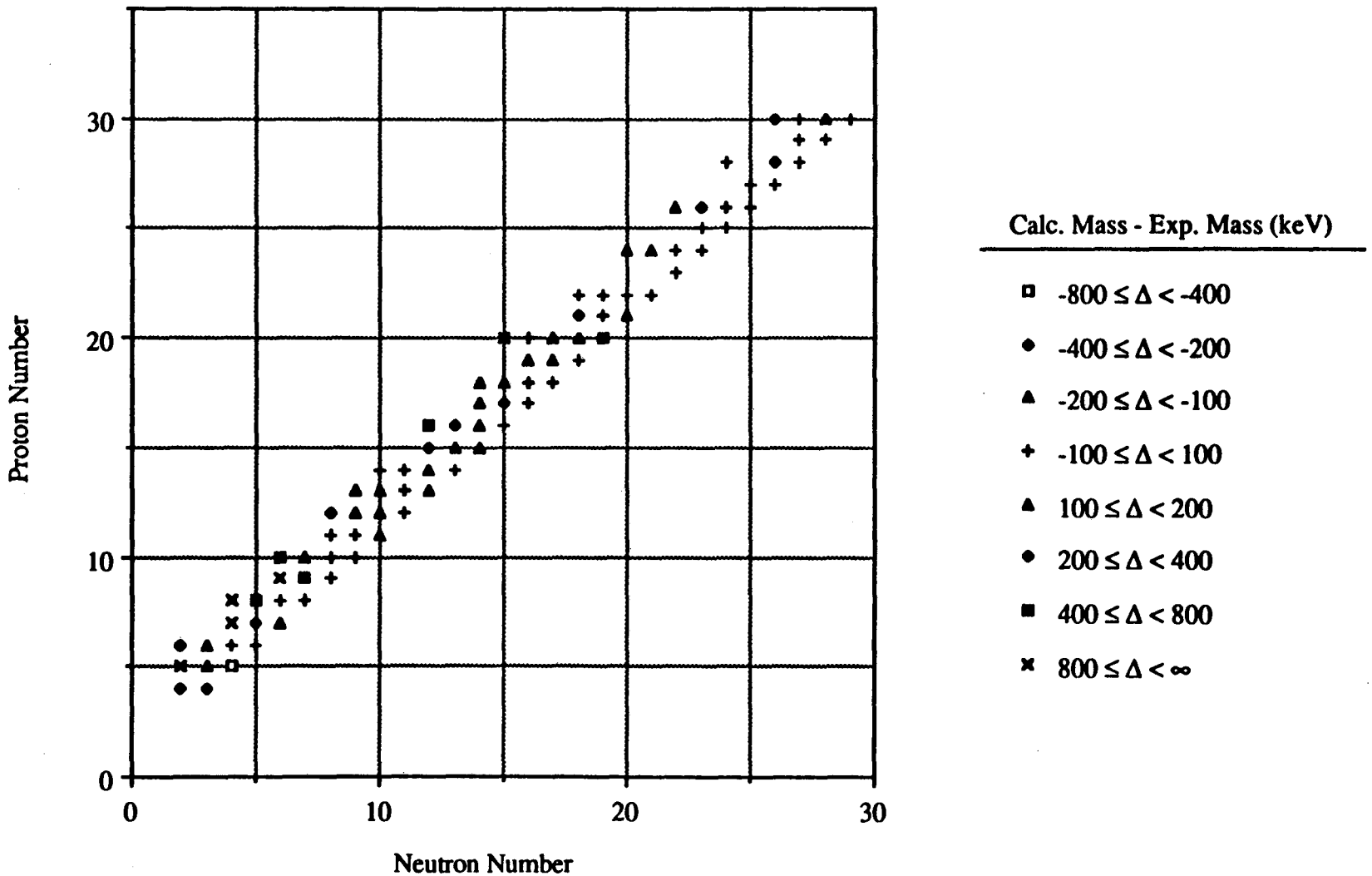

Figure II - 3

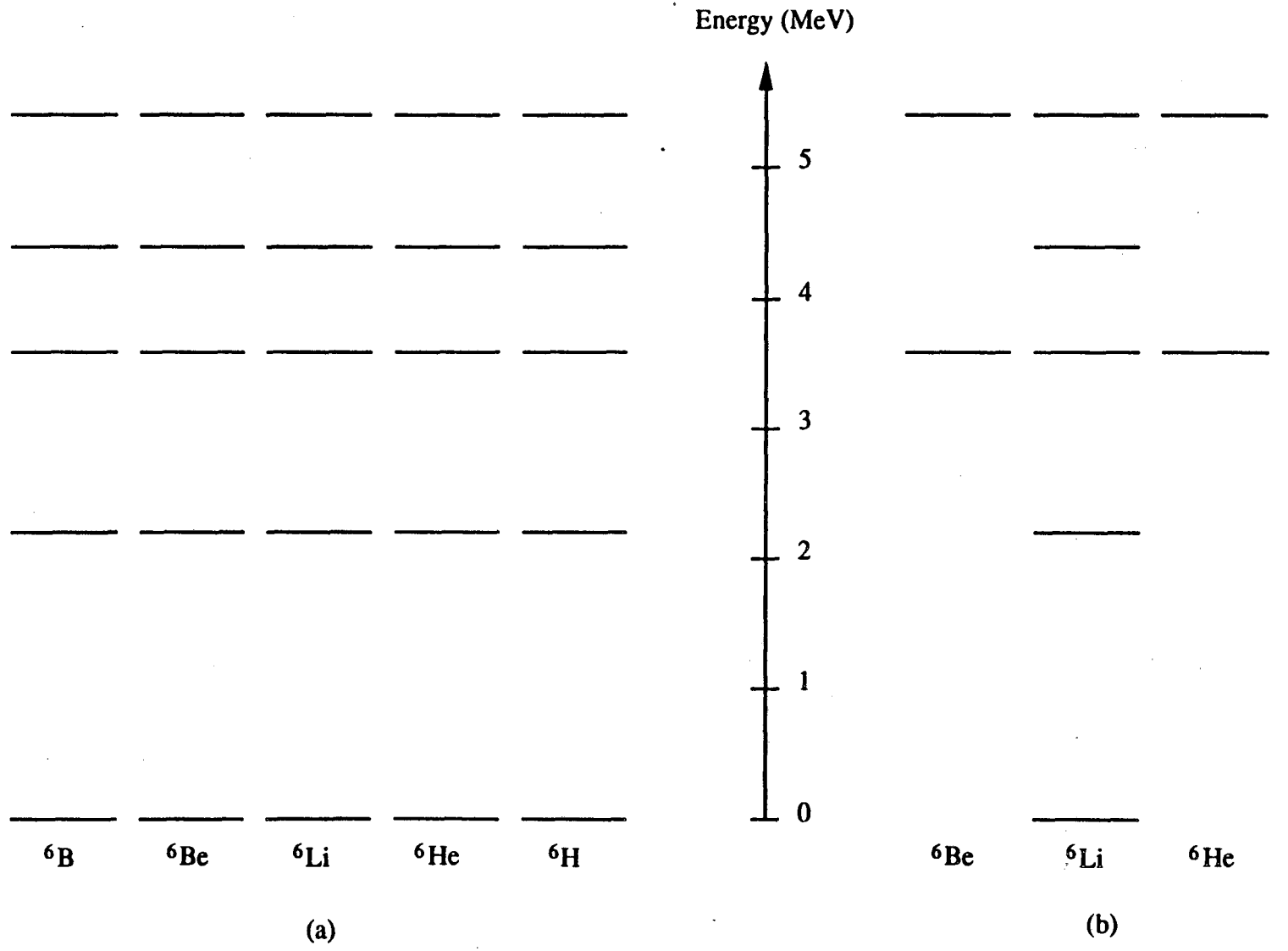

Figure II - 4

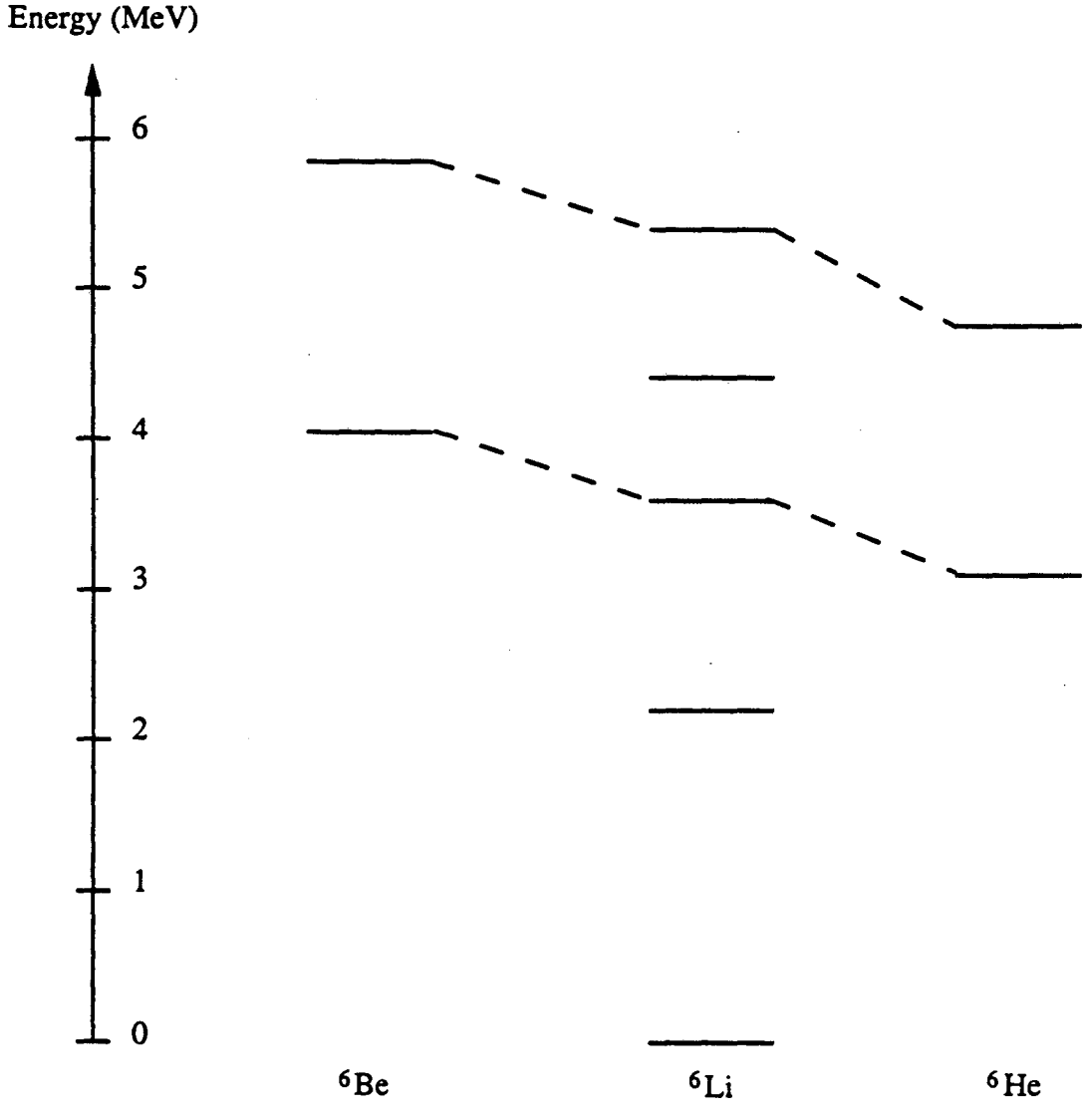

Figure II - 5

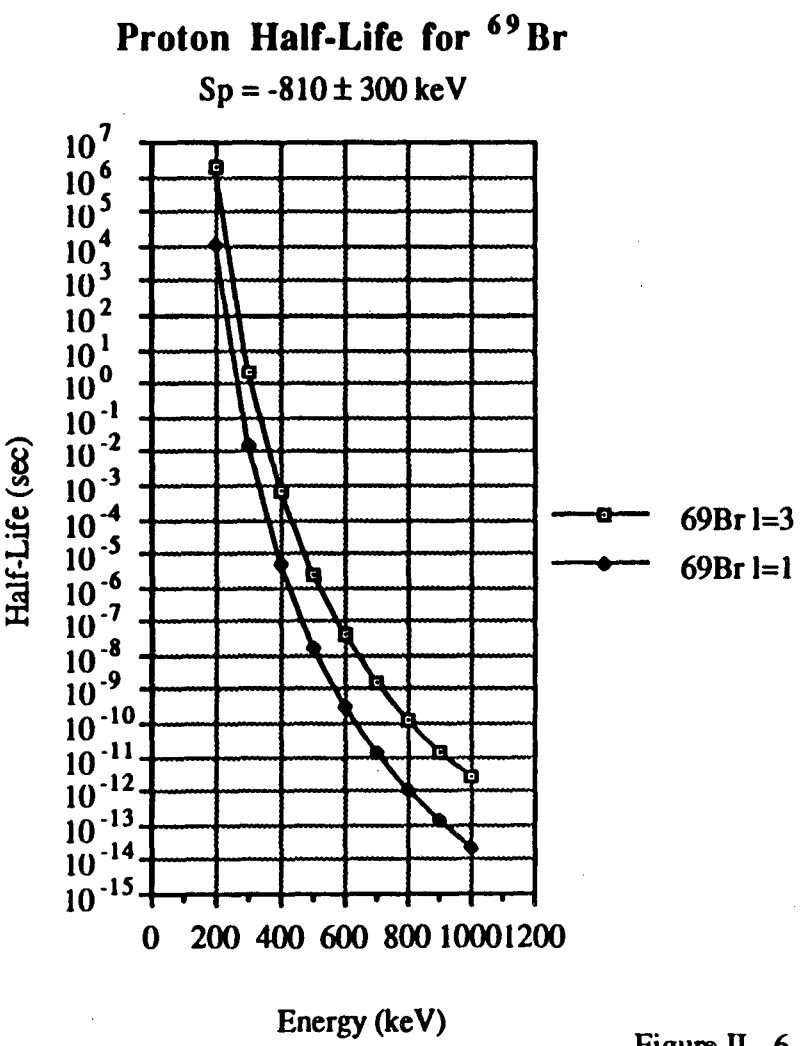
Proton Half-Life for ^{69}Br
Sp = -810 ± 300 keV
Half-Life (sec)
Energy (keV)
69Br l=3
69Br l=1

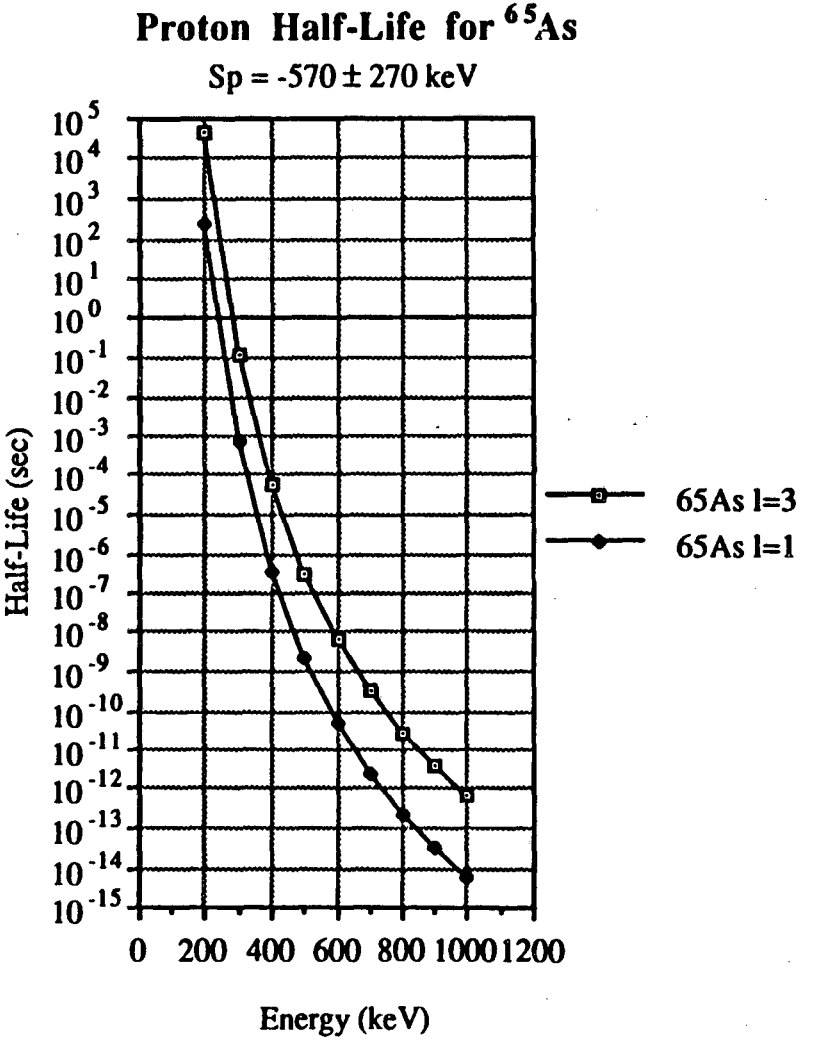
Proton Half-Life for ^{65}As
Sp = -570 ± 270 keV
Half-Life (sec)
Energy (keV)
65As l=3
65As l=1

Figure II - 6

III. Experimental Techniques

All the experiments which will be described were performed at the Lawrence Berkeley Laboratory 88-Inch Cyclotron. Different techniques were used for the different experiments, each one overcoming the limitations of the previous one. The discovery of the first $T_z = -5/2$ nuclide, ^{35}Ca, through its beta-delayed two-proton emission employed a helium-jet transport system. This system, however, could not be used to study the decay of another $T_z = -5/2$ nuclide, ^{31}Ar, or any noble gas for that matter. After considering several alternatives, an in-beam recoil catcher wheel was constructed. In order to search for the ground state proton emission from ^{69}Br and ^{65}As, low energy particle identification gas-silicon telescopes needed to be developed because traditional silicon detector telescopes became impractical.

A. The 88-Inch Cyclotron Facility

The Lawrence Berkeley Laboratory 88-Inch Cyclotron is a variable energy, sector-focused cyclotron where the maximum energy of an accelerated ion with charge Q and mass number $A \geq 4$ is

$$E_{max} = 140\left(\frac{Q^2}{A}\right)$$

The maximum energy for ions with $A < 4$ is limited by the radio frequency (RF) system of the cyclotron, which ranges from 5.5 MHz to 16.5 MHz, and/or the 100 kV limiting voltage output of the deflector power supply. Maximum energies for ions with $A < 4$ are 60 MeV for protons, 65 MeV for deuterons, and 145 MeV for $^3He^{2+}$ ions. Light ions (^3He in particular) were often produced in a conventional hot filament ion source [Eh 62]. All heavy ion beams ($A > 4$) as well as those light ion beams which required pulsing were produced in the Electron Cyclotron Resonance (ECR) source [Ly 87] coupled to the cyclotron. A schematic layout of the 88-Inch Cyclotron facility is shown in Fig. III - 1. The filament source is located below the cyclotron while the ECR source sits on the vault roof above the accelerator. All work described here was done at the location marked CAVE 2, EXOTIC NUCLEI. Light ion beams were transported to CAVE 2 with 70 - 80% transmission while the transmission for heavy ion beams was 40 - 60%.

Production of the light proton-rich radioactive nuclei under investigation is best accomplished by compound nucleus reactions where a $T_z = 0$ target is bombarded by a proton beam, a ^3He beam, or a $T_z = 0$ beam. This type of system produces the most proton-rich compound nuclei in the mass region. For the production of ^{35}Ca, the (^3He,

α4n) reaction on ^{40}Ca was used; ^{31}Ar was produced via the (^{3}He, 4n) reaction on ^{32}S, and the ^{69}Br and ^{65}As searches were performed using ^{28}Si and ^{32}S beams on calcium targets.

B. The Helium-Jet Transport System

Nuclear reaction products recoiling from a target must be carried to the detectors in such a manner that permits the accurate measurement of their decays. Thus, a thin source must be prepared in a vacuum chamber. One traditional method which accomplishes this is the helium-jet transport technique [Ma 74]. Such a system, used to discover the first T_z = -5/2 nuclide, ^{35}Ca, is shown schematically in Fig. III - 2. A water-cooled target chamber was pressurized with helium to 1.3 atm. The beam entered and exited through sets of nitrogen-cooled Havar [Ha 83] isolation windows. The target was situated in a slotted target holder so that the distance between the target and capillary could be optimized for the recoil range of the compound nucleus of interest. Nuclei recoiling out of the target were thermalized in the helium and were transported to the detector chamber via a 70 cm long 1.27 mm i.d. stainless steel capillary.

An important aspect of any helium-jet system is the use of additives to the helium. It is known that when large molecular clusters or aerosols (MW = 10^3 - 10^8 amu [Ju 71]) are in the helium, most nuclei recoiling from the target to stick to the aerosols, with the notable exception of the noble gases. The larger aerosols (and hence the reaction products) are transported by the laminar flow of the helium down the center of the capillary, thereby reducing the amount of activity lost by striking the capillary wall. Aerosols may be formed from a wide variety of materials including, but not limited to, mechanical pump oil, organic solvents such as acetone, ethylene glycol, carbon tetrachloride, benzene, and methanol, or inorganic salts such as sodium chloride, potassium chloride, or lead chloride. For the helium-jet experiment described here, sodium chloride was chosen as the additive because it resulted in the highest yield of reaction products transported to the detector chamber. A quartz tube containing the salt was heated in a tube furnace to a temperature of 600° C. This served to "soften" the salt so that as the helium passed over the sodium chloride, the force of the gas flow broke off salt clusters, thus forming the aerosols.

The transported activity was collected on a rotating aluminum disk in the detector chamber. The chamber was evacuated to 500 mTorr by a high speed Roots blower pump. The six inch diameter disk rotated at a speed of approximately 2 RPM in order to remove long-lived beta activity from the face of the detectors. This was an essential feature of the setup as beta decay background from simultaneously produced nuclei is a serious problem in low-yield experiments and must be reduced as much as possible. The beveled edge of the disk allowed the activity to be deposited under the detectors while the helium was

deflected away. The total transit time from the target chamber to the detector chamber was approximately 20 ms. The collection and transport efficiency of helium-jet transport systems is generally on the order of 50%.

Despite its high transport efficiency, the helium-jet technique has two limitations. First, due to the transport time through the capillary, nuclei whose half-lives are less than 10 to 15 ms and whose production cross sections are less than 100 μb will not be observed in any substantial yield. Second, noble gases do not adhere to the aerosols in the helium, thereby making it impossible to observe the decays of these radioactive isotopes. It thus became necessary to construct a new system which overcame these limitations in order to continue the investigation of the decays of very proton-rich nuclei.

C. Alternatives to the Helium-Jet Transport Technique

When developing new experimental equipment, the specifications of the system must always be clearly delineated. The criteria for this new spectroscopy system included the ability to detect the decays of short-lived nuclei ($t_{1/2} \geq 100$ μs), the versatility of observing single and/or two-proton decay modes (either direct or beta-delayed), and chemical universality.

One technique already in use for studying short-lived nuclei is the system developed by Gillitzer *et al.* [Gi 87] to study proton radioactivity in the tin region. The beam, after passing through a gas filled annular detector, impinges on a target mounted at the end of the annulus such that it is not visible to the detector. Behind the target is a catcher foil which stops reaction products recoiling from the target; the detector is then sensitive to activity emitted from the catcher foil. Counting between pulsed beam bursts, this system has been used to identify decays of nuclei with half-lives of 30 μs and has the capability of detecting the decays of nuclei whose half-lives are as small as 10 ns. In addition to being excellent for studying the decays of very short-lived nuclides, this technique has no chemical selectivity. The disadvantage of this system is highlighted when considering an experiment designed to search for two coincident particles: the subtended solid angle is rather small. Currently, the system subtends 7% of 4π sr for performing single particle spectroscopy; it would have a solid angle of only 3.5% of 4π sr in each side when looking for two particles in coincidence. A high geometry setup is important when performing two-particle spectroscopy because the detectors need to cover a fairly large angular range so that proton pairs emitted with small as well as with large opening angles can be detected. This system does not provide the solid angle necessary for a thorough investigation of such events.

The second system contemplated was a pulsed-beam target counting system such as the one was used by Cerny *et al.* [Ce 70] for measuring the proton radioactivity from

^{53m}Co. In this system the beam was pulsed so that the activities of the reaction products retained in the target could be detected. While the target was being irradiated, the detectors were shielded from the prompt radiation; counting was impossible during this phase. A single rotating wheel was used to control the pulsing of the beam, shield the detectors when the beam was on, and provide a slot so the target was visible to the detectors when the beam was off. This technique has the capability of measuring the decays of nuclei with very short half-lives ($\geq$ 100 μs) and has no chemical selectivity. The biggest disadvantage associated with this technique is, again, the subtended solid angle. Although the detector telescopes can be positioned so that a coincidence experiment can be performed at any given angle, the overall solid angle of the system is very small - approximately 2% of 4π sr per telescope. In addition, the uniform distribution of the activity in the necessarily thick target results in a somewhat broadened peak width of the observed activity - on the order of 200 keV measuring the full peak width at half its maximum height (FWHM).

The final option considered was an in-beam rotating catcher wheel. This system would catch nuclei recoiling from the target on catcher foils located around the circumference of a wheel. The deposited activity would then be transported to the detectors by the rotating wheel. Detectors placed above as well as below the plane of the wheel could detect both small and large angle coincidences. The advantages of such a system include the ability to detect nuclei with very short half-lives, the ability to measure these half-lives by varying the speed of the wheel, the versatility to look at recoils from different nuclear reactions by changing the thickness of the catcher foils, chemical universality, and a relatively large solid angle, approximately 20% of 4π sr, subtended by each telescope. The main disadvantage of this technique actually arises from such a high geometry. All the beta-delayed two-proton emitters examined to date decay via a sequential emission, thereby going through an intermediate nuclear state. As decays of this nature are isotropic (see Section II. D.) the observed peak widths would be adversely affected by this technique due to kinematics. The observed sum of the energies of two sequentially emitted particles is dependent upon the angle between them; the larger the angle, the higher the observed energy. This effect will cause a broadening of the observed peaks, perhaps by as much as 350 keV (FWHM). A much smaller component of the observed peak broadening would result from the uniform distribution of the recoiling nuclei in the catcher foils, similar to that described for the target counting method. However, due to the fact that the catcher foils would be much thinner than a typical target, this component of the broadening should not exceed 80 keV (FWHM).

The annular gas detector system is by far the fastest of the three alternatives considered, capable of measuring activities down to 10 ns. While the detector geometry for

performing single particle spectroscopy is reasonable, it would be rather small for the study of two-particle emission. The target counting system, which could measure activities down to 100 μs and coincidence events at either wide or narrow angles, suffers from the same limited solid angle problem. The rotating catcher wheel, which could also detect activities down to 100 μs, offers the best opportunity for detecting both one and two-proton decays simultaneously with a solid angle of approximately 20% of 4π per telescope; however the trade-off is that such a large subtended solid angle introduces greater uncertainty in the sum energy of coincident particles.

After considering these three alternatives to the helium-jet transport technique it was decided that the third option, the in-beam recoil catcher wheel, would best satisfy the requirements for studying both the single and two-proton decays of short-lived proton-rich nuclei.

D. The In-Beam Rotating Recoil Catcher Wheel

An aluminum alloy wheel with twelve removable catcher foils around its circumference was constructed and installed at an angle of 20° with respect to the beam. The target ladder, which held up to six targets, and the detector telescopes, which were placed to the side of the target ladder, were also inclined at 20°. This apparatus is schematically illustrated in Fig. III - 3. The angle of 20° presented an effective catcher foil 2.9 times thicker than the material the emitted protons must traverse, maximizing the catching efficiency of the foils while minimizing the recoil range effect on particle resolution. The wheel, driven by an external, variable speed motor, could be rotated at speeds ranging from 20 to 5000 RPM.

The beam needed to be pulsed as the wheel rotated for several reasons. The pulsing eliminated the beta background that would have been generated by irradiating the spokes, it prevented the spokes from melting, and it reduced the high radiation background present when the detectors were counting (see below). The customary method of pulsing the cyclotron beam had been to pulse of RF system. This method was used by Cerny *et al.* [Ce 70] with the pulsed-beam target counting system previously discussed. Pulsing the RF allowed the beam to be turned on or off in approximately 200 μs. At RF frequencies above 10 MHz, however, it took almost 500 μs for the beam to cease and another 500 μs for the bombardment to resume after the appropriate signal was sent. Therefore, in order to look for nuclei with very short half-lives, it became necessary to develop an alternate method of pulsing the beam.

Electrostatic deflection plates on the injection line between the ECR source and the cyclotron provided a faster method of beam pulsing. Since the ECR source extraction

voltage is ~10 kV, the beam was completely deflected before entering the accelerator by applying only 700 V to one plate while keeping the other at ground potential. Turning the voltage on or off required ~2 μs. The wheel, with twelve equally spaced slots, permitted a lamp and photodiode to generate the signal for pulsing the beam. The signal from the photodiode was used to generate a square wave which subsequently pulsed the controller for the bias supply to the deflection plates. The beam-on and beam-off times were set approximately equal because the distance between the beam and the detectors was designed such that the activated portion of the foils just reached the detectors as the beam was turned off. Because of the finite amount of time it takes for the cyclotron to empty after the beam is deflected (typically between 60 μs and 100 μs), slow wheel speeds, i.e., speeds in which the beam cycle is greater than 5 ms, required no corrective delays. Rapid rotation experiments, however, require that the beam-on and beam-off times be empirically determined to maximize the beam cycle.

E. Detection Systems

Each measurement that will be described had a detection system tailored to fit the experiment. The detector system used to discover the beta-delayed two-proton emission from ^{35}Ca via the helium-jet transport technique differed from that used to measure the beta-delayed two-proton emission from ^{31}Ar which employed the in-beam recoil catcher wheel. And because much lower energy protons were expected from ground state proton decay, the searches for ^{69}Br and ^{65}As required their own special detection techniques. A description of the characteristics and fabrication of the various types of silicon detectors used in these studies appears in Appendix 2.

1. Detector System Used in the Discovery of ^{35}Ca

The detector system used in conjunction with the helium-jet transport technique for the discovery of ^{35}Ca was shaped by two factors: the ubiquitous beta and beam-related backgrounds and the two-proton decay mechanism. The high beta background (~10 kHz) from the many co-produced reaction products necessitated the use of the three-element (ΔE1, ΔE2, E) silicon telescopes depicted in Fig. III - 4. These telescopes could be used either to measure high energy protons, or to identify protons which stop in the ΔE2 detectors while rejecting events which make it all the way to the E counter. This was a useful feature as beta particles could bounce all the way through the telescope until finally stopping in the E detector.

Another source of background that needed to be considered was neutrons produced by the high energy, high intensity ^{3}He beam. These neutrons could knock out protons

from the nuclei of atoms in the detectors or could result in severe radiation damage to the silicon crystal (see Section VII. F.). If these protons originated near the front of the ΔE1 detector, they could not be distinguished from the beta-delayed protons. One way of reducing the production of "knock out" protons was to situate the detector chamber upstream from the target and have the detectors face down, as the neutrons should be forward peaked at small angles relative to the beam axis. Most "knock out" protons originating in the E detector however, could be filtered out in the analysis via the particle identification software (see Section III. G. 1.), the exception being very high energy protons ($E_p \geq 15$ MeV) which tend to leave signals very similar to those of the beta-delayed protons. Despite these background sources, the imposed two-proton coincidence requirement was so stringent that very little background actually survived the analysis. The betas that did persist bounced around so much in one telescope while a legitimate proton event was detected in the other, that the resulting signal looked like a two-proton coincidence event.

The second factor used to determine the detector design was the two-proton decay mechanism (see Section II. D.). If the protons were to be emitted via a correlated mechanism (^{2}He emission), then there would exist a most probable laboratory angle at which the protons may be observed. Assuming that the break-up energy of the diproton is 500 keV as reaction experiments suggest [Co 80, St 79], then this most probable angle is 40°. If, on the other hand, sequential emission were to be the dominant mechanism, the protons would be emitted isotropically. As such, the best system to use was one where proton pairs emitted via either mechanism could be observed.

The detector setup for this experiment consisted of two three-element telescopes perched above the rotating disk in the helium-jet detector chamber (see Fig. III - 2). This chamber was located upstream from the target box. The unusual aspect about these telescopes was that the ΔE1 and ΔE2 detectors were constructed such that the surface contact on one side of each detector was divided down the center line, thus creating two detectors on one silicon wafer. This narrow line (~0.1 mm thick) permitted the detection of proton pairs whose opening angles ranged from very close to 0° to 70°. These halves will be referred to as left and right, and the individual elements will be called ΔE1 - L, ΔE1 - R, ΔE2 - L, and ΔE2 - R. Typical thicknesses for the phosphorus-diffused ΔE detectors were 15 μm for the ΔE1 wafer, 250 μm for the ΔE2 wafer, while that for the lithium-drifted silicon E detector was 500 μm. Each two-element telescope (ΔE1, ΔE2), which could identify protons with energies between 920 keV and 5.5 MeV, subtended a solid angle of 4.5% of 4π sr while the three-element telescopes each subtended 1.5% of 4π sr.

2. Detector System Used to Identify the Beta-Delayed Two-Proton Decay of ^{31}Ar

As shown in Fig. III - 3, the detector telescopes used with the in-beam recoil catcher wheel sandwiched the catcher foils. Each telescope consisted of a phosphorus diffused ΔE detector and an ion-implanted E detector. For this measurement, the thicknesses of the ΔE and E detectors were 20 μm and 300 μm, respectively. This setup permitted proton pairs with opening angles between 40° and 180° to be observed; the subtended solid angle was 19% of 4π sr for each telescope.

During the initial experiments it became obvious that the beam bursts were preventing the observation of the beta-delayed proton activities. It was clear that counting could not take place while the beam was on as the detectors were overwhelmed by the prompt radiation produced by the beam. This included high energy electrons scattered from the target, catcher foils, and the upstream collimator, as well as neutrons produced by the decomposition of some of the ^{3}He ions in the beam. To remedy this predicament, a second photodiode was set up to pulse the electronics in anti-coincidence with the beam. However, this system proved to be unreliable and was subsequently eliminated. Finally, a single photodiode was used to pulse the beam as well as the counting system. The signal from the photodiode ge. .rated a uniform counting pulse which subsequently produced the gating signal for the beam. The timing, typically set such that the beam would come on 100 μs after the counting was disabled and would be deflected 200 μs before the counting period began, eliminated the prompt electron and neutron background.

Additional measures were taken to reduce the stray electrons and neutrons from reaching the detectors. An L shaped tantalum collimator was hung from the roof of the box between the entrance collimator and the target. This served to reduce the electron spray coming from the entrance collimator from reaching the detectors. Tantalum shielding was also attached to the telescope mount just in front of the ΔE detectors. Although this cut down slightly on the solid angle of the system, it had the advantageous effect of further shielding the detectors from the prompt radiation. Finally, the target and wheel were biased to +2.5 kV to suppress the electron background; this, however, was subsequently abandoned as it had no discernable effect on measured results.

It was soon discovered that the detectors were suffering severe radiation damage from being so close to the beam (see Section VII. F.). This problem was so acute that surface barrier detectors lasted only 1 hour in the presence of a 110 MeV ^{3}He beam with an intensity of only 250 particle nA. Uncooled ion implanted detectors survived 24 to 48 hours. Cooling the ion implanted detectors down to -35° C with thermoelectric coolers or cold nitrogen increased their lifetimes by a factor of ten.

3. Detector System Used in The Search for the Ground State Proton Decays of ^{69}Br and ^{65}As

The protons emitted in ground state proton emission are expected to be much lower in energy than those emitted in the beta-delayed proton decay of nuclei in this mass region. In fact, the proton energies predicted for the ground state proton decays of ^{69}Br and ^{65}As are 810 keV and 530 keV, respectively, and their half-lives are expected to be well below 10 ms (see Section II. C.). Therefore, telescopes had to be constructed which permitted the identification of low energy protons in the relatively high radiation background that is inherent with the in-beam recoil catcher wheel system (~10^5 cps).

The low energy particle identification telescopes that were initially developed consisted of a gas counter for the ΔE detector and a 300 μm ion-implanted silicon detector for the E counter. The cross section of such a telescope is schematically illustrated in Fig. III - 5. The entrance window was made from 30 μg/cm^2 stretched polypropylene; the gas chosen was CF_4 (freon-14). The active volume of the gas counter was defined by two one-dimensional wire grids composed of 10 μm diameter gold-coated tungsten wires at ground potential located 3 mm above and below the 70 μg/cm^2 nickel electrode. These telescopes were eventually incorporated into two arrays each of which contained six such telescopes. In these arrays, the distance from the window to the electrode was 6 mm and the distance from the electrode to the silicon detector was 3 mm. The silicon detectors for these arrays were manufactured on a single wafer by Micron Semiconductor, Ltd. of Lancing, Sussex, England. It was the arrays that were used in the actual searches for the ground state proton decays.

The choice of gas used in detectors of this type is governed by how much voltage can be applied to the electrode at a given pressure, the resulting signal amplification (the gain), and the counting rate which can be achieved. While polyatomic gases such as methane or isobutane are generally regarded quite favorably because they are fairly easy to ionize and they require fairly low electric fields, gains of more than 10^4 cannot be attained without a continuous discharge. This problem can be alleviated by adding a noble gas, such as argon, to the polyatomic gas. Because of the great electronic stability of noble gases, the added gas acts as a quencher absorbing the photons produced in the de-excitation of the polyatomic gas molecules. Even a small amount of quencher can result in gains of 10^6. Electronegative gases such as freon or ethyl bromide serve to trap electrons extracted from the cathode before they reach the anode. Addition of these gases can provide gains of up to 10^7. A problem which often arises when using gas counters is the large amount of quencher consumed for each detected event [Le 87]. At a gain of 10^6 and assuming 100 electron-ion pairs per event, about 10^8 quencher molecules are dissociated per event. A

continuous gas flow prevents the depletion of the quencher gas. Such a gas flow was used in these experiments.

Gases that were tested on-line in the ΔE counter included P10 gas (a mixture composed of 90% argon and 10% methane), isobutane, propane, and freon-14. It was found that isobutane and freon-14 gave the best gas amplification for protons, but the freon-14 was least sensitive to high energy positrons and electrons, and also gave the best shaped signal. By placing a potential of 520 V to 540 V on the nickel electrode while maintaining the pressure inside the detector at 0.2 psi (10.3 Torr), the gas detector operated at the upper end of the proportional region - just below the avalanche mode. This high electric field (~2000 V/cm) was required to provide the amplification necessary for particle identification (see Section III. G. 2.).

Although the ΔE signals were used for particle identification, the final energy signal was taken solely from the silicon E counter. This was possible because of the small amount of energy the protons lost in the gas. For incident proton energies ranging from 100 keV to 6.0 MeV, Table III - 1 gives the energy lost in traversing a telescope within the array.

The efficiency curve for the telescopes was derived by measuring the beta-delayed proton spectrum of ^{29}S as well as through proton scattering measurements. Proton groups arising from the decay of ^{29}S range in energy from 740 keV to 5.5 MeV [Vi 79]. To determine the detection efficiency for protons with energies below 740 keV, protons were scattered off a 20 $\mu g/cm^2$ carbon foil. Low energy proton beams (500 keV, 1 MeV, 1.5 MeV, and 2 MeV) were produced by the Tandem Van de Graaff accelerator at the Lawrence Livermore National Laboratory in Livermore, California. The results of these measurements indicated that the efficiency of the telescopes remained constant for protons with energies in the range of 350 keV to 5.5 MeV.

F. Data Acquisition

While the detector systems used in the beta-delayed two-proton decay measurements of ^{35}Ca and ^{31}Ar employed similar electronics, the use of the low-energy particle identification gas detectors necessitated a different electronics design.

1. Acquisition System Used in the Proton-Proton Coincidence Experiments

All the signals from the silicon detectors used in the proton-proton coincidence measurements were initially amplified by charge sensitive preamplifiers equipped with a slow linear output and a fast timing signal. Each output fed a separate system of electronics. The slow output signals were further amplified with high rate linear amplifiers.

Energy Loss of Protons in the Various Components of the Gas - Silicon Telescope

Incident Energy (MeV)	Loss in Window (keV)	Loss in Gas (keV)	Loss in Electrode (keV)	Loss in Gas (keV)	Final Energy (MeV)
0.100	23	32	13	10	0.022
0.200	24	25	16	13	0.122
0.300	23	22	14	12	0.229
0.400	21	18	13	10	0.338
0.500	18	16	12	8	0.446
0.600	15	15	11	7	0.552
0.700	15	14	10	7	0.654
0.800	12	12	10	6	0.760
0.900	12	11	10	5	0.862
1.000	11	10	9	5	0.965
2.000	6	6	6	3	1.979
3.000	4	5	4	2	2.985
4.000	3	4	4	2	3.987
5.000	2	3	3	2	4.990
6.000	2	3	3	1	5.991

Table III - 1

Logic signals were generated for each detector and sent to a master coincidence system. Each amplified signal was sent through a delay gate, which was gated by the master gate, and then stretched to 2 μs by a pulse stretcher. The stretched signals were read by an LBL 16-channel Multiplexer-ADC unit.

The fast timing signals from the preamplifiers were sent through fast amplifiers and then to constant fraction discriminators (CFD). The CFD signal was used to produce a fast timing signal that started and stopped the corresponding time-to-amplitude converters (TAC). TACs were set up between the following pairs of detectors: ΔE1 - L and ΔE2 - L, ΔE1 - R and ΔE2 - R, ΔE1 - L and ΔE1 - R, and ΔE2 - L and ΔE2 - R. Of course in the ^{31}Ar experiments, the ΔE2 detectors were actually the E detectors. All the TAC outputs were sent to pulse stretchers (2 μs) and then read by the Multiplexer-ADC unit.

Master gate signals for these proton-proton coincidence experiments were generated whenever the first two elements of either the left or the right telescope fired, or whenever the first two elements of one telescope fired and the ΔE2 (or E in the ^{31}Ar experiments) of the other telescope fired. All signals that met only the first requirement were sent to a scale down unit which sampled a predesignated percentage of these events. This way, the co-produced beta-delayed proton emitters could be used to monitor the experiment and internally calibrate the energy axes without filling up the data tapes with "uninteresting" events.

With all the parameters and the master gate signal present at the LBL Multiplexer, each parameter was individually sent to a 5 μs analog-to-digital converter (ADC). Digital output was sent to a buffer area in a ModComp Classic computer. Magnetic tape recording of event-by-event data was performed by the routine ORDER1 [Ma 79], and the on-line analysis and display were handled by MULTID [Ma 79]. The entire data acquisition and analysis procedure was controlled by the program CHAOS [Ma 79].

2. Acquisition System Used in the Ground State Proton Searches

Because protons emitted in ground state proton decay of ^{69}Br and ^{65}As are expected to have energies of less than 1 MeV, new electronics modules needed to be designed so that the small energy signals left in the gas could be picked off the noise and amplified. These sensitive modules were designed by the LBL Electronics Engineering Group. The newly designed preamplifiers were equipped with special low noise FETs with an additional high voltage protective network included on those attached to the gas detectors. As before, each preamplifier had a slow linear output signal as well as a fast timing output signal. The slow output signals were fed into redesigned dual shaping amplifiers which had about ten times the gain of the high rate linear amplifiers previously

used. These new amplifiers were also equipped with both fast and slow outputs. The slow outputs were sent directly to ADCs which were part of the CAMAC data acquisition system; the fast signals were used to generate logic pulses for the master coincidence.

The fast output of these preamplifiers required the development of a fast amplification system. One set of fast amplifiers was located in the cave just after the preamplifiers and a second set was in the counting area feeding the rest of the fast electronics circuit. The resulting signal was then used to drive a standard CFD. As in the previous system, the CFD produced a fast timing pulse that started and stopped appropriate TACs. The TAC signals, resulting from a ΔE (gas) start and an E stop for each of the twelve telescopes, were then sent into the CAMAC ADCs.

The master gate signal was generated whenever any complete telescope (ΔE and E) fired in anticoincidence with the beam. This pulse was then used to strobe the ADCs in the CAMAC crate. The CAMAC system was required in these experiments because the Multiplexer-ADC system previously described could not handle more than 16 parameters per event; this system could easily handle the 36 parameter per event data that was taken. As before, the digital output of the ADCs was stored in a buffer in a ModComp Classic computer. The CHAOS package previously mentioned was used to record the event-by-event data on magnetic tape and perform the on-line data analysis and display.

G. Data Analysis

On-line as well as post-run analyses were performed by the program CHAOS. Basically, the analyses consisted of gating on proton events and relevant TAC spectra. In order to gate on just the protons, particle identification spectra were created in the proton-proton coincidence data while two-dimensional ΔE-E spectra were generated in the ground state protons analyses.

1. Analysis of the Beta-Delayed Two-Proton Data

The particle identification spectra which were created for the analyses of these data use an empirical relationship between the range and energy of a particle in a given medium [Ha 69]:

$$R = aE^{1.73}$$

R is the range of a particle with energy E and a is a constant which depends only upon the mass and charge of the particle. Because two detectors were used to stop the delayed protons, the total range of these protons may be written as

$$R = t + R_E$$

where t is the thickness of the first detector and R_E is the range of the proton in the second. Substituting the empirical relationship given above,

$$aE^{1.73} = t + aE_E^{1.73}$$

so that

$$E^{1.73} - E_E^{1.73} = \frac{t}{a}$$

Since $\frac{t}{a}$ is constant for a given particle in a given experiment, it serves to identify the particle.

Using the TAC spectra to measure the time between two coincident protons removed most of the background present in the proton-gated coincidence spectra. The cleanest spectra were obtained by gating on the TAC spectrum which measured the timing between the two ΔE2 detectors in the ^{35}Ca experiment, or the two E detectors in the ^{31}Ar experiment. The width of the gates used was approximately 20 ns (~10 ns FWHM).

The program FILTER [Mc 82] was used initially to scan the raw data tapes. This program created new tapes which contained only those events which met certain coincidence requirements. Typically, the requirement was that in order to be written onto the new tape the event needed to fire both ΔE1 detectors and at least one of the ΔE2 (or E for ^{31}Ar) detectors. Sorting through the new tapes was much faster than doing the coincidence sort with the raw data tapes. The program MULTID [Ma 79] was used to display the data and fit the peaks, while the program SPECTR [Wo 79] was used to plot the final sorted spectra.

2. Analysis of the Proton Radioactivity Experiments

Because the ΔE detectors for these experiments were gas instead of silicon, the energy deposited in these detectors was greatly reduced while many more beta particles and scattered electrons triggered the master gate. Additionally, the signals left in the gas detectors by protons did not form a discrete peak; instead, they appeared as a smear over an energy range (see Section IV - D.). As a result, it became impractical to use the empirical relationship previously discussed. Instead, two-dimensional ΔE-E spectra were created to identify proton events. Due to the proportionality

$$\frac{dE}{dx} \alpha \frac{MZ^2}{E}$$

plotting the energy lost by various particles in the E detector against the energy lost in the gas detector yields several bands, each one corresponding to a different mass and charge, i.e., a beta band, a proton band, and an alpha band. By setting a gate on the proton band, most of the background caused by alpha and beta particles was eliminated.

It was discovered that the TACs would give a signal only when the energy lost in the gas was larger than some arbitrary value. This value was such that betas and most protons with more than 1 MeV of energy would not give a valid TAC. The efficiency of the TAC for these proton events could be increased only by raising the bias on the electrode in the gas. However, it was better not to increase the bias too much because the TACs acted as a very nice beta filter while permitting the observation of low energy protons (see Section IV. C.). Most of the TAC gates were set 30 ns to 40 ns wide (15 ns to 20 ns FWHM).

Figure Captions

Figure III - 1: A schematic layout of the Lawrence Berkeley Laboratory 88-Inch Cyclotron facility. The experiments described here were done at the location marked CAVE 2, EXOTIC NUCLEI.

Figure III - 2: A schematic illustration of the helium-jet transport system.

Figure III - 3: A schematic diagram of the in-beam rotating catcher wheel.

Figure III - 4: A schematic representation of the split detectors used in the discovery of the first $T_z = -5/2$ nuclide, ^{35}Ca.

Figure III - 5: A schematic diagram of the low-energy proton telescope.

88-INCH CYCLOTRON FACILITY

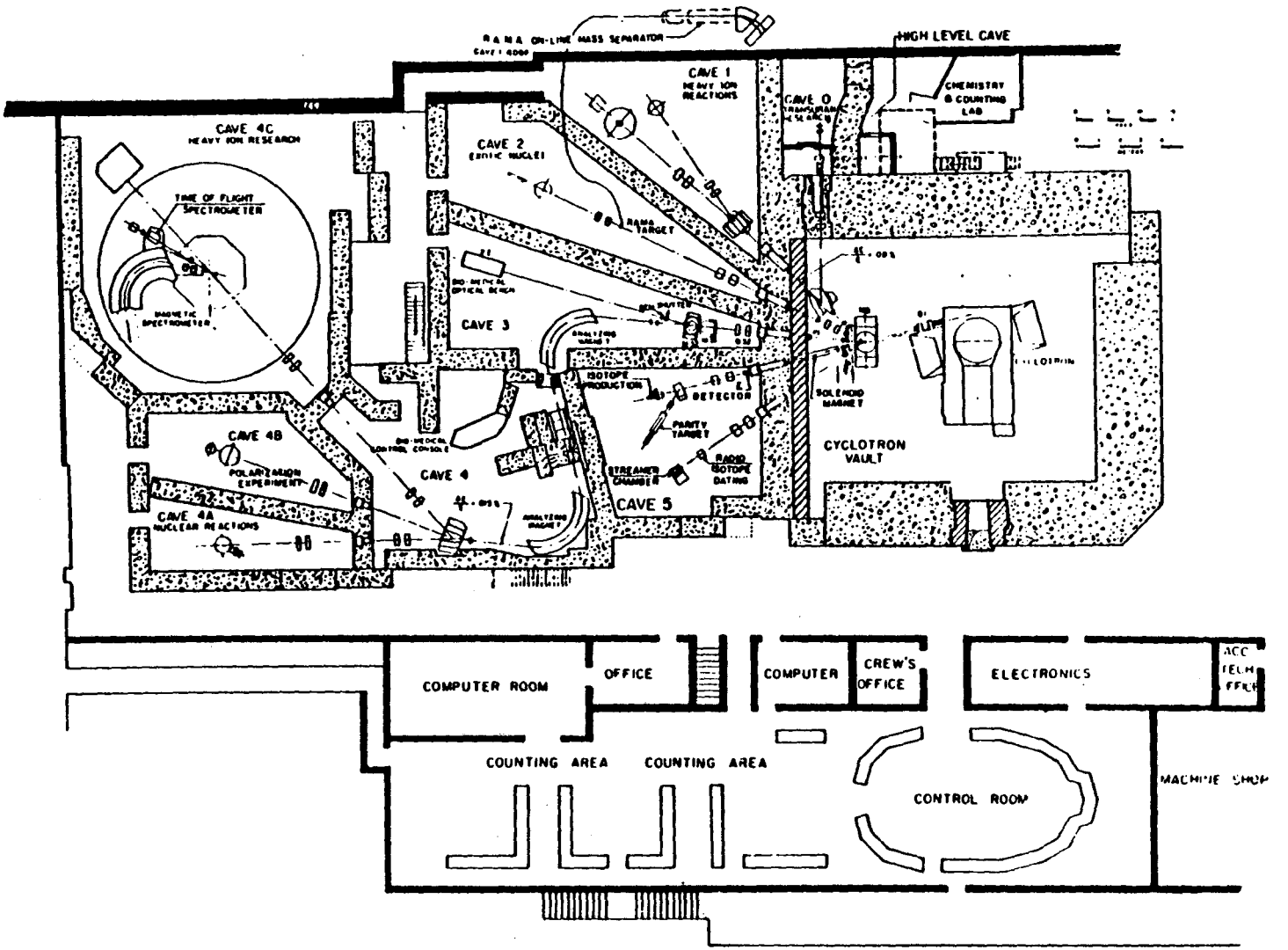

Figure III - 1

XBL 721-331F

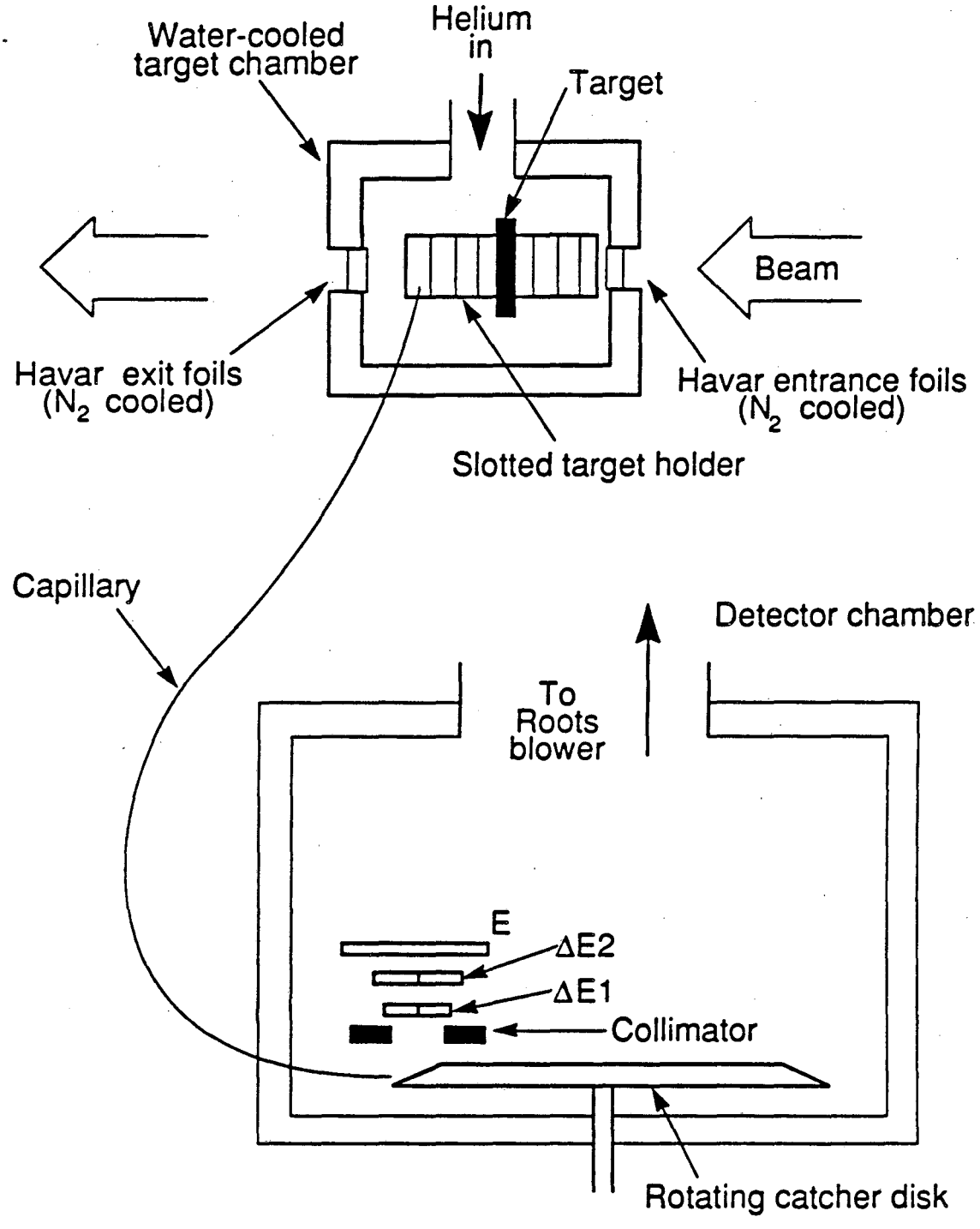
Water-cooled
target chamber
Helium
in
Target
Beam
Havar exit foils
(N_2 cooled)
Havar entrance foils
(N_2 cooled)
Slotted target holder
Capillary
Detector chamber
To
Roots
blower
E
ΔE2
ΔE1
Collimator
Rotating catcher disk
XBL 893-6166

Figure III - 2

In-Beam Rotating Catcher Wheel

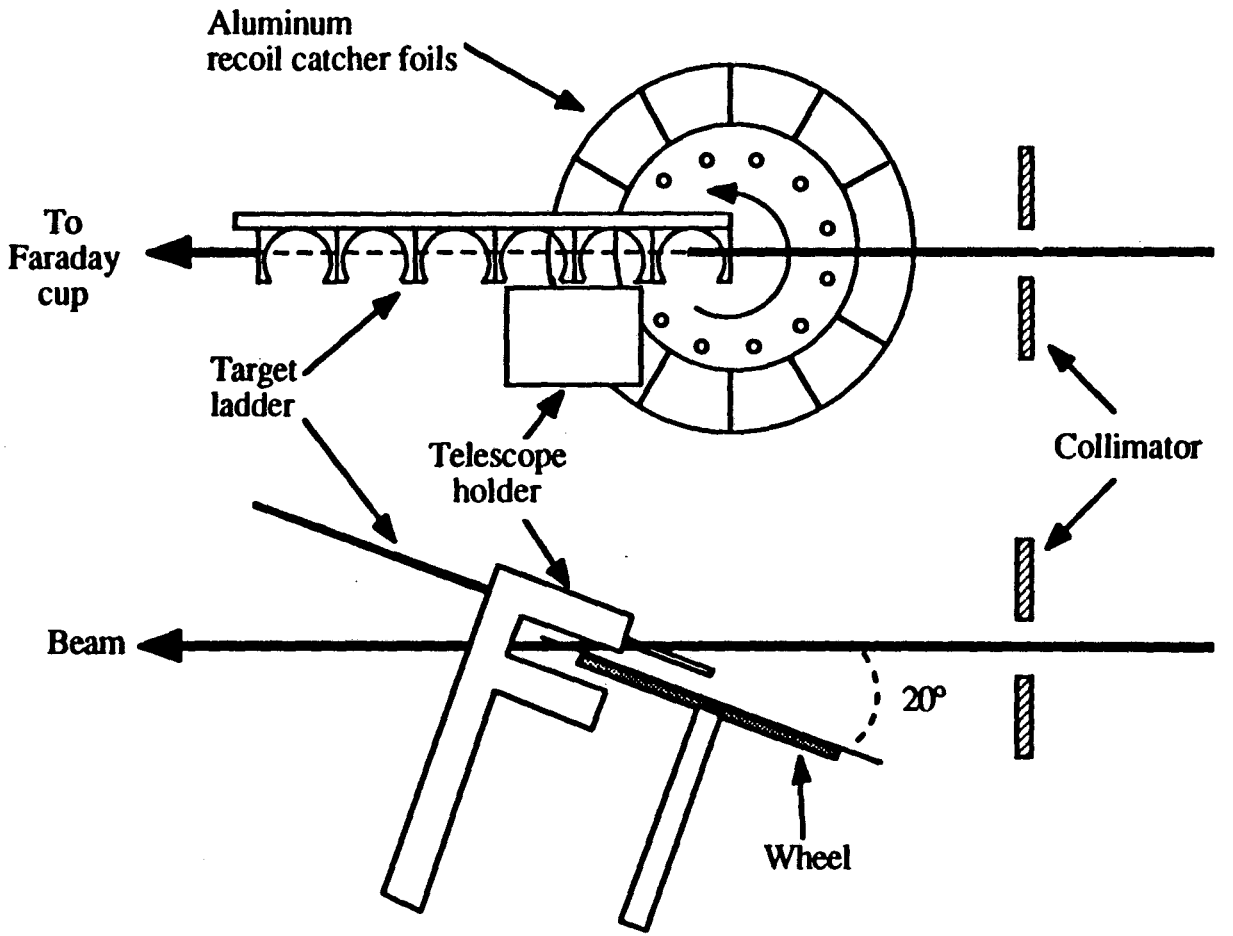

Figure III - 3

XBL 893-6167

Figure III - 4

Cross Section Of The Low-Energy Proton Telescope

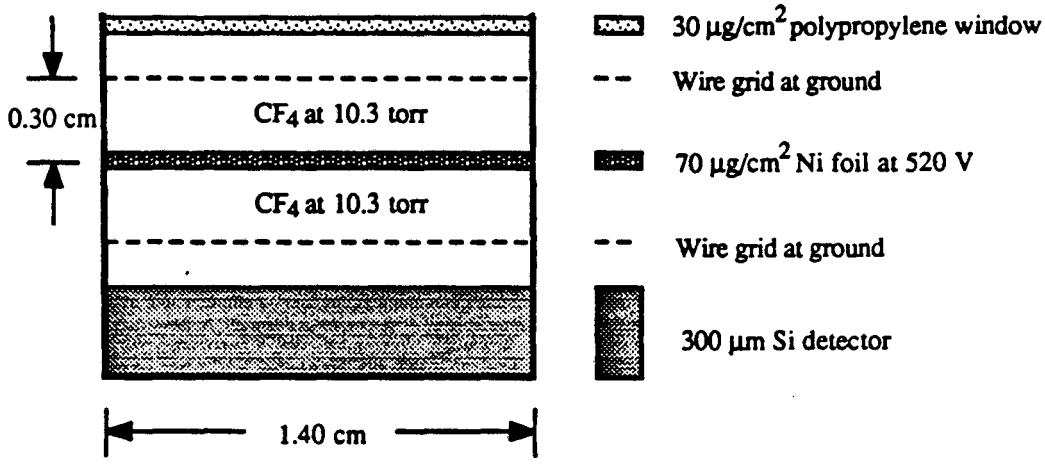

Figure III - 5

IV. Results and Discussion

A. The Beta-Delayed Two-Proton Decay of ^{35}Ca

Prior to searching for the decay of the hitherto undiscovered nucleus ^{35}Ca, the calibration of the helium-jet transport system was established by measuring the beta-delayed two-proton decay of ^{22}Al [Ca 84]. ^{22}Al was produced via the ^{24}Mg (^{3}He, p4n) ^{22}Al reaction using a 135 MeV ^{3}He beam with an intensity ranging from 3 μA to 7 μA. The two-proton summed energy spectrum arising from this decay is shown in Fig. IV - 1b; it is the result of 86 mC of beam on target. The energy calibration of the telescopes was provided by the co-produced T_z = -3/2 beta-delayed proton emitters ^{21}Mg and ^{25}Si. The peaks labelled X and G correspond to the two-proton transitions to the first excited and ground states in the ^{20}Ne daughter, respectively. The energy of the X peak at 4.112 MeV agrees quite well with the previous results of the decay of ^{22}Al to the first excited state of ^{20}Ne. Using the observed two-proton decay energy to the ^{20}Ne first excited state, the knowledge of the energies of the first and second protons [Ca 84], and the known center-of-mass energy of 4.484 MeV for this decay branch, it was determined that the average angle between the telescopes was 33°.

Once it was established that the system was functioning properly, ^{35}Ca was produced by the ^{40}Ca (^{3}He, α4n) ^{35}Ca reaction also at 135 MeV. The energy calibration of the telescopes was verified by the beta-delayed protons emitted from the T_z = -3/2 nuclei ^{41}Ti, ^{37}Ca, and ^{29}S. The two-proton coincidence spectrum collected during the bombardment of the 2 mg/cm^2 natural calcium target for 2.1 C is shown in Fig. IV - 1a. Two peaks with laboratory energies of 4.089 ± 0.030 MeV and 3.287 ± 0.030 MeV are evident. Gating on these peaks and projecting out the individual proton spectra comprising them produced Figs. IV - 2a and IV - 2b. The events in these proton peaks met the 40 ns coincident requirement and have been assigned to the beta-delayed two-proton decay of ^{35}Ca.

The assignment of the observed groups to ^{35}Ca is supported by the strong agreement between several theoretically predicted values and their experimentally deduced counterparts. These quantities include the excitation energy of the isobaric analog state (IAS) in ^{35}K, the laboratory and center-of-mass decay energies from the IAS in ^{35}K to the ground state of ^{33}Cl, the excitation energy of the first excited state in ^{33}Cl, and the half-life of ^{35}Ca. Additionally, other candidates for beta-delayed two-proton emission in this region have been eliminated as possible sources of these peaks.

Using masses from the table "Updated Atomic Masses From (Mainly) Experimental Data" [Wa 88], the Kelson-Garvey mass relation estimates the mass excess for ^{35}Ca to be 4.684 ± 0.080 MeV. Based on this, the Coulomb displacement energy formula predicts

the T = 5/2 IAS in ^{35}K to have an excitation energy of 9.071 ± 0.040 MeV. This excitation energy taken in conjunction with the known mass excess of ^{33}Cl and the fact that the first excited state in ^{33}Cl lies 0.81 MeV above the ground state [En 78], gave the predicted center-of-mass two-proton decay energies from the IAS in ^{35}K to the ground and first excited states of ^{33}Cl as 4.329 ± 0.040 MeV and 3.519 ± 0.040 MeV, respectively. The corresponding two-proton decay energies expected to be observed in the laboratory with the average angle of the telescopes at 33° are 4.160 ± 0.040 MeV and 3.350 ± 0.040 MeV, respectively. Assuming a log ft of 3.09 for the superallowed beta decay to the IAS in ^{35}K and using the available experimental information on the beta decay of the mirror nucleus ^{35}P, the half-life of ^{35}Ca has been predicted to be 35 ms [Äy 80].

The individual proton spectra in Figs. IV - 2a and IV - 2b exhibit a discrete peak structure, thereby suggesting the sequential emission of the protons rather than the correlated ^{2}He decay mechanism. Additionally, both spectra have a peak at 2.213 ± 0.045 MeV. Because the observed energy of the first proton in the sequential emission of two protons is unaffected by the opening angle of the pair, it has been assumed that this 2.2 MeV proton is emitted first in the decays to both the ground and first excited states of ^{33}Cl. As such, the experimentally deduced center-of-mass two-proton decay energies to these states in ^{33}Cl are 4.311 ± 0.040 MeV and 3.501 ± 0.040 MeV, respectively. This yields an excitation energy of 9.053 ± 0.045 MeV for the T = 5/2 IAS in ^{35}K.

The measurement of the excitation energy of the T = 5/2 level in ^{35}K provides the mass of the third member of the A = 35, T = 5/2 isospin sextuplet and can be used in conjunction with the known T = 5/2 levels in ^{35}S and ^{35}P to predict the mass of the ground state of ^{35}Ca via the isobaric multiplet mass equation (IMME) as described in Section II. A. 2. The mass excess and excitation energy of the lowest T = 5/2 state in ^{35}S has been determined from the ^{37}Cl (p, ^{3}He) ^{35}S reaction [Gu 75] to be -19.692 ± 0.010 MeV and 9.155 ± 0.010 MeV, respectively. Although a state at 8.430 ± 0.010 MeV is given as another possibility for the lowest T = 5/2 state, it has been eliminated due to its inconsistency with the Coulomb displacement energy calculations and with the observed excitation energy of the T = 5/2 isobaric analog state in ^{35}K. The ground state of ^{35}P was determined to have a mass excess of -24.884 ± 0.004 MeV by using the weighted average of four previous measurements [Go 72, Th 84, Ma 84, Dr 85]. The IMME predicted the ground state of ^{35}Ca to have a mass of 4.453 ± 0.060 MeV. This value is 233 keV more bound than that which was predicted by the Kelson-Garvey mass relation. This provides some evidence that the Kelson-Garvey mass relation tends to underpredict the binding energy of nuclei as one looks toward the proton drip line.

Other candidates for beta-delayed two-proton emission in this region include ^{27}S, ^{31}Ar, ^{39}Sc, ^{38}Sc, ^{34}K, ^{30}Cl, and ^{39}Ti. These have all been eliminated as the source of the two-proton peaks. ^{27}S is not predicted to have beta-delayed two-proton branches at these energies, ^{31}Ar cannot be observed in a helium-jet experiment, ^{39}Sc is known to be proton unbound [Mo 88], ^{38}Sc, ^{34}K, and ^{30}Cl are predicted to be proton unbound by more than 600 keV, and ^{39}Ti is predicted to be unbound with respect to ground state two-proton emission.

Because the two-proton G peak from ^{35}Ca is so close in energy to the two-proton X peak from ^{22}Al, the calcium target was analyzed for possible magnesium impurities by performing an electron induced x-ray fluorescence analysis. The results showed that magnesium comprised less than 0.1% of the composition of the target. If ^{22}Al were to undergo beta-delayed two-proton emission to the second excited state of ^{20}Ne, the two-proton sum energy would be approximately 1.7 MeV. As there is no evidence of any protons at this energy, it was concluded that there was no significant concentration of magnesium in the target and the 4.089 MeV peak is, in fact, due solely to the beta-delayed two-proton decay of ^{35}Ca.

The beta-delayed single proton decay of ^{35}Ca was not definitively observed in these experiments. A single proton emitted from the isobaric analog state in ^{35}K leaving the ^{34}Ar daughter in its ground state would have an energy of almost 9 MeV. The high energy single proton spectra did not show unambiguous evidence of a proton group near this energy. Decays from other levels in ^{35}K to various low-lying states in ^{34}Ar would give rise to many low-intensity proton groups. The numerous beta-delayed proton peaks coming from the co-produced $T_z = -3/2$ nuclei made such peaks from the decay of ^{35}Ca extremely difficult to identify.

A half-life of 50 ± 30 ms was estimated for both the X and the G groups shown in Fig. IV - 1a. This was established by comparing the relatives yields of ^{35}Ca, ^{22}Al, and the observed $T_z = -3/2$ beta-delayed proton emitters at several rotating disk speeds. In theory, if the helium-jet had a precise transit time for each nuclide transported, this method could give the exact half-life of ^{35}Ca. However, each nuclide has a distribution of transit times in the helium-jet. It is this distribution as well as the low yield of ^{35}Ca that account for such a large error bar on the measured half-life.

All the values which were predicted and subsequently deduced from the experimental results are tabulated in Table IV - 1. Based on these measurements and calculations, a proposed partial decay scheme for ^{35}Ca was constructed and is presented in Fig. IV - 3. The solid lines represent the observed decay branch and the broken lines show other possible decay branches. The ground state spin and parity for ^{35}Ca ($1/2^+$) is taken

from its mirror nucleus ^{35}P [En 78]. Based on this partial decay scheme, a lower limit of 6 nb was set for the production cross section of ^{35}Ca in this experiment.

Theoretical and Experimentally Deduced Quantities From The Beta-Delayed Two-Proton Decay of ^{35}Ca

Quantity	Theory	Experiment
Mass Excess of ^{35}Ca (MeV)	4.684 ± 0.080 [a]	4.453 ± 0.060 [b]
Excitation Energy of the IAS	9.071 ± 0.040	9.053 ± 0.045
Center-of-Mass Decay Energy (G)	4.329 ± 0.040	4.311 ± 0.040
Center-of-Mass Decay Energy (X)	3.519 ± 0.040	3.501 ± 0.040
Observed 2p Decay Energy (G)	4.160 ± 0.040	4.089 ± 0.030
Observed 2p Decay Energy (X)	3.344 ± 0.040	3.287 ± 0.030
Level of 1st Excited State in ^{33}Cl	0.81 [En 78]	0.802 ± 0.042
Half-Life of ^{35}Ca (ms)	35 [Äy 80]	50 ± 30

[a] Mass excess predicted by the Kelson-Garvey mass relation
[b] Mass excess calculated by the IMME

Table IV - 1

B. Testing the New In-Beam Recoil Catcher Wheel

As with any new piece of experimental apparatus, the in-beam recoil catcher wheel and its associated electronics required on-line testing by performing experiments which would give known positive results. As described in Section III. E. 2., the beam bursts and high energy electrons scattered from the upstream collimator initially prevented the observation of any proton activities. After making the appropriate changes to the system as outlined in that section, experiments could be carried out without interference from either the beam or other scattered particles.

In order to test the new system, the major beta-delayed proton groups from the easily produced $T_z = -3/2$ nuclei ^{17}Ne [Ha 71], ^{21}Mg [Se 73a], and ^{25}Si [Re 66, Ro 89] were measured. These nuclides were made in reactions resulting from the bombardment of a 2 mg/cm^2 natural magnesium target with a 1 μA, 110 MeV ^3He beam. The recoil catcher wheel was fitted with 500 μg/cm^2 aluminum catcher foils, and the wheel speed was set at 20 RPM. This wheel speed corresponded to a complete pulsing cycle of 250 ms (125 ms

beam on, 125 ms beam off). The two-element detector telescopes each consisted of a 20 μm ΔE detector and a 500 μm E detector.

The total beta-delayed proton spectrum obtained from this bombardment (i.e., the sum of the beta-delayed proton spectra of both telescopes) is presented in Fig. IV - 4. The major peaks from ^{17}Ne, ^{21}Mg, and ^{25}Si are labelled; the energies of these peaks agree with those previously reported. The observed peak width of 140 keV (FWHM) is due primarily to the activity being spread throughout the thickness of the catcher foils. During the 125 ms transit time to the telescopes, 55% of the ^{17}Ne ($t_{1/2}$ = 109 ms) had decayed, 51% of the ^{21}Mg ($t_{1/2}$ = 120 ms) had decayed, and 33% of the ^{25}Si ($t_{1/2}$ = 220 ms) had decayed. Although a substantial fraction of the activity had disintegrated before the counters were turned on, the relatively large solid angle subtended by each telescope (19% of 4π sr) helped counter this loss of activity.

Having clearly observed beta-delayed proton emission with the recoil catcher wheel system, the next step before searching for the decays of new nuclides was to make sure the coincident emission of two protons from a known beta-delayed two-proton emitter could be detected. This was accomplished by observing the decay of the now standard beta-delayed two-proton emitter ^{22}Al ($t_{1/2}$ = 70 ms). A 135 MeV ^{3}He beam was used to bombard a 2 mg/cm^2 natural magnesium target. 135 MeV was chosen as the bombarding energy because this beam would be used for the production of ^{31}Ar, a T_z = -5/2 nuclide predicted to possess a beta-delayed two-proton branch. Using exactly the same beam guaranteed that the detectors would be exposed to the identical radiation environment in both experiments. Again, 500 μg/cm^2 aluminum catcher foils were used, but now the wheel speed was increased to 50 RPM (50 ms beam on, 50 ms beam off). The detector telescopes, each consisting of a 20 μm ΔE detector and a 300 μm E detector, were sensitive to proton pairs whose opening angles ranged from 40° to 180°.

Figure IV - 5a shows the beta-delayed two-proton summed energy spectrum obtained from the decay of ^{22}Al after a 27 mC bombardment; the coincidence requirement for the two protons was 20 ns. Two distinct groups are evident in this spectrum: a peak at 4.2 MeV and a peak at 5.9 MeV. Again, these results are consistent with previous observations of this decay branch. The break up of these two-proton summed energy peaks into their individual proton spectra [Ca 84] taken in conjunction with the previously observed isotropy of the emitted protons [Ja 85] indicated that a predominantly sequential decay mechanism was being observed. As described in Section II. D., the observed sum of the energies of two sequentially emitted particles is dependent upon the opening angle between them; the larger the angle, the higher the observed total energy. Because proton pairs with such a wide range of opening angles were detected, the summed energy peaks

were kinematically broadened. The width of the peaks (FWHM) were 220 keV (G peak) and 340 keV (X peak); virtually all of the observed peak widths were due to this kinematic broadening.

At this point it is instructive to compare the ^{22}Al yield obtained with the helium-jet transport method to that obtained with the recoil catcher wheel. Fig. IV - 5b shows the ^{22}Al beta-delayed two-proton summed energy spectrum obtained with the helium-jet transport technique [Ca 84]. Although the bombarding energies in the two spectra were different, the production cross section for ^{22}Al was on the order of 100 nb for both reactions. Because the detectors were not in the environment of the beam with the helium-jet method, the beam on target was 5 times more intense than when the recoil catcher wheel system was used. However the recoil catcher wheel system required only 2% of the integrated beam to produce 80% of the statistics acquired with the helium-jet. There were several factors contributing to this effect. The more energetic beam used with the recoil catcher wheel resulted in 17% more ^{22}Al nuclei recoiling from the target than with the helium-jet system. Also, the aluminum catcher foils were able to stop 77% of the ^{22}Al nuclei produced at the higher energy while the helium gas stopped all of the ^{22}Al recoils produced at 110 MeV but subsequently transported only ~50% of them to the detectors [Ma 74]. However, the most important element for observing the enhanced yield with the recoil catcher wheel was its subtended solid angle: the telescopes used with the recoil catcher wheel each subtended 19% of 4π sr while those used with the helium-jet system each subtended only 4.5% of 4π sr. This represented an increase of 320% more solid angle subtended per telescope with the recoil wheel system, thus accounting for its huge increase in yield.

C. The Beta-Delayed Two-Proton Decay of ^{31}Ar

Upon successfully observing the beta-delayed two-proton decay of ^{22}Al, the search for a similar decay branch of the T_z = -5/2 nuclide ^{31}Ar was initiated. The half-life of ^{31}Ar has been measured to be 15 ± 3 ms [Bo 87] from its beta-delayed proton decay branch. A 2.5 mg/cm^2 ZnS target on a 1.5 mg/cm^2 aluminum backing was bombarded with a 135 MeV ^{3}He beam to produce ^{31}Ar via the ^{32}S (^{3}He, 4n) ^{31}Ar reaction. 500 μg/cm^2 aluminum catcher foils were mounted around the wheel whose speed was set at 130 RPM. This corresponded to a 38 ms pulsing period (19 ms beam on, 19 ms beam off). The two-element detector telescopes used in this experiment contained a 20 μm ΔE detector and a 300 μm E counter.

The two-proton summed energy spectrum from the decay of ^{22}Al is presented again in Fig. IV - 6a for reference. The corresponding two-proton summed energy spectrum

resulting from the 240 mC ^{3}He + S bombardment is shown in Fig. IV - 6b; the two-proton coincidence requirement was again 20 ns. The known beta-delayed two-proton emitters ^{22}Al and ^{26}P were produced in this bombardment and their two-proton summed energy peaks are labelled. Also labelled is a cluster of events ranging from ~7.3 MeV to ~7.7 MeV; these have been assigned to the beta-delayed two-proton decay of ^{31}Ar.

The assignment of this high energy group to the beta-delayed two-proton decay of ^{31}Ar is based on several arguments: the agreement of the two-proton summed energy with the predicted two-proton decay energy from the isobaric analog state in ^{31}Cl to the ground state of ^{29}P, the fact that ^{31}Ar has the highest available two-proton decay energy of any nuclide possibly formed in this reaction, and that the number of events of ^{31}Ar compared to the yield of ^{22}Al and ^{26}P agrees with production cross section predictions.

Using recently updated masses [Wa 88], the Kelson-Garvey mass relation estimated the mass excess of ^{31}Ar to be 11.65 ± 0.07 MeV; this gave a Q_{EC} for ^{31}Ar of 18.71 ± 0.10 MeV. Based on these predictions, the Coulomb displacement energy formula calculated the excitation energy of the T = 5/2 IAS in ^{31}Cl to be 12.49 ± 0.10 MeV. Two protons emitted from this state to the ^{29}P ground state are thus expected to have a center-of-mass decay energy of 7.81 ± 0.11 MeV. The observed two-proton summed energy group between 7.3 MeV and 7.7 MeV is consistent with these calculations as the beta-delayed two-proton decay of ^{31}Ar. Unfortunately, due to the very small number of observed events, unambiguous individual proton spectra could not be produced.

The unusually large peak width of this cluster can be explained quantitatively by the geometry of the experimental setup. Tables IV - 2a and IV - 2b list four hypothetical energy distributions for the individual protons comprising the two-proton group, opening angles for each distribution, and the corresponding observed peak widths. The first column of the table gives the hypothetical center-of-mass energy for the first proton emitted in the two-proton decay and the second column gives the center-of-mass energy of the second proton. These values assume that the center-of-mass two-proton decay energy is 7.81 MeV as calculated above. In the third and fourth columns are the opening angles between the two protons as seen from the laboratory and center-of-mass reference frames, respectively. The fifth and sixth columns show the laboratory energies of the two protons, the seventh column gives their sum, and the eighth column has the observed peak width for each energy distribution. The average laboratory angle between the two telescopes was 110°. The average peak width over the energy distributions listed in this table is 425 keV. This peak width is consistent with the width of the observed group ascribed to ^{31}Ar in Fig. IV - 6b.

Hypothetical Individual Proton Energies and Their Corresponding Two-Proton Sum Peak Widths

E_1 (MeV)	E_2 (MeV)	η	θ	E_1^L (MeV)	E_2^L (MeV)	Lab Sum (MeV)	Width (keV)
2	5.81	40°	41°	1.94	5.45	7.39	
		60°	63°		5.52	7.46	
		90°	92°		5.62	7.56	
		110°	112°		5.70	7.64	390
		120°	122°		5.73	7.67	
		150°	151°		5.81	7.75	
		180°	180°		5.84	7.78	
3	4.81	40°	41°	2.90	4.46	7.36	
		60°	63°		4.54	7.44	
		90°	92°		4.66	7.56	
		110°	112°		4.74	7.64	440
		120°	122°		4.78	7.68	
		150°	151°		4.87	7.77	
		180°	180°		4.90	7.80	

Table IV - 2a

E_1 (MeV)	E_2 (MeV)	η	θ	E_1^L (MeV)	E_2^L (MeV)	Lab Sum (MeV)	Width (keV)
4	3.81	40°	41°	3.87	3.49	7.36	
		60°	63°		3.57	7.44	
		90°	92°		3.69	7.56	
		110°	112°		3.78	7.65	450
		120°	122°		3.82	7.69	
		150°	151°		3.91	7.78	
		180°	180°		3.94	7.81	
5	2.81	40°	41°	4.39	2.54	6.93	
		60°	63°		2.61	7.00	
		90°	92°		2.73	7.12	
		110°	112°		2.81	7.20	420
		120°	122°		2.85	7.24	
		150°	151°		2.93	7.32	
		180°	180°		2.96	7.35	

Table IV - 2b

The two other prime candidates for beta-delayed two-proton emission which could have been produced in this bombardment are ^{27}S and ^{23}Si. The Kelson-Garvey mass relation and the Coulomb displacement energy formula suggest that the two-proton center-of-mass decay energies for the beta-delayed two-proton decay of these nuclides to the ground state of their daughters (^{25}Al and ^{21}Na) are 6.59 ± 0.07 MeV and 5.86 ± 0.17 MeV, respectively. As these energies are well below that for ^{31}Ar, it can be assumed that these nuclides are not the source of the peak assigned to the beta-delayed two-proton decay of ^{31}Ar.

The ratios of the number of events assigned to the decay of ^{31}Ar to the number of counts observed from the decays of ^{22}Al and ^{26}P were compared to the corresponding ratios of the predicted production cross sections. The predicted values were obtained from the statistical model fusion-evaporation code ALICE [Bl 76]. According to this code, ^{22}Al and ^{26}P have production cross sections 15 and 50 times higher than that of ^{31}Ar in this reaction. After correcting for the differences in half-lives, this is approximately the ratio that is seen in Fig. IV - 6b.

Based on the preceding arguments and calculations, a proposed partial decay scheme for the T_z = -5/2 nuclide ^{31}Ar was constructed. This is presented in Fig. IV - 7. As with the decay scheme of ^{35}Ca, the solid lines represent the decay observed in this work and the broken lines represent alternate, unobserved decay modes.

D. The Search for Proton Radioactivity from ^{69}Br and ^{65}As

The search for the ground state proton decays of ^{69}Br and ^{65}As employed the recoil catcher wheel and the gas-silicon telescopes which were described in Sections III. E. 2. and III. E. 3. The overall performance of the experimental system and energy calibration of the proton telescopes were established by measuring the beta-delayed proton decay of ^{25}Si. This particular nuclide was chosen as the calibrant for two main reasons: 1) it is fairly easy to produce in large yields, and 2) it possesses a beta-delayed proton group at approximately 370 keV [Ro 89]. This is the lowest energy proton transition known among the easily produced A = 4n + 1, T_z = -3/2 beta-delayed proton emitters. As it was previously determined that the efficiency of the telescopes for detecting protons was constant in the energy range of 350 keV to 5.5 MeV (see Section III. E. 3.), observation of this low energy decay branch would prove that the system could, in fact, measure low energy protons.

The ^{24}Mg (^{3}He, 2n) ^{25}Si reaction on a 1.5 mg/cm^2 natural magnesium target was once again used to produce ^{25}Si. This time, however, the energy of the ^{3}He beam was only 40 MeV. This particular beam energy selection was based on ALICE calculations

which predicted that the cross section for this reaction should peak at approximately 40 MeV. For this series of experiments, the 500 $\mu g/cm^2$ aluminum catcher foils were replaced by 200 $\mu g/cm^2$ aluminum foils. Thinner catcher foils were required at this lower beam energy in order to obtain a uniform distribution of the activity throughout the foils. The wheel speed was once again set at 20 RPM (250 ms beam cycle) to measure this 220 ms activity.

A typical two-dimensional ΔE-E spectrum obtained from this bombardment and the proton band is shown in Fig. IV - 8. The region just below and to the left of the proton band (near the origin) are beta particle events. The ^{25}Si beta-delayed proton spectrum presented in Fig. IV - 9a was generated simply by gating on the proton band shown in Fig. IV - 8. By also requiring a 25 ns TAC coincidence between both elements of the telescope, the 370 keV and 910 keV beta-delayed proton peaks became readily apparent, as is shown in Fig. IV - 9b. These beta-delayed proton measurements were used to determine that the product of the collection efficiency for the ^{25}Si recoil nuclei and the detection efficiency of the telescopes for protons whose energies range from 350 keV to 5.5 MeV was $3 \pm 2\%$. This "overall system" efficiency was calculated using the measured cross section of 150 μb for the (^3He, 2n) reaction on magnesium [Es 71] in conjunction with the absolute proton intensities reported by Robertson *et al.* [Ro 89], the fraction of the ^{25}Si nuclei which recoiled out of the target and were subsequently stopped by the catcher foils, the solid angle of the system, and the running time. These measurements verified the fact that the detector efficiencies remained constant over this proton energy range.

In order to determine whether or not the overall system efficiency changed when heavier bombarding beams were used, the beta-delayed proton spectrum resulting from the bombardment of a calcium target with a 180 MeV ^{14}N beam was also measured. The activity was again collected on 200 $\mu g/cm^2$ aluminum catcher foils and measured at a wheel speed of 30 RPM (170 ms beam cycle). The spectrum shown in Fig. IV - 9c resulted from the bombardment of a 1.75 mg/cm^2 natural calcium target with a 400 pna beam. Decays of the two $T_z = -3/2$, $A = 4n + 1$ beta-delayed proton emitters ^{37}Ca ($t_{1/2}$ = 170 ms) [Ha 72] and ^{41}Ti ($t_{1/2}$ = 80 ms) [Se 74] are obvious in this spectrum. The production cross sections for these reactions have not been measured experimentally; instead, they were predicted by ALICE to be 0.5 μb and 3 μb, respectively. By gating on the proton band in the two-dimensional ΔE-E spectrum and using the predicted cross sections from ALICE, the absolute proton intensities reported by Sextro *et al.* [Se 74], and the experimental parameters mentioned above, it was determined that the overall system efficiency for these beta-delayed proton emitters was again $3 \pm 2\%$. Although these calculations relied upon the absolute value of the predicted cross sections (as opposed to the ^{31}Ar analysis where

the ratios of the predicted values were used in the arguments), it has been observed that ALICE predictions are good to, at worst, an order of magnitude. As examples, the ratios of the predicted to measured cross section for several similar reactions in this mass region are listed in Table IV - 3.

After the system performance tests and calibrations were completed, a 1.75 mg/cm^2 natural calcium target was bombarded by a 200 MeV ^{32}S beam in order to search for the ground state proton decays of the $T_z = -1/2$ nuclides ^{69}Br and ^{65}As via the ^{40}Ca (^{32}S, p2n) ^{69}Br and ^{40}Ca (^{32}S, αp2n) ^{65}As reactions. At this beam energy, ALICE predicts that the cross sections for the production of ^{69}Br and ^{65}As via these reactions are 150 μb and 110 μb, respectively. The bombardments were carried out at wheel speeds of 5000 RPM (1 ms beam cycle) and 1250 RPM (4 ms beam cycle) with beam currents ranging from 130 pnA to 150 pnA. The total integrated beam on target in the 5000 RPM and 1250 RPM bombardments was 3.4 mC and 4.8 mC, respectively. After this, a cross bombardment of the calcium target with a 175 MeV ^{28}Si beam was performed in order to search for ^{65}As via the ^{40}Ca (^{28}Si, p2n) ^{65}As reaction. The predicted cross section for this reaction at 175 MeV is 120 μb. In addition to the two wheel speeds used in the sulfur bombardments, this cross bombardment was also performed at a wheel speed of 50 RPM (100 ms beam cycle). The ^{28}Si beam current ranged from 80 pnA to 100 pnA and the amount of integrated beam at each wheel speed was: 1.4 mC at 5000 RPM, 460 μC at 1250 RPM, and 5.4 mC at 50 RPM.

The ^{32}S + Ca bombardments at 5000 RPM and 1250 RPM revealed no proton groups in any telescope which could be assigned to either ^{69}Br or ^{65}As ground state proton decay. An example of the proton spectrum obtained in the ^{32}S bombardments is shown in Fig. IV - 10. From the overall system efficiency determined in the two calibration experiments, the number of counts that would have been seen given a specific cross section and half-life has been estimated. The total number of counts expected in the first three telescopes of an array from the 5000 RPM and 1250 RPM experiments are plotted in Figs. IV - 11a and IV - 11b as a function of reaction product half-life. These curves were calculated assuming a 100% proton decay branch and the reaction cross sections listed on the figures. In the half-life range of 10 μs to 1 ms, a 100% ground state proton branch is a good estimate as the beta decay half-lives are at least 5 ms.

From the expected count rate values, an upper limit can be set for the ^{69}Br ground state proton half-life for a given production cross section. The minimum number of counts, N_x, that must be observed in a peak to meet a 95% confidence level is typically taken as

Comparison of Cross Sections Predicted by ALICE with Experimental Results

Reaction	E_{Beam} (MeV)	σ_{ALICE} (μb)	$\sigma_{Experiment}$ (μb)	Ratio (ALICE/Exp)	Reference
^{24}Mg (^{3}He, 2n) ^{25}Si	40	16	150	0.11	[Es 71]
^{24}Mg (^{16}O, 3n) ^{37}Ca	77	1.5	0.2	7.5	[Ja 74]
^{32}S (^{16}O, 3n) ^{45}Cr	75	3.6	0.3	12	[Ja 74]
^{48}Ti (^{12}C, pn) ^{58}Co	47.5	197×10^3	40×10^3	4.9	[Du 85]
^{48}Ti (^{12}C, 3n) ^{57}Ni	47.5	86×10^3	16×10^3	5.4	[Du 85]
^{48}Ti (^{12}C, p2n) ^{57}Co	47.5	323×10^3	215×10^3	1.50	[Du 85]
^{48}Ti (^{12}C, 2pn) ^{57}Fe	47.5	30×10^3	80×10^3	0.38	[Du 85]
^{48}Ti (^{12}C, p3n) ^{56}Co	47.5	50×10^3	18×10^3	2.8	[Du 85]

Table IV - 3

$$N_x = 3\,(N_B)^{1/2}$$

where N_B is the number of background counts under the peak [Ca 80]. In both the 5000 RPM and 1250 RPM experiments, the backgrounds observed in the sum spectra obtained by adding the data from the first three telescopes in an array yields a minimum detectable limit of 100 counts for a proton peak in the energy range of 500 keV to 1 MeV. The width of a proton peak in this energy range was taken as the width of the 370 keV proton peak observed in the beta-delayed proton decay of ^{25}Si. Application of this minimum detectable limit to the expected number of counts in the three-telescope sum spectrum (see Fig. IV - 11a and Fig. IV - 11b) indicates that if the production cross section for ^{69}Br is on the order of 150 μb as predicted by ALICE, then ^{69}Br must have a half-life shorter than 100 μs. Furthermore, even if the production cross section was an order of magnitude lower than the predicted value, a proton peak would have been observed in the 5000 RPM experiment if ^{69}Br had a half-life in the range of 200 μs to 1 ms. Although the absence of a ^{69}Br proton peak in these experiments could be due to a production cross section of less than 1 μb, it is most likely due to the fact that the half-life of ^{69}Br is less than 100 μs. The assignment of an upper half-life limit of 100 μs is consistent with the mass predictions as it indicates that ^{69}Br is proton unbound by at least 450 keV (see Fig. II - 6).

The ^{28}Si + Ca bombardments at 5000 RPM and 1250 RPM also revealed no proton groups in any telescope which could be attributed to the ground state proton decay of ^{65}As. By making a similar set of statistical arguments to those made for the sulfur bombardments, the minimum detectable limit for these experiments was again determined to be 100 counts for a proton peak in the energy range of 500 keV to 1 MeV. In the case of ^{65}As, however, the absence of a proton peak in the sulfur and silicon bombardments at 5000 RPM and 1250 RPM can be used to assign either a lower half-life limit of 100 μs, an upper half-life limit of 40 ms, or a lower production cross section limit (for either reaction) of 1 μb. Again, such a low cross section is not consistent with other p2n and 2pn evaporation channels (see Table IV - 3). Moreover, although the 100 μs limit is consistent with the predicted separation energy of -530 ± 230 keV, the tendency of this type of mass prediction to underestimate the binding energies of nuclei near the proton drip line suggests that the absence of a proton group is most likely due to the fact that ^{65}As is more bound than predicted, and thus decays predominantly by beta emission.

The ^{28}Si + Ca bombardment was performed again, but this time at a wheel speed of 50 RPM. This wheel speed, corresponding to a 100 ms beam cycle, permitted the detection of a ground state proton decay branch in nuclei whose half-lives were consistent with the beta decay process (≥ 5 ms). However, no low energy proton peaks which could

be attributed to the decay of ^{65}As were observed. A typical single-telescope spectrum produced by the ^{28}Si bombardment at a wheel speed of 50 RPM is presented in Fig. IV - 12. The number of protons from ^{65}As which are expected to be observed with our system was calculated in the same manner as the expectations for ^{69}Br. This time however, various direct proton decay branches were used. The total number of proton counts expected in each telescope of the array as a function of the ground state proton branching ratio is listed in Table IV - 4. In these calculations, a 50 ms half-life was assumed and the predicted ALICE cross section of 120 μb was used. Based on the minimum detectable limit of 100 counts used to claim that a peak does in fact rise above the background, it was concluded that ^{65}As undergoes beta-decay as its primary decay mode. However, as can be seen from the plot of the ground state proton decay branch versus the expected number of counts shown in Fig. IV - 13, a ground state proton decay branch of 0.25% cannot be excluded.

Recently, a similar set of pulsed-beam experiments were performed by Hotchkis *et al.* at the Daresbury Recoil Spectrometer [Ho 89]. In these experiments, which also employed the ^{32}S + Ca reaction to make ^{69}Br and ^{65}As, the reaction products were separated from the beam, mass-analyzed, and then implanted into a 50 μm silicon detector. The energy and time of deposition for each recoil were recorded. Low energy proton events arising from the decays of these recoils would be stopped in the detector, giving a full energy signal, while the positrons from the beta decays of the more prolifically produced nuclei would lose only a small amount of energy in the detector. Preliminary data at mass 69 showed evidence for a proton peak at 450 keV with a half-life between 50 μs and 100 μs. This peak, initially believed to arise from the ground state proton decay of ^{69}Br, was subsequently disregarded as a "statistical aberration" after several confirmatory experiments failed to reproduce the peak [Ho 89a]. The minimum half-life that a nucleus could possess and still be seen at the Daresbury facility was 5 μs. It was thus concluded that the half-life of ^{69}Br is less than 5 μs or that the beta background in these measurements was too high to search for protons whose energies ranged from 300 keV to 1 MeV.

In addition to searching for the ground state proton decay of ^{69}Br, proton radioactivity from ^{65}As was also searched for at the Daresbury spectrometer. Again, no evidence of proton peaks which could be assigned to the decay of ^{65}As [Ho 89] was observed. Thus, Hotchkis *et al.* also concluded that ^{65}As has a half-life shorter than 5 μs, or that ^{65}As decays predominantly by positron emission with only a weak, if any, ground state proton decay branch.

Expected Number of Ground State Protons to be Observed from ^{65}As

Wheel Speed = 50 RPM

Assumed Half-Life = 50 ms

Assumed Cross Section = 110 μb

Proton Branch	Telescope 1	Telescope 2	Telescope 3	Telescope 4	Telescope 5	Telescope 6
1%	191	136	60	13	20	39
0.5%	96	68	30	7	10	19
0.1%	19	14	6	1	2	4
0.05%	10	7	3	1	1	2
0.01%	2	1	1	0	0	0

Table IV - 4

Figure Captions

Figure IV - 1a: The two-proton summed energy spectrum produced by the beta-delayed two-proton decay of ^{35}Ca. Groups labelled X and G correspond to transitions to the first excited and ground states of ^{33}Cl, respectively. Part of the continuum in the spectra below 3 MeV is due to positron scattering between the detector wafers.

Figure IV - 1b: The two-proton summed energy spectrum arising from the beta-delayed two-proton decay of ^{22}Al. The groups labelled X and G correspond to transitions to the first excited and ground states of ^{20}Ne, respectively.

Figure IV - 2a: The individual proton energy spectrum from the beta-delayed two-proton decay of ^{35}Ca to the ground state of ^{33}Cl (those protons comprising group G in Fig. IV - 1a).

Figure IV - 2b: The individual proton energy spectrum from the beta-delayed two-proton decay of ^{35}Ca to the first excited state of ^{33}Cl (those protons comprising group X in Fig. IV - 1a).

Figure IV - 3: A proposed partial decay scheme for the T_z = -5/2 nucleus ^{35}Ca. The solid lines indicate the observed decay branches and the broken lines indicate other possible decay branches.

Figure IV - 4: The total beta-delayed proton spectrum (the sum of the top and bottom telescopes) from the simultaneously produced T_z =-3/2 nuclei ^{17}Ne, ^{21}Mg, and ^{25}Si collected with solid state telescopes in conjunction with the recoil catcher wheel.

Figure IV - 5a: The two-proton summed energy spectrum from the decay of ^{22}Al obtained with solid state telescopes in conjunction with the recoil catcher wheel. The X and G groups are as before.

Figure IV - 5b: The two-proton summed energy spectrum from the decay of ^{22}Al obtained with the helium-jet transport technique.

Figure IV - 6a: The two-proton summed energy spectrum from the decay of ^{22}Al obtained with the helium-jet transport technique (same as Fig. IV - 5a).

Figure IV - 6b: The two-proton summed energy spectrum from the decay of the $T_z = -5/2$ nuclide ^{31}Ar obtained with the recoil catcher wheel.

Figure IV - 7: A proposed partial decay scheme for ^{31}Ar. The solid lines indicate the observed decay branch and the broken lines indicate other possible decay branches.

Figure IV - 8: The two dimensional ΔE-E spectrum showing the gate around the proton band. This spectrum was obtained from the ^{24}Mg (^{3}He, 2n) ^{25}Si reaction with a beam energy of 40 MeV. The bands from the 4.09 MeV and 3.33 MeV beta-delayed proton groups are most easily seen.

Figure IV - 9a: The ^{25}Si beta-delayed proton spectrum which was produced by gating on the proton band shown in Fig. IV - 8.

Figure IV - 9b: The 370 keV and 910 keV beta-delayed proton peaks become evident when the proton gate shown in Fig. IV - 8 is placed in coincidence with a 25 ns TAC gate.

Figure IV - 9c: The beta-delayed proton spectrum arising from the 180 MeV ^{14}N + Ca bombardment which confirmed the overall efficiency of the catcher and detector systems. See text.

Figure IV - 10: A typical single telescope spectrum obtained from the ^{32}S + Ca bombardment with a wheel speed of 5000 RPM. No proton groups which could be attributed to decay of either ^{69}Br or ^{65}As were observed.

Figure IV - 11a: A plot of the number of counts needed to see a peak at the 95% confidence level versus the half-life of the given nuclide for a wheel speed of 5000 RPM. In these experiments, approximately 100 counts would have had to be seen to attain this level.

Figure IV - 11b: The same plot as in Fig. IV - 11a, but for a wheel speed of 1250 RPM. Again, approximately 100 counts would have had to be observed in order to reach the 95% confidence level.

Figure IV - 12: A typical single telescope spectrum obtained from the ^{28}Si + Ca bombardment with a wheel speed of 5000 RPM. No proton groups which could be attributed to decay of ^{65}As were observed.

Figure IV - 13: A plot of the ground state proton decay branch of ^{65}As versus the number of counts expected to be observed, assuming a 110 μb production cross section, a 50 ms half-life and using a 50 RPM wheel speed.

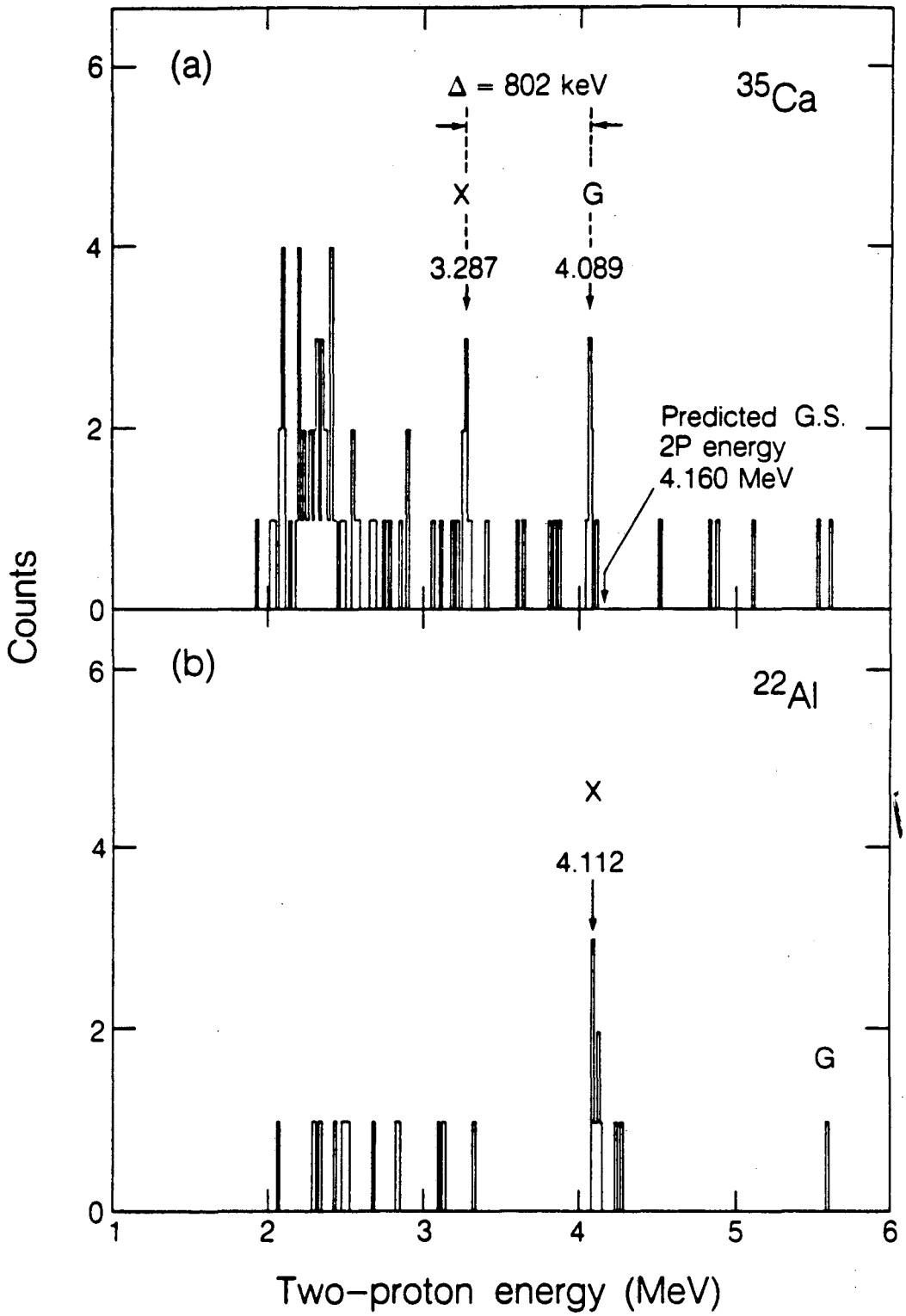
(a)
Δ = 802 keV
^{35}Ca
X
G
3.287
4.089
Predicted G.S.
2P energy
4.160 MeV
(b)
^{22}Al
X
4.112
G
Counts
Two-proton energy (MeV)
XBL 855-8888

Figure IV - 1

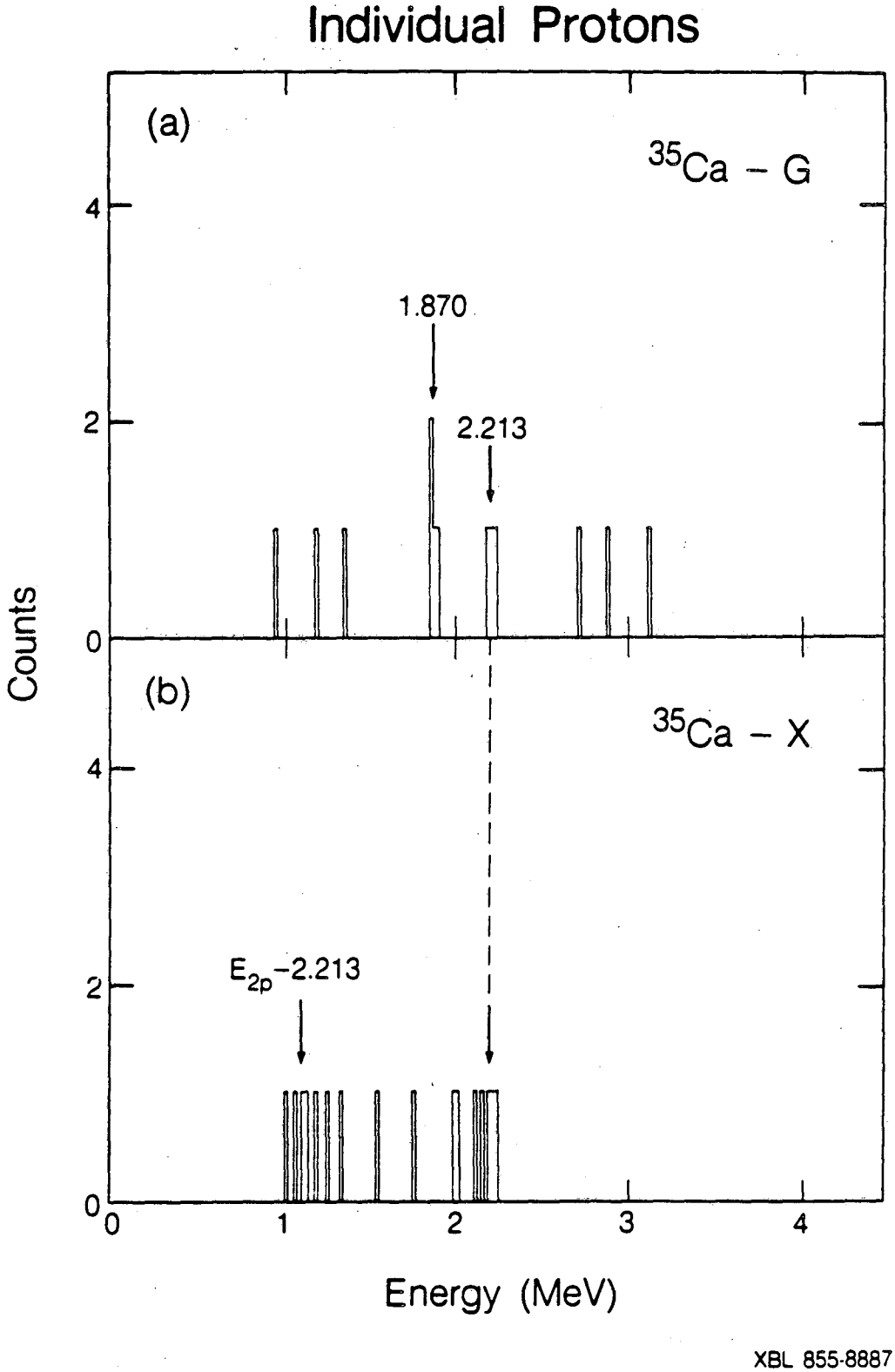
Individual Protons
(a)
^{35}Ca – G
1.870
2.213
(b)
^{35}Ca – X
E_{2p}–2.213
Counts
Energy (MeV)
0
1
2
3
4
XBL 855-8887

Figure IV - 2

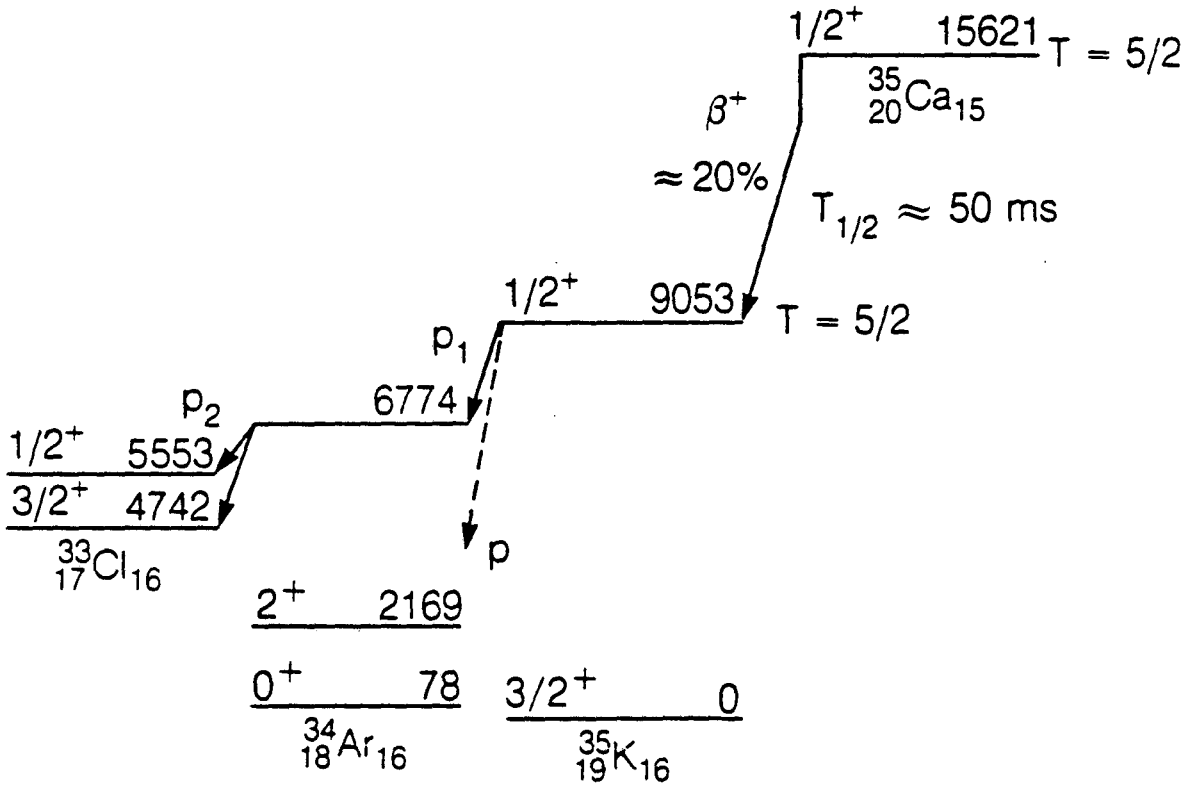

XBL 855-8889

Figure IV - 3

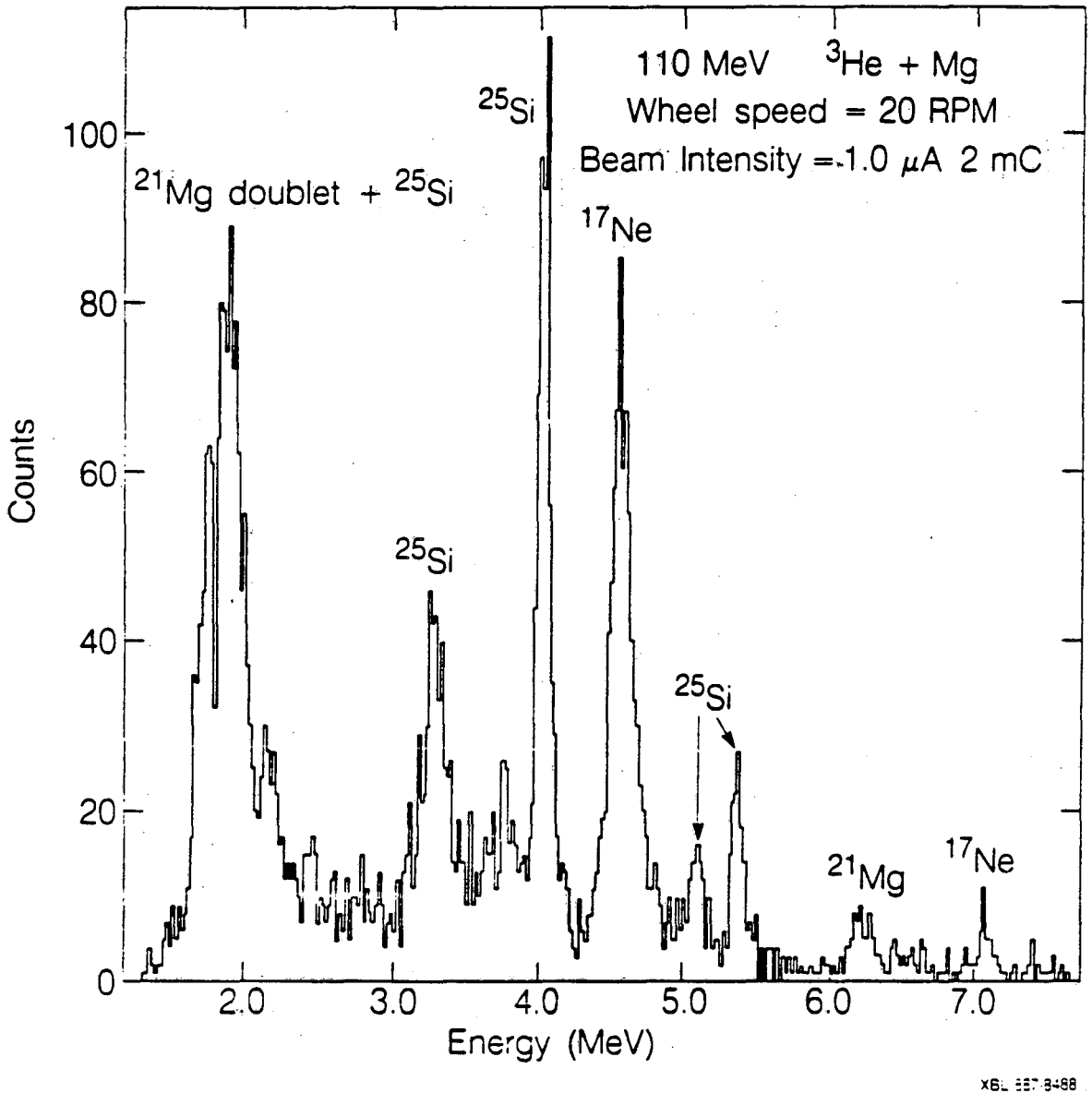
110 MeV ^{3}He + Mg
Wheel speed = 20 RPM
Beam Intensity = 1.0 μA 2 mC
^{21}Mg doublet + ^{25}Si
^{25}Si
^{17}Ne
^{25}Si
^{25}Si
^{21}Mg
^{17}Ne
Counts
Energy (MeV)
0
20
40
60
80
100
2.0
3.0
4.0
5.0
6.0
7.0

Figure IV - 4

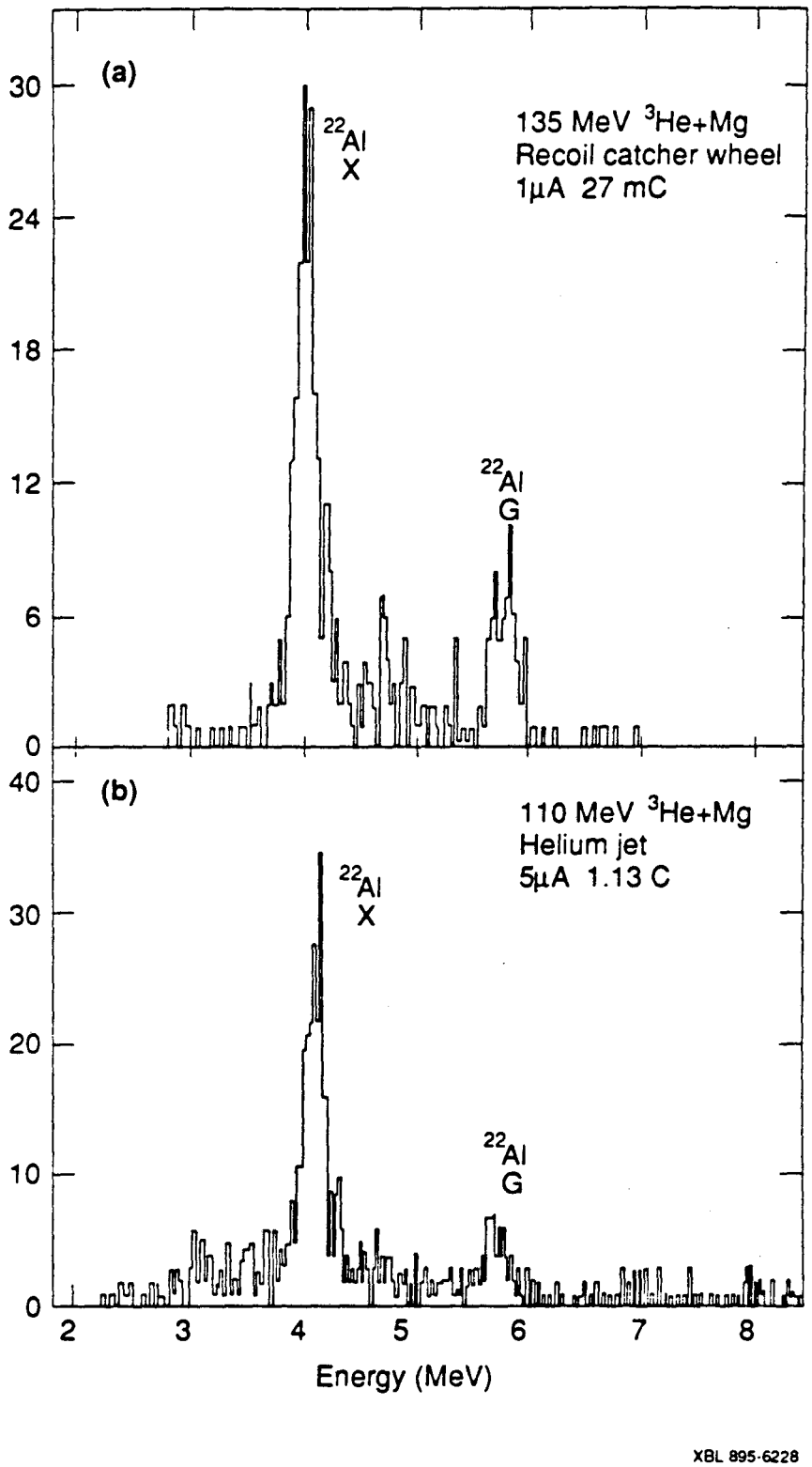
(a)
135 MeV ^{3}He+Mg
Recoil catcher wheel
1μA 27 mC
^{22}Al
X
^{22}Al
G
(b)
110 MeV ^{3}He+Mg
Helium jet
5μA 1.13 C
^{22}Al
X
^{22}Al
G
Energy (MeV)
XBL 895-6228

Figure IV - 5

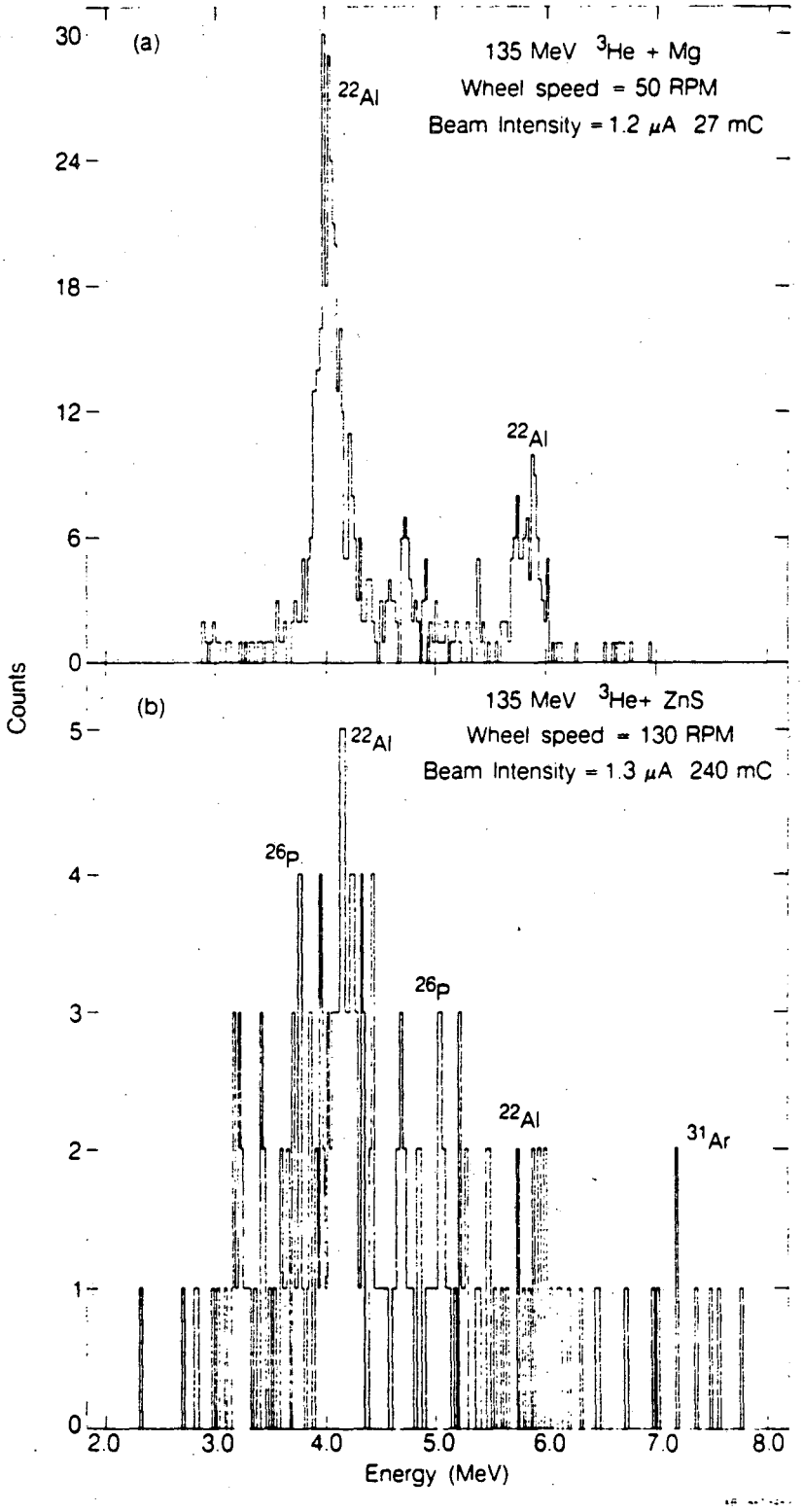
(a)
135 MeV ^{3}He + Mg
Wheel speed = 50 RPM
Beam Intensity = 1.2 μA 27 mC
^{22}Al
^{22}Al
(b)
135 MeV ^{3}He+ ZnS
Wheel speed = 130 RPM
Beam Intensity = 1.3 μA 240 mC
^{22}Al
^{26}P
^{26}P
^{22}Al
^{31}Ar
Counts
Energy (MeV)

Figure IV - 6

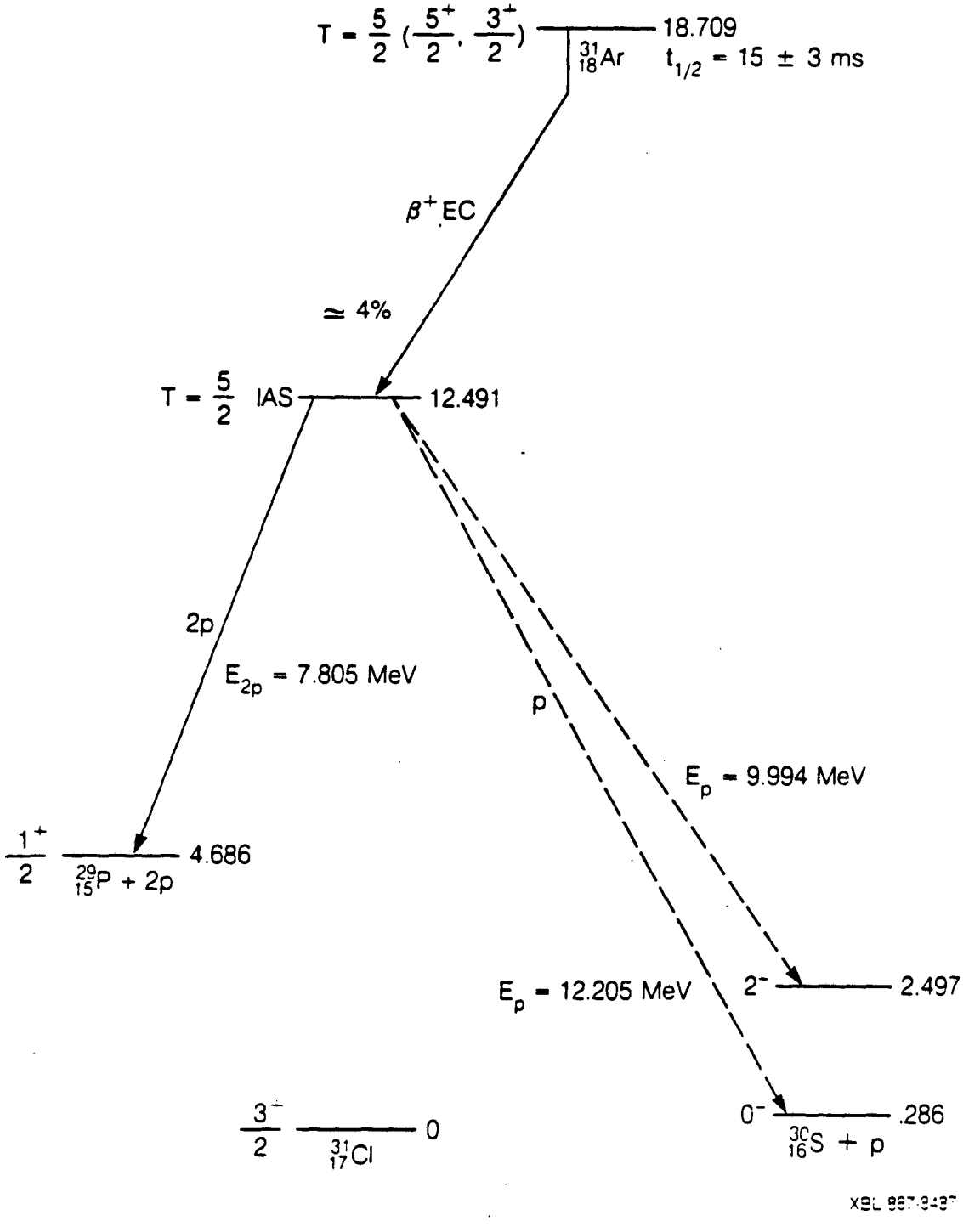
T = 5/2 (5+/2, 3+/2)
18.709
31 18Ar
t1/2 = 15 ± 3 ms
β+EC
≃ 4%
T = 5/2 IAS
12.491
2p
E2p = 7.805 MeV
p
Ep = 9.994 MeV
1+/2
29 15P + 2p
4.686
Ep = 12.205 MeV
2−
2.497
3−/2
31 17Cl
0
0−
.286
30 16S + p

Figure IV - 7

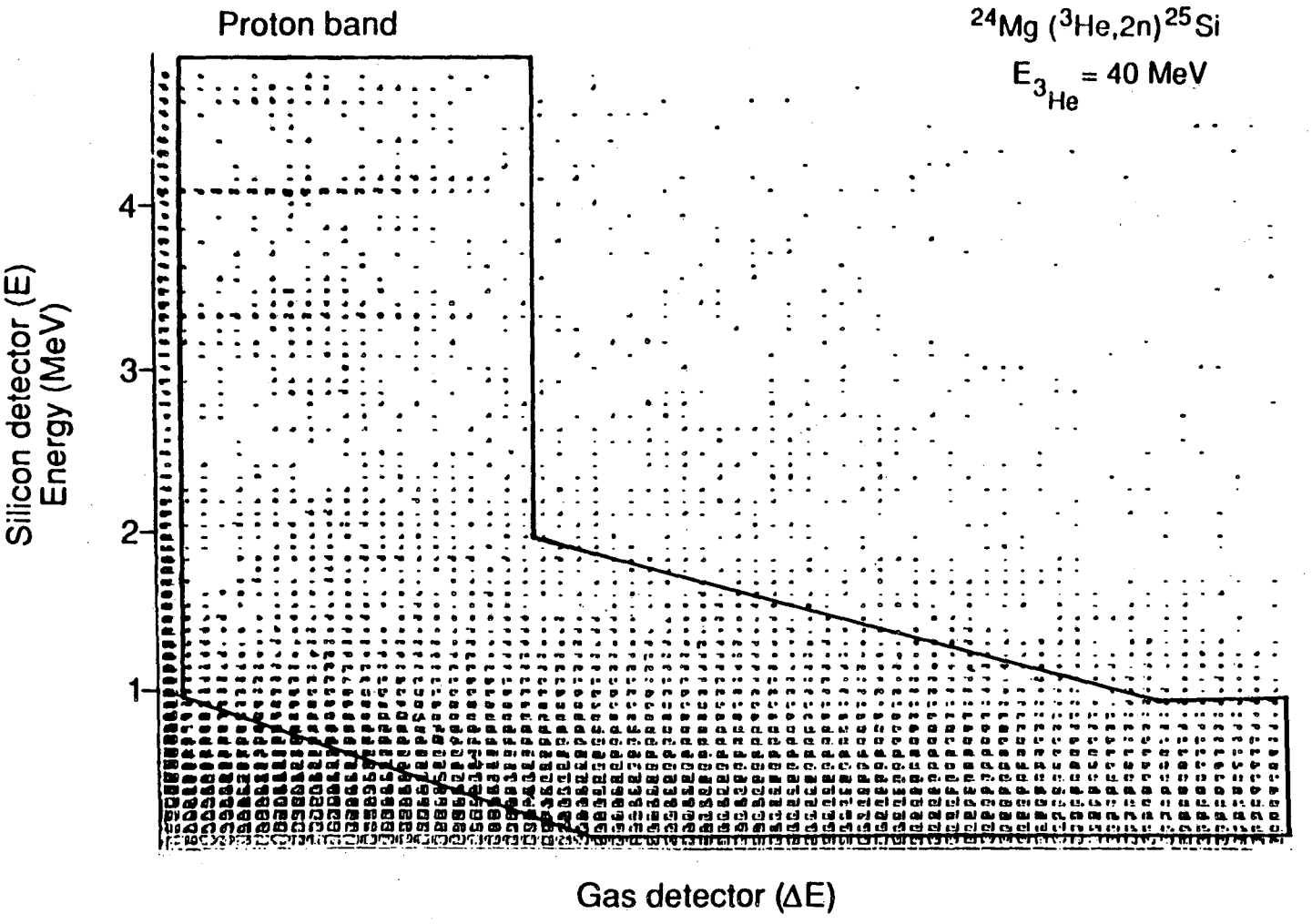
Proton band
^{24}Mg (^{3}He,2n)^{25}Si
$E_{^{3}He}$ = 40 MeV
Silicon detector (E)
Energy (MeV)
4
3
2
1
Gas detector (ΔE)
XBL 895-6229

Figure IV - 8

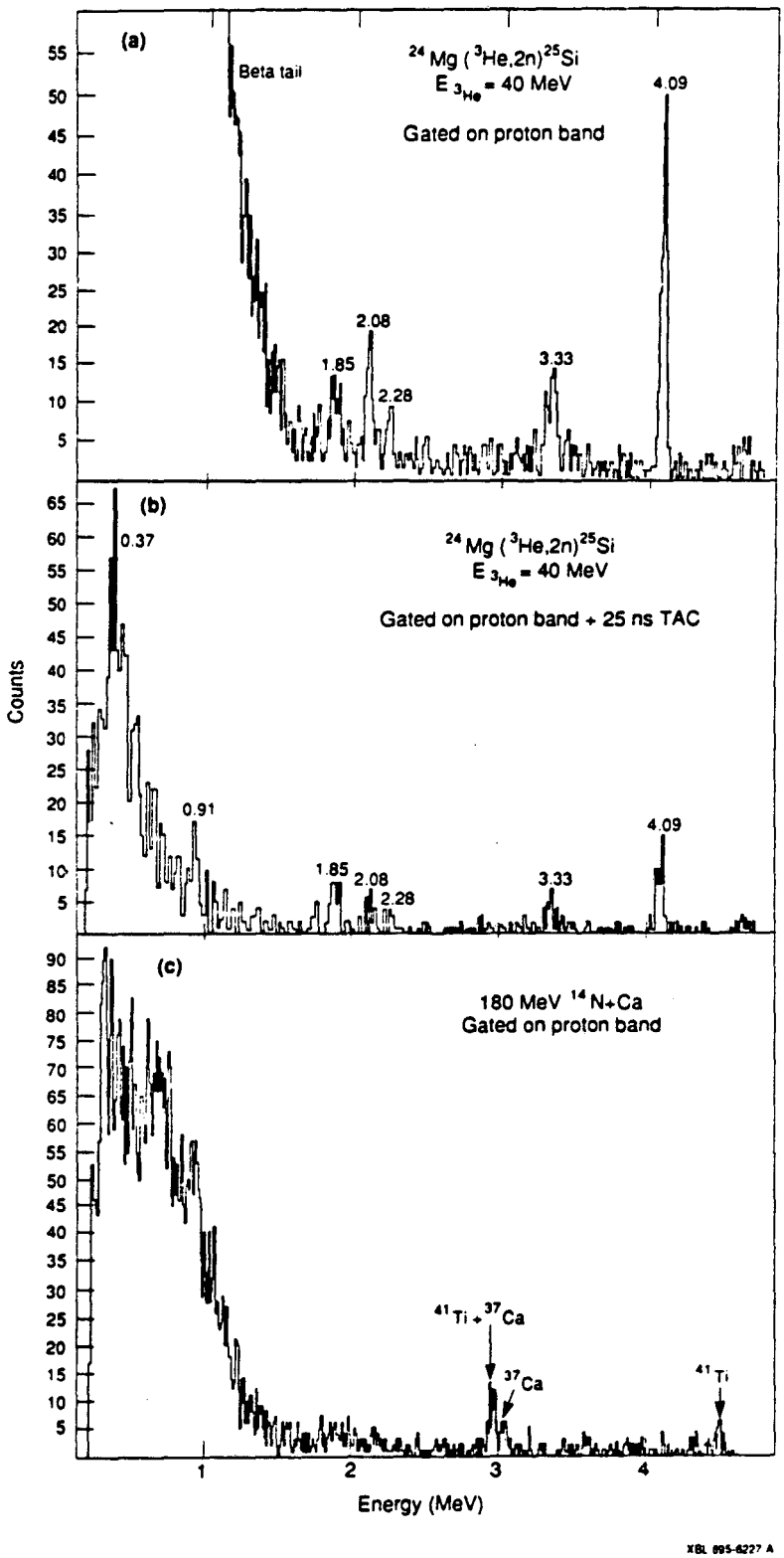
(a)
Beta tail
^{24}Mg (^{3}He,2n)^{25}Si
E $_{^{3}He}$ = 40 MeV
Gated on proton band
4.09
2.08
1.85
2.28
3.33
(b)
0.37
^{24}Mg (^{3}He,2n)^{25}Si
E $_{^{3}He}$ = 40 MeV
Gated on proton band + 25 ns TAC
0.91
4.09
1.85
2.08
2.28
3.33
(c)
180 MeV ^{14}N+Ca
Gated on proton band
^{41}Ti + ^{37}Ca
^{37}Ca
^{41}Ti
Counts
Energy (MeV)
XBL 895-6227 A

Figure IV - 9

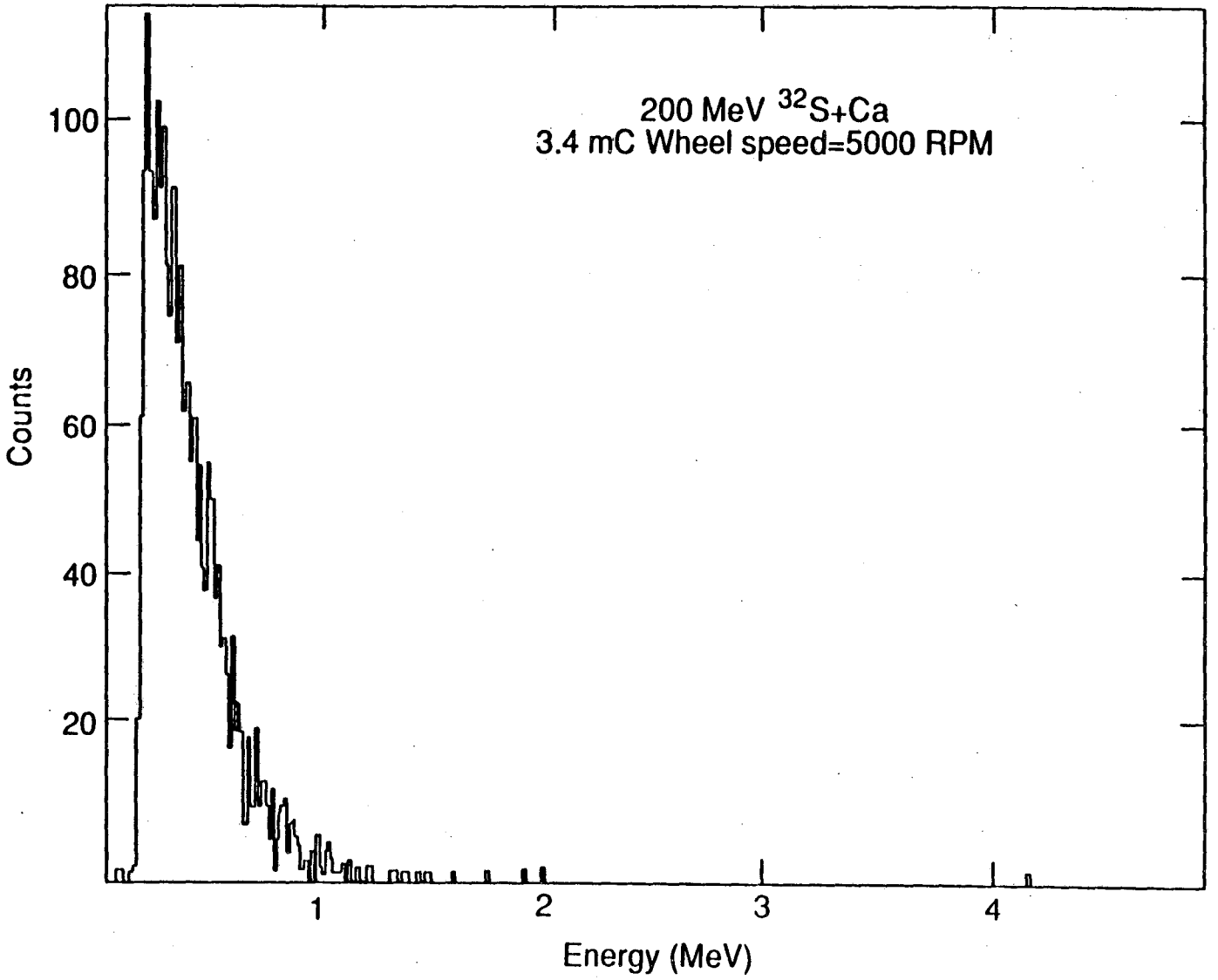

Figure IV - 10

XBL 896-6251

95% Confidence Level Curves for 5000 RPM

a)

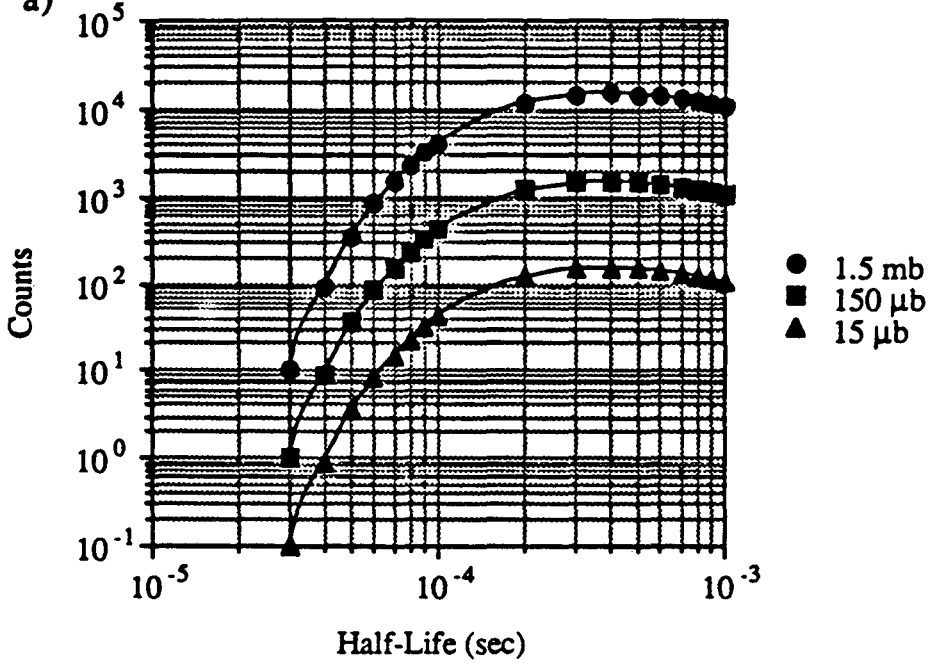

95% Confidence Level Curves for 1250 RPM

b)

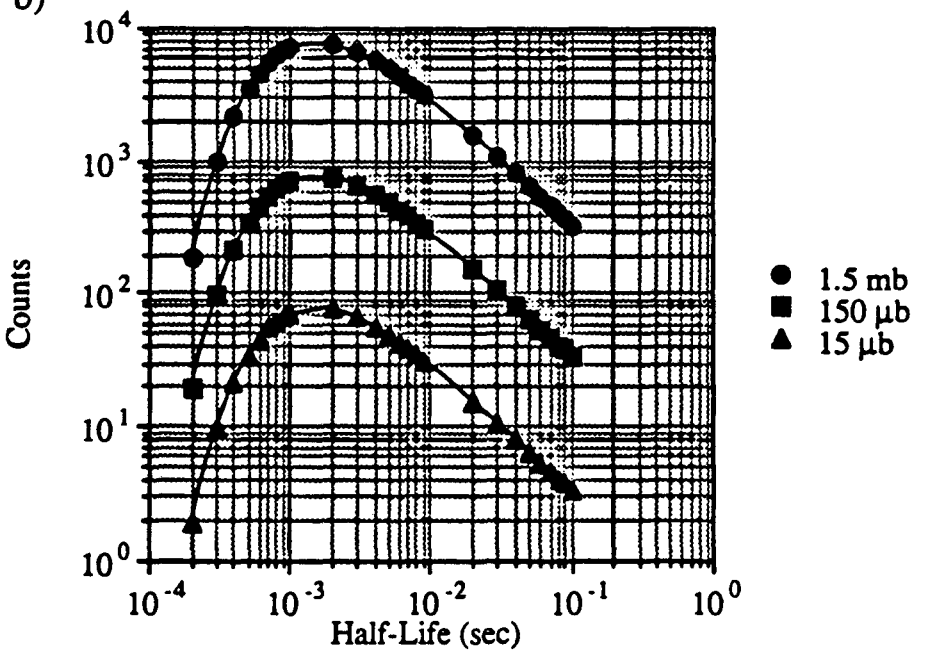

Figure IV - 11

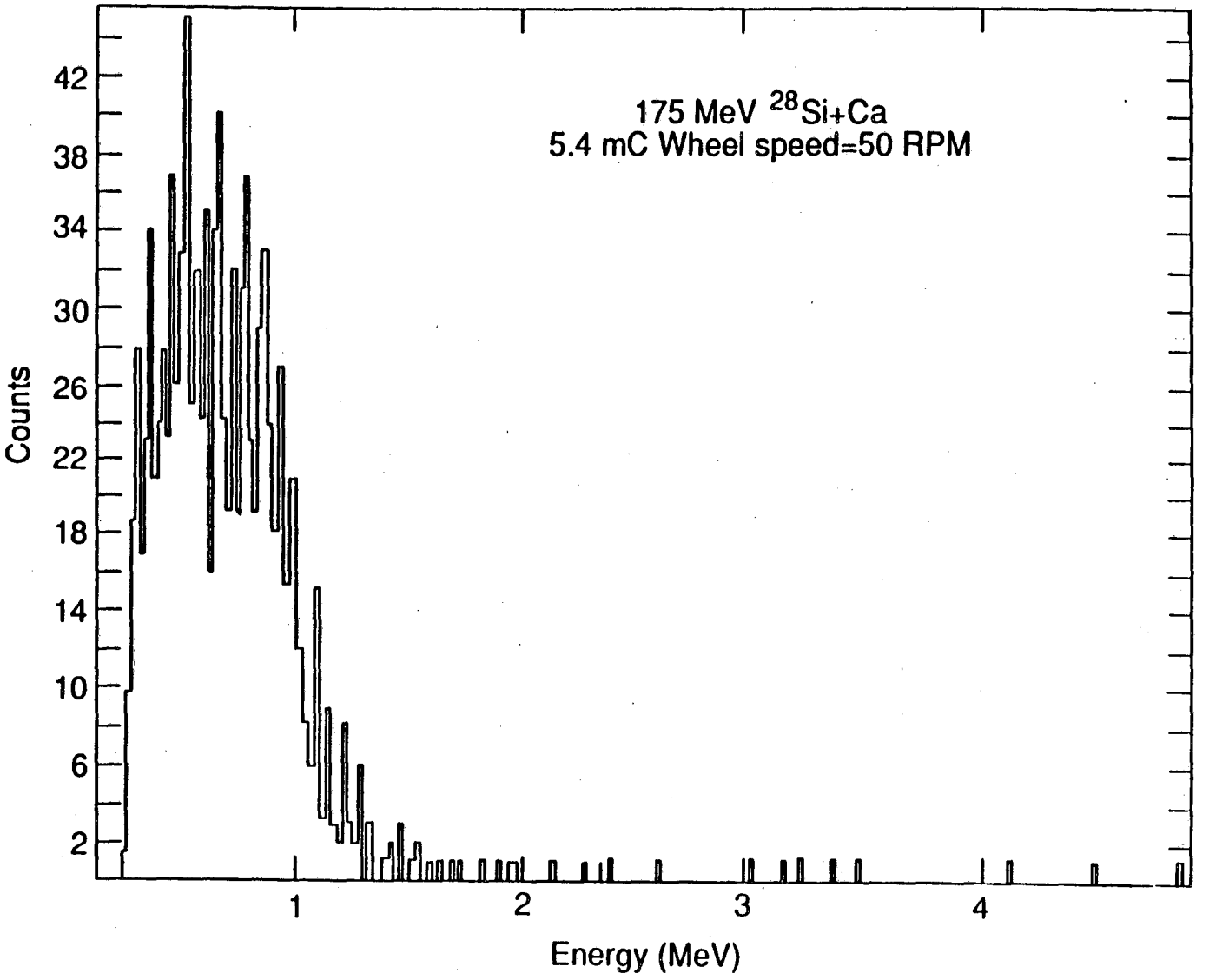

Figure IV - 12

XBL 896-6252

Ground State Proton Decay Branch vs. Expected Number of Counts

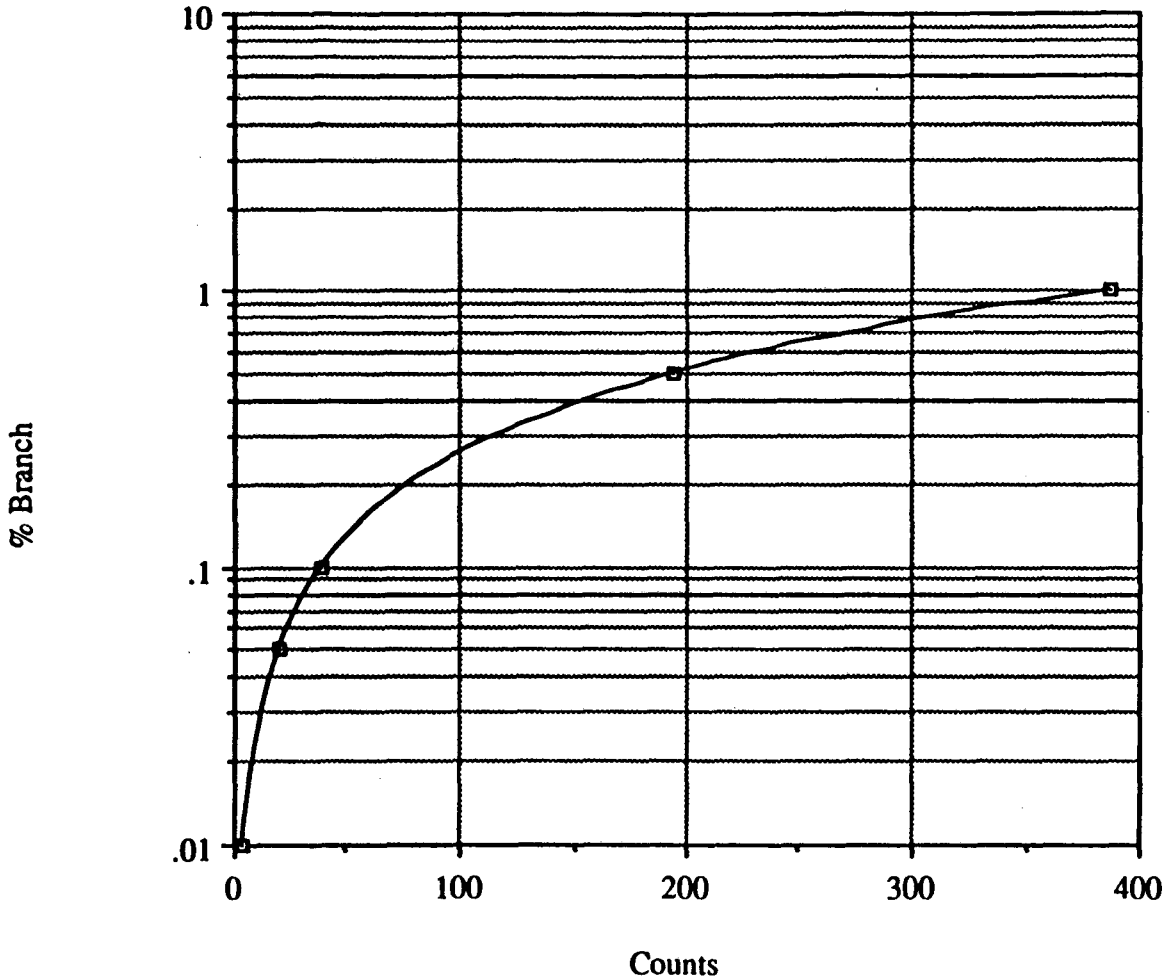

Figure IV - 13

V. Summary and Conclusions

Several experimental techniques have been used to study the decays of nuclei far from stability. Included among them are the helium-jet transport technique, a rapidly rotating in-beam recoil catcher wheel, silicon detector systems, and gas-silicon, low energy particle identification telescopes.

The discovery of the first $T_z = -5/2$ nucleus, ^{35}Ca ($t_{1/2} = 50 \pm 30$ ms), through its beta-delayed two-proton decay employed the helium-jet transport technique [Äy 85]. This measurement showed that ^{35}Ca possesses two such decay branches, one to the ground state of ^{33}Cl and the other to its first excited state. Furthermore, from these decays, the energy of the isobaric analog state in ^{35}K was inferred to be 9.053 ± 0.045 MeV. As this provided the mass of the third member of the A = 35, T = 5/2 isospin sextuplet, the IMME was invoked to determine the mass excess of ^{35}Ca to be 4.453 ± 0.060 MeV. It is interesting to note that this is 231 keV more bound than what is predicted by the charge symmetric Kelson-Garvey mass relation.

In order to study nuclei with half-lives shorter than ~15 ms, an alternative to the helium-jet transport system needed to be devised. After considering several options, a rapidly rotating in-beam recoil catcher wheel was designed and constructed. This wheel allows the detection of decays from nuclei whose half-lives are as short as 100 μs. Additionally, it permits the detection of noble gas nuclei which are unobservable with the helium-jet system [Re 89].

After testing the recoil catcher wheel by observing the decays of known beta-delayed proton and beta-delayed two-proton emitters, beta-delayed two-proton emission from another $T_z = -5/2$ nuclide, ^{31}Ar, was observed [Re 89]. The two protons, emitted from the isobaric analog state in ^{31}Cl, leave the ^{29}P daughter in its ground state. The fact that ^{31}Ar is a beta emitter at all is itself significant because the Kelson-Garvey mass relation predicts that this nucleus should be unbound to ground state two-proton decay by 230 ± 180 keV.

The final set of experiments were designed to search for the ground state proton emission from the $T_z = -1/2$ nuclides ^{69}Br and ^{65}As. Because protons emitted from ground states of nuclei must be very low in energy (or else these nuclei would be "unbound"), special low energy, particle identification telescopes were developed and used in these searches together with the recoil catcher wheel. Although no proton groups were detected which could be assigned to the decays of either of these nuclei, certain limits were set.

It was determined that the half-life of ^{69}Br does not exceed 150 μs, implying that it is unbound with respect to ground state proton emission by at least 450 keV. Because no proton groups were observed, the actual separation energy could not be compared to the

predicted value of 810 ± 300 keV. However, if the trend that has been observed continues in this somewhat heavier mass region, i.e., the mass predictions are roughly 200 keV more unbound than what is observed experimentally, then ^{69}Br will be unbound by approximately 600 keV, resulting in a half-life of 50 ns to 100 ns.

On the other hand, ^{65}As has been predicted to be proton unbound by 530 ± 270 keV. Again, if the predictions err on the side of instability by 200 keV, the separation energy of ^{65}As would be 330 keV. This energy corresponds to a half-life of 1 ms to 10 ms, and therefore makes beta decay a competitive decay mode. Even after optimizing the system to search for decays on this time scale, no proton groups were observed. It was thus concluded that ^{65}As is a beta emitter with, at most, a 0.1% ground state proton decay branch.

VI. Appendix 1 - Derivation of the Beta Decay Probability Formula

The expression for the probability of a nucleus to emit a beta particle with energy E and momentum p given in Section II - B will be derived in Appendix 1. Since the experimental work described in this thesis pertains to nuclei on the proton-rich side of stability, I shall proceed through this section assuming that the beta decay is the decay of a proton into a neutron, positron, and neutrino:

$$p \rightarrow n + e^+ + \nu$$

The perturbation potential responsible for this transition, $H_{\beta+}$, can be given by

$$H_{\beta+} = g\ \psi^*_{e+}(\vec{r_n})\ \psi^*_{\nu}(\vec{r_n})\ Q_p$$

where g is the strength of the weak interaction, $\psi^*_{e+}(\vec{r_n})$ and $\psi^*_{\nu}(\vec{r_n})$ are the complex conjugates of the positron and neutrino wave functions at the site of the decay, r_n, and Q_p is the operator which converts the proton into the neutron. The decay probability per unit time, W_{fi}, also known as Fermi's Golden Rule #2 [Fe 50], is given by

$$W_{fi} = \frac{2\pi}{\hbar} \left| \langle \psi_f | H_{\beta-} | \psi_i \rangle \right|^2 \rho(E_f)$$

where ψ_f and ψ_i are the final and initial wave functions of the nucleus, respectively, and $\rho(E_f)$ is the density of final states. The matrix element in this expression may be given by

$$\langle \psi_f | H_{\beta-} | \psi_i \rangle = g \sum_{\text{protons}} \langle \psi_f | \langle \psi_{e+} | \langle \psi_\nu | Q_p | \psi_i \rangle$$

$$= g \int \psi^*_f\ \psi^*_{e-}(\vec{r_n})\ \psi^*_{\nu}(\vec{r_n})\ Q_p\ \psi_i\ d\tau$$

where Q_p is the operator which converts a proton into a neutron. Because the probability of a neutrino interacting with matter is extremely small, its wave function may be taken to be that of a plane wave, i.e., the particle is moving in a force-free region:

$$\psi_\nu = A \exp\left(\frac{i}{\hbar}(\vec{p_\nu} \cdot \vec{r})\right)$$

Assuming that the neutrino is confined to an arbitrary volume V, ψ_ν must be normalized such that

$$\langle\psi_\nu|\psi_\nu\rangle = \int_V \psi_\nu^* \psi_\nu \, dV = |A|^2 V = 1$$

Therefore,

$$A = \frac{1}{\sqrt{V}}$$

The interaction occurs only at the position of the nucleus so that ψ_ν must be within the nuclear volume.

The energy of the neutrino is equal to

$$E_\nu = h\nu_\nu = \frac{hc}{\lambda_\nu} = \frac{2\pi\hbar c}{\lambda_\nu}$$

so that its wavelength is equal to

$$\lambda_\nu = \frac{2\pi\hbar c}{E_\nu} = \frac{2\pi\,(197.3)}{E_\nu}$$

From these expressions it can be seen that the maximum neutrino energy corresponds to the minimum neutrino wavelength. The maximum energy for neutrinos resulting from beta decay is about 10 MeV, which corresponds to a wavelength of 124 fm. This length is clearly much longer than the radius of even the heaviest of nuclei. Therefore, the long wavelength approximation may be invoked: over nuclear dimensions, the amplitude of the neutrino wave function is about constant. That is,

$$\psi_\nu^*(\vec{r_n}) \approx \psi_\nu^*(0) = \text{a constant}$$

and thus may be removed from the integral.

The deBroglie wavelength of the emitted positron is equal to

$$\lambda_{e+} = \frac{h}{p} = \frac{2\pi\,(197.3)}{(E^2 - E_o^2)^{1/2}}$$

where E is the total positron energy, and E_o is its rest mass. Again, the maximum positron energy corresponds to the minimum wavelength. Thus, a 10 MeV positron will have a deBroglie wavelength of 118 fm, which is again larger than nuclear dimensions. Unlike the neutrino, however, the positron's wave function cannot be set equal to a plane wave and then be considered constant over nuclear dimensions and subsequently removed from the integral because the ambient Coulomb field in the nucleus will affect the shape of the wave function. Therefore, the positron wave function must be expressed as

$$\psi^*_{e+}(\vec{r_n}) = F(Z,E)^{1/2}\,\psi^*_{e+}(0)$$

The function F(Z,E) is known as the Fermi function. The Fermi function has the form

$$F(Z,E) \approx \frac{2\pi\eta}{1-e^{-2\pi\eta}}$$

where

$$\eta = \frac{Ze^2}{\hbar v} \quad \text{for } \beta^- \text{ decay}$$

and

$$\eta = -\frac{Ze^2}{\hbar v} \quad \text{for } \beta^+ \text{ decay}$$

In the above expressions, v is the velocity of the emitted lepton.

Substituting these results for the matrix element in Fermi's Golden Rule #2, we obtain

$$\langle \psi_f | H_{\beta^-} | \psi_i \rangle = g\,F(Z,E)^{1/2}\;\psi^*_{\nu}(0)\,\psi^*_{e+}(0) \langle \psi_f | Q_p | \psi_i \rangle .$$

From the normalization we know that

$$\psi^*_{\nu}(0) = \psi^*_{e+}(0) = \frac{1}{\sqrt{V}}$$

which yields

$$\langle \psi_f | H_{\beta^-} | \psi_i \rangle = \frac{g}{V} F(Z,E)^{1/2} \langle \psi_f | Q_p | \psi_i \rangle$$

Substituting this expression into the equation for the decay probability, we obtain

$$W_{fi} = \frac{2\pi}{\hbar} \frac{g^2}{V^2} F(Z,E) \left| \langle \psi_f | Q_p | \psi_i \rangle \right|^2 \rho(E_f)$$

The last aspect that must be considered is the density of final nuclear states. This quantity may be thought of as the number of ways the available total energy E can be divided between the positron and the neutrino, and may be stated mathematically by

$$\rho(E_f) = \frac{dn}{dE}$$

The total number of momentum states for either lepton is N,

$$N = \frac{4\pi}{3} \frac{p^3}{h^3} V$$

and the total number of ways each lepton may be in volume V with momentum between p and p + dp is

$$dN = 4\pi \frac{p^2}{h^3} V \, dp$$

The total number of momentum states available is therefore

$$d_n = (dN_{e^+})\,(dN_\nu) = 16\pi^2 V^2 \frac{p_{e^+}^2 \, p_\nu^2}{h^6} \, dp_{e^+} \, dp_\nu$$

The relativistic momentum of a particle with rest mass m and kinetic energy E is

$$p = \frac{1}{c} \sqrt{E(E + 2mc^2)}$$

$$\therefore\ p_\nu = \frac{E_\nu}{c} = \frac{E_0 - E_{e^+}}{c}$$

where E_0 is the total decay energy and E_{e^+} is the energy of the emitted positron. For a given positron energy

$$dp_\nu = \frac{dE_0}{c}$$

and

$$dn = 16\,\pi^2\,V^2 \frac{(E_0 - E_{e^+})^2\,p_{e^+}^2}{h^6\,c^3}\,dp_{e^+} + dE_0$$

$$\frac{dn}{dE_0} = \frac{16\pi^2\,V^2}{h^6 c^3}(E_0 - E_{e^+})^2\,p_{e^+}^2\,dp_{e^+}$$

Upon a final substitution into the expression for the decay probability, one obtains the expression for emitting a beta particle with energy E and momentum p:

$$W_{fi} = P(E)\,dE = \frac{g^2}{2\pi^3\,\hbar^7\,c^3}\left|\langle \psi_f | Q_p | \psi_i \rangle\right|^2 F(Z,E)\,(E_0 - E)^2\,p^2\,dp$$

VII. Appendix 2 - Silicon Detectors

Several styles of silicon detectors were used to detect protons emitted in the decays of the proton-rich nuclei. Included among them were phosphorus-diffused, surface barrier, and ion-implanted detectors. This section will describe the basic properties of semiconductor detectors, their fabrication of the various styles, and their relative advantages and disadvantages. The section concludes with a discussion of radiation damage to silicon detectors.

A. Basic Properties of Semiconductor Materials

The outer electron shell levels of crystalline materials exhibit a band structure. These bands, a valence band and a conduction band, are separated by a region where there are no energy levels available to the electrons. This is known as the forbidden energy gap. The width of this gap is determined by the lattice spacing of the atoms in the crystal. Electrons in the conduction band are detached from the atoms in the lattice and are free to roam over the entire crystal, while those in the valence band are more tightly bound to their lattice atoms.

The forbidden energy gap is on the order of 6 eV in insulators. The gap in conductors, however, does not exist because the valence band and conduction band overlap. In semiconductors, the band gap is about 1 eV high - small enough for thermal energy to excite a few valence electrons into the conduction band. This excitation creates a hole in the valence band. It is fairly easy for a neighboring valence electron to break its covalent bond and fill the newly created hole. This generates a hole in the neighboring position thus permitting another valence electron to move over. As this sequence is repeated, the hole appears to move through the crystal. Since the hole is positively charged relative to the sea of electrons in the valence band, it acts like a positive charge carrier; the movement of holes in semiconductors constitutes an electric current just as the movement of electrons constitutes a current in conductors.

Under an externally applied electric field (which is the usual way silicon detectors are operated - see Section VII. B.), the holes and electrons exhibit a drift velocity through the semiconductor. This velocity is equal to the product of the magnitude of the electric field and the mobility of the charge carrier. The mobility is itself a function of the operating temperature and the applied electric field. At room temperature, the mobility of an electron in silicon [Le 87] is 1350 cm^2/Vs and that of a hole is 480 cm^2/Vs. The mobility of the charge carriers at room temperature is unaffected by electric fields which are smaller than 1000 V/cm, thus creating a linear relationship between the drift velocity and the applied electric field. At temperatures between 100 K and 400 K, the mobility varies as $1/T^m$

where T is the temperature and m depends on the material and the charge carrier. In silicon, m = 2.5 for electrons and 2.7 for holes.

Just as an electron-hole pair may be generated by exciting a valence electron into the conduction band, an electron may recombine with a hole by dropping from the conduction band to an open level in the valence band accompanied by the emission of a photon. This is known as recombination. The most important recombination mechanism, however, is through recombination centers which result from impurities in the crystal. Recombination centers are energy levels provided by the impurities which can be located anywhere in the forbidden energy gap. These centers are available to electrons in the conduction band for de-excitation as well as to electrons in the valence band . Electrons captured by these levels may be released back into an "allowed" band, or may be annihilated if a hole is captured in the same level. Some impurities can capture only one type of carrier, thereby not permitting annihilation. These levels hold the carrier for a time characteristic of the impurity, and then release it. This process is known as trapping.

Both recombination and trapping are detrimental to radiation detectors as they reduce the mean free time of the charge carriers. If the trapping time is on the order of the charge collection time, then incomplete charge collection will result. While impurities in the crystal are the biggest source of recombination and trapping, structural defects may also give rise to similar states in the forbidden energy gap. These defects may be caused by imperfect crystal growth, thermal shock, or radiation damage. Radiation damage is the most common cause and will be discussed later in this Appendix.

B. Doped Semiconductors and the Semiconductor Junction

If an atom of phosphorus, which has five valence electrons, is introduced into a silicon crystal (silicon is tetravalent), four of the electrons are used in bond formation and the fifth goes into a level which lies just below the conduction band. Unlike recombination and trapping states, however, this level is so close to the conduction band (just 0.05 eV away) that the extra electron is easily excited into it. This, in turn, enhances the conductivity of the semiconductor. In addition, these extra electrons fill the holes normally formed by electron migration. The concentration of electrons in the crystal is therefore enhanced. Semiconductors of this type are called n-type semiconductors.

Analogously, if a trivalent atom such as boron is introduced into the silicon, a hole is formed at the site of the boron atom. The hole can be filled with an electron from the valence band; this electron then occupies a level just slightly above the valence band. This excess of holes decreases the normal concentration of electrons. Such semiconductors are called p-type semiconductors.

Silicon diodes are formed when a piece of p-type silicon is brought in intimate contact with n-type material. This is known as a p-n junction. Because of the difference in the concentration of electrons and holes between the two materials, the holes drift toward the n-region and the electrons drift toward the p-region. This redistribution of holes and electrons causes a charge build up to occur on both sides of this junction; the p-region becomes negative while the n-region becomes positive. The resulting electric field across the junction creates a potential difference known as a contact potential. This contact potential, on the order of 1 V [Le 87], causes the relative band energies in the n-type material to drop below their counterparts in the p-type material. This region of changing potential is known as the depletion zone and has the special property of being devoid of all charge carriers.

When an ionizing particle passes through the depletion zone, electrons and holes are formed. The electrons immediately migrate toward the n side and the holes toward the p side. Due to experimental constraints, the charge collection process must be limited to several microseconds. The intrinsic electric field is not intense enough to provide efficient charge collection on such short time scales. The situation is remedied by applying a reverse-bias voltage to the junction, i.e., either a positive voltage to the n-side or a negative voltage to the p-side. This has the effect of providing a charge collection time of just a few microseconds as well as increasing the depletion zone so higher energy particles can be detected.

C. Diffused Junction Detectors

Diffused junction detectors are produced by diffusing n-type material into one end of a homogeneous p-type silicon wafer. Phosphorus is the n-type material most frequently chosen. By regulating the phosphorus concentration, the temperature of the process (usually ~1000° C), and diffusion time, p-n junctions lying from .1 μm to 2 μm beneath the surface can be produced. The silicon surface becomes so heavily doped during the diffusion process that the depletion zone extends largely into the p-side of the junction. Although this process leaves a dead layer through which the ionizing radiation must pass, the width of this layer is much smaller than the depletion zone which is created, and unlike the the depletion zone, it does not vary much with applied bias. The high temperature needed to diffuse the phosphorus through the silicon tends to increase the intrinsic noise level of the detector and decrease its lifetime. The major advantages of diffused junction detectors are their relative ruggedness compared to other semiconductor detectors and their greater resistance to contamination of the detector surface.

Phosphorus-diffused silicon detectors work very well with the helium-jet transport technique. However when used in conjunction with the in-beam recoil catcher wheel, the intense radiation field produced by the nearby beam causes the diffused junction detectors to breakdown quite rapidly - usually within a few hours. However cooling them to -35° C seems to extend their lifetimes by a factor of 10. In this strenuous environment, ion-implanted detectors have been found to give much better results.

D. Surface Barrier Detectors

Surface barrier detectors are usually made by forming a junction with n-type silicon and gold, although p-type silicon and aluminum work just as well. The contact potential established is similar to that in the p-n junctions previously described, however the depletion zone created in surface barrier detectors is much larger than in diffused junction detectors. In fact, the depletion zone in surface barrier detectors can extend entirely through a thin silicon wafer. A benefit of using a completely depleted detector is that by increasing the applied bias, the charge collection time can be greatly reduced. Depletion zones 5 mm deep have been obtained routinely in surface barrier detectors.

The process for manufacturing surface barrier detectors is quite a bit simpler than that for diffused junction detectors. After etching the surface of the silicon wafer and allowing it to oxidize slightly, a thin layer of gold (~40 $\mu g/cm^2$) is evaporated onto it. The wafer is then mounted in an insulating ring that has metallic surfaces for electrical contacts. Because the fabrication process takes place at room temperature, the lifetime of surface barrier detectors is not compromised as it is when higher temperatures are used.

A disadvantage associated with surface barrier detectors is their sensitivity to light. Visible wavelengths have energies of 2 eV to 4 eV. Because the thin layer of gold on the silicon is not enough to stop the ambient light, and because the forbidden energy gap is only about 1 eV high, unwanted signals can be obtained from the detector if it is not properly shielded from the light.

E. Ion-Implanted Detectors

Ion-implanted junctions are formed by shooting the impurities directly into the silicon wafer with an accelerator. By regulating the energy of the beam, the depth of the junction can be controlled. As some radiation damage is incurred in this process, ion-implanted detectors must be annealed at a temperature of ~500° C prior to use. Although this temperature slightly reduces the lifetime of the detector, the effect is not nearly as severe as the 1000° C temperature used to manufacture diffused junction detectors.

Ion-implanted detectors tend to be more stable than surface barrier detectors and have shown the most favorable characteristics of all silicon detectors, i.e., lowest noise, lowest leakage current, etc. However, as can be inferred from the fabrication process, they are also the most expensive.

Cooling ion-implanted detectors to -35° C not only reduces the noise in the counters, but also decreases the leakage current. After approximately 50 hours of use, the leakage current in the uncooled detectors was greater than 10 μA with an applied bias of 60 V. After cooling the detectors, the leakage current was reduced to 0.2 μA. The same cooled ion-implanted detectors were used for close to 350 hours before they were replaced.

F. Radiation Damage

The distance between the beam and the detectors in the in-beam recoil catcher wheel box is only about 1 cm . Therefore damage to the detectors from the radiation associated with the beam (particularly neutrons when a ^{3}He beam is used) poses a severe problem. Radiation damage in silicon detectors results primarily from changes within the crystal lattice [Kr 84]. Incident radiation of sufficient energy can displace a silicon atom from its equilibrium site to an interstitial position. The resulting vacancy-interstitial pair, known as a Frenkel defect, acts as a carrier trapping site. Neutrons, through transmutations of the silicon, also introduce trapping and recombination centers. The main effects of the radiation damage are 1) an increase in the leakage current, 2) a decrease in the energy resolution of the detector, 3) an increase in the charge collection time, and 4) a material change from n-type to p-type.

When charge carriers are caught in or released from the trapping centers, the bulk current inside the crystal increases. This gives rise to the increase in the leakage current. The energy resolution of the detector is decreased because capturing the charge carriers results in the incomplete collection of charge produced by the incoming particle. Trapping centers reduce charge carrier mobility and therefore increase the time required for charge collection. Also, crystal defects tend to act as electron acceptors; over time, the silicon can actually change from n-type to p-type.

Cooling the detectors tends to minimize the effects of radiation damage. Decreasing the operating temperature generally results in a decrease of leakage current on the order of a factor of 3 for each 10° C drop [Eg 85]. This subsequently reduces the noise in the detectors. The detectors used in conjunction with the in-beam recoil catcher wheel are cooled to -35° C with either thermoelectric coolers or cold nitrogen.

VIII. References

[An 84] M.S. Antony and A. Pape, Phys. Rev. C 30, 1286 (1984).

[An 85] M.S. Antony, J. Britz, J.B. Bueb, and A. Pape, At. Data and Nucl. Data Tables 33, 447 (1985).

[An 86] M.S. Antony, J. Britz, and A. Pape, At. Data and Nucl. Data Tables 34, 279 (1986).

[Äy 80] J. Äystö and J. Cerny, "Current and Future Directions in the Study of Light Nuclei Employing an On-Line Mass Separator", in Future Directions in Studies of Nuclei Far From Stability, edited by J.H. Hamilton, E.H. Spejewski, C.R. Bingham, and E.F. Zganjar, North-Holland Publishing Company, Amsterdam, The Netherlands, 1980, p. 257.

[Äy 85] J. Äystö, D.M. Moltz, X.J. Xu, J.E. Reiff, and J. Cerny, Phys. Rev. Lett. 55, 1384 (1985).

[Äy 89] J. Äystö and J. Cerny, "Proton-Rich Light Nuclei", in Treatise on Heavy-Ion Science, edited by D. Allan Bromley, Plenum Press, New York, New York, 1989, p. 207.

[Ba 63] R. Barton, R. McPherson, R.E. Bell, W.R. Frisken, W.T. Link, and R.B. Moore, Can. J. Phys. 41, 2007 (1963).

[Bl 76] M. Blann and J. Bisplinghoff, Lawrence Livermore National Laboratory, Report No. UCID-19614 (1976).

[Bo 69] A. Bohr and B. Mottelson, Nuclear Structure, Volume I, W.A. Benjamin, Inc., New York, New York, 1969, p. 326.

[Bo 86] P. Bopp, D. Dubbers, L. Hornig, E. Klemt, J. Last, H. Schütze, S.J. Freedman, and O. Schärpf, Phys. Rev. Lett. 56, 919 (1986).

[Bo 87] V. Borrel, J.C. Jacmart, F. Pougheon, A. Richard, R. Anne, D. Bazin, H. Delagrnage, C. Détraz, D. Guillemaud-Mueller, A.C. Mueller, E. Roeckl, M.G. Saint-Laurent, J.P. Dufour, F. Hubert, and M.S. Provikoff, Nucl. Phys. A473, 331 (1987).

[Br 36] G. Breit and E. Feenberg, Phys. Rev. 50, 850 (1936).

[Br 85] B.A. Brown and B.H. Wildenthal, At. Data and Nucl. Data Tables 33, 347 (1985).

[Ca 80] T.A. Cahill, Ann. Rev. Nucl. Part. Sci. 30, 221 (1980).

[Ca 83] M.D. Cable, J. Honkanen, R.F. Parry, S.H. Zhou, Z.Y. Zhou, and J. Cerny, Phys. Rev. Lett. 50, 404 (1983).

[Ca 83a] M.D. Cable, J. Honkanen, R.F. Parry, S.H. Zhou, Z.Y. Zhou, and J. Cerny, Phys. Lett. 123B, 25 (1983).

[Ca 84] M.D. Cable, J. Honkanen, E.C. Schloemer, M. Ahmed, J.E. Reiff, Z.Y. Zhou, and J. Cerny, Phys. Rev. C 30, 1276 (1984).

[Ca 84a] M.D. Cable, J. Honkanen, E.C. Schloemer, M. Ahmed, J.E. Reiff, Z.Y. Zhou, and J. Cerny, Proc. of the 5th Nordic Meeting on Nuclear Physics, Jyväskylä, Finland, 1984, p. 119.

[Ce 70] J. Cerny, J.E. Esterl, R.A. Gough, and R.G. Sextro, Phys. Lett. 33B, 284 (1970).

[Ce 77] J. Cerny and J.C. Hardy, Ann. Rev. Nucl. Sci. 27, 333 (1977).

[Co 75] W.J. Courtney and J.D. Fox, At. Data and Nucl. Data Tables 15, 141 (1975).

[Co 80] T.V. Congedo, I.S. Lee-Fan, and B.L. Cohen, Phys. Rev. C 22, 985 (1980).

[Dr 85] P.V. Drumm, L.K. Fifield, R.A. Bark, M.A.C. Hotchkis, C.L. Woods, and P. Maier-Komor, Nucl. Phys. A441, 95 (1985).

[Du 85] H. Dumont, B. Delaunay, J. Delaunay, D.M. De Castro Rizzo, A. Brondi, P. Cuzzocrea, A. D'Onofrio, R. Moro, M. Romano, and F. Terrasi, Nucl. Phys. A435, 301 (1985).

[Eg 85] EG&G Ortec, The Whys and Wherefores of Charged Particle Detector Spectrometry, EG&G Ortec, Oak Ridge, Tennessee, 1985, p. 5.

[Eh 62] K.W. Ehlers, Nucl. Instr. and Meth. 18, 571 (1962).

[En 78] P.M. Endt and C. van der Leun, Nucl. Phys. A310, 1 (1978).

[Es 71] J.E. Esterl, Ph.D. Thesis, University of California Radiation Laboratory Report No. UCRL - 20840, unpublished (1971).

[Fa 84] T. Faestermann, A. Gillitzer, K. Hartel, P. Kienle, and E. Nolte, Phys. Lett. 137B, 23 (1984).

[Fa 88] T. Faestermann, A. Gillitzer, K. Hartel, P. Kienle, and E. Nolte, Proc. 5th Int. Conf. on Nuclei Far From Stability, edited by I. Towner, American Institute of Physics, New York, New York, 739 (1988).

[Fe 50] E. Fermi, Nuclear Physics, Revised Edition, notes compiled by J. Orear, A.H. Rosenfeld, and R.A. Schluter, University of Chicago Press, Chicago, Illinois, 1950.

[Fr 81] G. Friedlander, J.W. Kennedy, E.S. Macias, and J.M. Miller, Nuclear and Radiochemistry, Third Edition, John Wiley & Sons, New York, New York, 1981, p. 89.

[Ga 66] G.T. Garvey and I. Kelson, Phys. Rev. Lett. 16, 197 (1966).

[Gi 87] A. Gillitzer, T. Faestermann, K. Hartel, P. Kienle, and E. Nolte, Z. Phys. A326, 107 (1987).

[Go 60] V.I. Gol'danskii, J. Exptl. Theoret. Phys. 39, 497 (1960); Soviet Phys. JETP 12, 348 (1961).

[Go 61] V.I. Gol'dnaskii, Nucl. Phys. 27, 648 (1961).

[Go 66] V.I. Gol'danskii, Ann. Rev. Nucl. Sci. 16, 1 (1966).

[Go 72] D.R. Goosman and D.E. Alburger, Phys. Rev. C 6, 820 (1972).

[Go 80] V.I. Gol'danskii, Pis'ma Zh. Eksp. Teor. Fiz. 32, 572 (1980); JETP Lett. 32, 554 (1980).

[Gu 75] A. Guichard, H. Nann, and B.H. Wildenthal, Phys. Rev. C 12, 1109 (1975).

[Ha 69] B.G. Harvey, Introduction to Nuclear Physics and Chemistry, Second Edition, Prentice-Hall, Englewood Cliffs, New Jersey, 1969, p. 356.

[Ha 71] J.C. Hardy, J.E. Esterl, R.G. Sextro, and J. Cerny, Phys. Rev. C 3, 700 (1971).

[Ha 72] J.C. Hardy, Nucl. Data Tables 11, 327 (1972).

[Ha 83] Havar is an alloy composed primarily of Co (42.5%), Cr (20.0%), Fe (19.9%), and Ni (13.0%) and has a specific gravity of 8.3 . It is manufactured by Hamilton Precision Metals, A Division of HMW Industries, Inc., Lancaster, Pennsylvania 17604.

[Ha 88] P. Haustein, At. Data and Nucl. Data Tables 39, 185 (1988).

[Ho 82] S. Hofmann, W. Reisdorf, G. Münzenberg, F.P. Heßberger, J.R.H. Schneider, and P. Armbruster, Z. Phys. A305, 111 (1982).

[Ho 83] J. Honkanen, M.D. Cable, R.F. Parry, S.H. Zhou, Z.Y. Zhou, and J. Cerny, Phys. Lett. 133B, 146 (1983).

[Ho 87] M.A.C. Hotchkis, J.E. Reiff, D.J. Vieira, F. Blönnigen, T.F. Lang, D.M. Moltz, X. Xu, and J. Cerny, Phys. Rev. C 35, 315 (1987).

[Ho 89] M.A.C. Hotchkis, R. Chapman, J.H. McNeill, R.A. Cunningham, B.R. Fulton, R.D. Page, P.J. Woods, and G.D. Jones, Manchester Nuclear Physics Report, August 1987 - December 1988, Schuster Laboratory, University of Manchester, Manchester, England, p. 13.

[Ho 89a] M.A.C. Hotchkis, private communication.

[Ja 70] K.P. Jackson, C.U. Cardinal, H.C. Evans, and N.A. Jelley, Phys. Lett. 33B, 281 (1970).

[Ja 70a] W. Jaus and G. Rasche, Nucl. Phys. A143, 202 (1970).

[Ja 72] W. Jaus, Phys. Lett. 40, 616 (1972).

[Ja 74] K.P. Jackson, J.C. Hardy, H. Schmeing, R.L. Graham, J.S. Geiger, and K.W. Allen, Phys. Lett. 49B, 341 (1974).

[Ja 85] R. Jahn, R.L. McGrath, D.M. Moltz, J.E. Reiff, X.J. Xu, J. Äystö, and J. Cerny, Phys. Rev. C 31, 1576 (1985).

[Jä 88] J. Jänecke and P.J. Masson, At. Data and Nucl. Data Tables 39, 265 (1988).

[Ju 71] H. Jungclas, R.D. Macfarlane, and Y. Fares, Phys. Rev. Lett. 27, 556 (1971).

[Ka 64] V.A. Kanaukhov and G.M. Ter-Akopyan, Phys. Lett. 12, 339 (1964).

[Ke 66] I. Kelson and G.T. Garvey, Phys. Lett. 23, 689 (1966).

[Kl 82] O. Klepper, T. Batsch, S. Hofmann, R. Kirchner, W. Kurcewicz, W. Reisdorf, E. Roeckl, D. Schardt, and G. Nyman, Z. Phys. A305, 125 (1982).

[Kr 84] H.W. Kraner, Nucl. Instr. and Meth. A225, 615 (1984).

[Le 87] W.R. Leo, Techniques for Nuclear and Particle Physics Experiments, Springer-Verlag, Berlin, 1987, pp. 207ff.

[Li 80] R.L. Liboff, Introductory Quantum Mechanics, Addison-Wesley Publishing Company, Inc., Reading, Massachusetts, 1980, pp. 232ff.

[Ly 87] C.M. Lyneis, Proc. 11th Int. Conf. on Cyclotrons and Their Applications, Tokyo, Japan, 1987, p. 707.

[Ma 69] P. Marmier and E. Sheldon, Physics of Nuclei and Particles, Volume 1, Academic Press, New York, New York, 1969, pp. 351ff.

[Ma 74] R.D. Macfarlane and W.C. McHarris, Nuclear Spectroscopy and Reactions, Part A, edited by J. Cerny, Academic Press, New York, 1974, p. 243.

[Ma 79] C. Maples and J. Sivak, IEEE Trans. Nucl. Sci. NS-26, 4409 (1979).

[Ma 84] W.A. Mayer, W. Henning, R. Holzwarth, H.J. Korner, G. Korschinek, W.U. Mayer, G. Rosner, and H.J. Scheerer, Z. Phys. A319, 287 (1984).

[Mc 82] Program written by R.J. McDonald.

[Mo 88] M.F Mohar, E. Adamides, W. Benenson, C. Bloch, B.A. Brown, J. Clayton, E. Kashy, M. Lowe, J.A. Nolen Jr., W.E. Ormand, J. van der Plicht, B. Sherrill, J. Stevenson, and J.S. Winfield, Phys. Rev. C 38, 737 (1988).

[Mo 89] D.M. Moltz and J. Cerny, "Beta-Delayed Two-Proton Emission", in Particle Emission from Nuclei, Volume III, edited by D.N. Poenaru and M.S. Ivascu, CRC Press, Boca Raton, Florida, 1989, p. 133.

[Oh 65] G.G. Ohlsen, Nucl. Instr. and Meth. 37, 240 (1965).

[Ra 75] S. Raman, T.A. Walkiewicz, and H. Behrens, At. Data and Nucl. Data Tables 16, 451 (1975).

[Re 66] P.L. Reeder, A.M. Poskanzer, R.A. Esterlund, and R. McPherson, Phys. Rev. 147, 781 (1966).

[Re 89] J.E. Reiff, M.A.C. Hotchkis, D.M. Moltz, T.F. Lang, J.D. Robertson, and J. Cerny, Nucl. Instr. and Meth. A276, 288 (1989).

[Ro 89] J.D. Robertson, J.E. Reiff, D.M. Moltz, T.F. Lang, and J. Cerny, Lawrence Berkeley Laboratory Report No. LBL - 26335 (1989).

[Se 73] Program written by R. Sextro.

[Se 73a] R.G. Sextro, R.A. Gough, and J. Cerny, Phys. Rev. C 8, 258 (1973).

[Se 74] R.G. Sextro, R.A. Gough, and J. Cerny, Nucl. Phys. A234, 130 (1974).

[Si 87] A. Sirlin, Phys. Rev. D 35, 423 (1987).

[St 79] D.P. Stahel, Ph.D. Thesis, Lawrence Berkeley Laboratory Report Number LBL - 9706 (1979).

[Sy 71] K.R. Symon, Mechanics, Addison-Wesley, Reading, Massachusetts, 1971, pp. 175 - 182.

[Th 84] C.E. Thorn, J.W. Olness, and E.K. Warburton, Phys. Rev. C 30, 1442 (1984).

[Vi 79] D.J. Vieira, R.A. Gough, and J. Cerny, Phys. Rev. C 19, 177 (1977).

[Wa 88] A.H. Wapstra, G. Audi, and R. Hoekstra, At. Data and Nucl. Data Tables, 39, 281 (1988).

[Wi 57] E.P. Wigner, Proc. of the Robert A. Welch Found. Conf. on Chem. Res., Houston, Texas, edited by W.O. Milligan, 1957, p. 67.

[Wi 70] D.H. Wilkinson and B.E.F. Macefield, Nucl. Phys. A158, 110 (1970).

[Wi 74] D.H. Wilkinson and B.E.F. Macefield, Nucl. Phys. A232, 58 (1974).

[Wi 84] B.H. Wildenthal, Prog. Part. Nucl. Phys. 11, 5 (1984).

[Wo 79] Program written by J.M. Wouters.

LAWRENCE BERKELEY LABORATORY
TECHNICAL INFORMATION DEPARTMENT
1 CYCLOTRON ROAD
BERKELEY, CALIFORNIA 94720